
**รายงานวิจัยฉบับสมบูรณ์**

# อิทธิพลของความเค้นแบบแกนเดี่ยวต่อสมบัติไดอิเล็กตริกของสารเซรามิกเฟร์โรอิเล็กตริก

**โดย**

**ผศ. ดร. รัตติกร ยิ้มนิรัญ**

**สิงหาคม 2550**

สัญญาเลขที่ RSA4780002

# รายงานวิจัยฉบับสมบูรณ์

# อิทธิพลของความเค้นแบบแกนเดี่ยวต่อสมบัติไดอิเล็กตริกของสารเซรามิกเฟร์โรอิเล็กตริก

ผศ. ดร. รัตติกร ยิ้มนิรัญ
ภาควิชาฟิสิกส์ คณะวิทยาศาสตร์
มหาวิทยาลัยเชียงใหม่

สนับสนุนโดยสำนักงานกองทุนสนับสนุนการวิจัย

(ความเห็นในรายงานนี้เป็นของผู้วิจัย สกว.ไม่จำเป็นต้องเห็นด้วยเสมอไป)

# กิตติกรรมประกาศ

ผู้วิจัยใคร่ขอขอบพระคุณ สำนักงานกองทุนสนับสนุนการวิจัย (สกว.) ที่ได้ให้การสนับสนุนงานวิจัยและพัฒนาครั้งนี้ ผ่านทางทุนพัฒนานักวิจัย ประจำปี พ.ศ. 2547 ขอขอบพระคุณศาสตราจารย์ ดร. ทวี ตันฆศิริ และบุคลากรของห้องปฏิบัติการวิจัยอิเล็กโทรเซรามิกส์ที่ได้ให้การสนับสนุนและคำแนะนำในทุกด้าน ขอขอบคุณภาควิชาฟิสิกส์ คณะวิทยาศาสตร์ มหาวิทยาลัยเชียงใหม่ ที่ช่วยอำนวยความสะดวกในการใช้เครื่องมือ อุปกรณ์ และสถานที่ จนทำให้งานวิจัยเรื่องนี้สามารถดำเนินการจนสำเร็จผลได้ด้วยดี ขอขอบคุณผู้ร่วมงานและนักศึกษาทุกท่าน ที่มีส่วนช่วยเหลือผู้วิจัยให้ดำเนินงานชิ้นนี้สำเร็จลุล่วงได้ดี โดยเฉพาะ ดร. วรรณวิลัย ไชยสาร คุณสุพัตรา วงศ์แสนใหม่ คุณอธิพงศ์ งามจารุโรจน์ คุณสวรินทร์ ฉมังลาภ คุณเรวดี วงศ์มณีรุ่ง คุณเมืองใจ อุ่นเรือน และคุณนฤทธ์ ตรีอำนรรค ขอขอบคุณผู้ช่วยศาสตราจารย์ ดร.ยงยุทธ เหล่าศิริถาวร สำหรับด้านงานคำนวณและงานด้านฟิสิกส์อื่นๆ ขอขอบคุณรองศาสตราจารย์ ดร.สุพล อนันตา ที่ได้ให้ความช่วยเหลือส่งเสริมเกื้อกูลในการทำงานเสมอมานับตั้งแต่วันเริ่มต้น ตลอดจนเป็นกำลังใจให้กันเสมอที่จะสู้และอยู่รอดในการทำวิจัย ผู้วิจัยต้องขอบคุณความร่วมมือที่ได้รับอย่างดีจากนักวิจัยที่ปรึกษาและเพื่อนร่วมงานในต่างประเทศ ได้แก่ Prof. Robert Newnham Prof. Kenji Uchino และ Prof. Amar Bhalla แห่ง The Pennsylvania State University Prof. Xiaoli Tan แห่ง Iowa State University และ Prof. David Cann แห่ง Oregon State University

ท้ายที่สุดนี้ขอมอบความดีทั้งหมดให้แทนคำขอบคุณสำหรับ คุณวิภา ยิ้มนิรัญ ภรรยา และด.ช. รัญชน์ ยิ้มนิรัญ ลูกชาย คงไม่มีความสำเร็จใดๆเกิดขึ้นได้ถ้าปราศจากความรักและความเข้าใจ รอยยิ้มแห่งความสุข คำปลอบเมื่อยามท้อ ตลอดจนกำลังใจและความอดทนที่ครอบครัวมอบให้ผู้วิจัยตลอดมาจนสามารถมาถึง ณ วันนี้ได้

(ผศ.ดร. รัตติกร ยิ้มนิรัญ)
หัวหน้าโครงการ

# บทคัดย่อ

**รหัสโครงการ :** RSA4780002

**ชื่อโครงการ :** อิทธิพลของความเค้นแบบแกนเดี่ยวต่อสมบัติไดอิเล็กตริกของสารเซรามิกเฟร์โรอิเล็กตริก

**ชื่อนักวิจัย :** ผศ.ดร. รัตติกร ยิ้มนิรัญ

ภาควิชาฟิสิกส์ คณะวิทยาศาสตร์ มหาวิทยาลัยเชียงใหม่

**E-mail Address :** rattikornyimnirun@yahoo.com

**ระยะเวลาโครงการ :** 31 สิงหาคม 2547 ถึง 30 สิงหาคม 2550

ในการวิจัยนี้ได้ทำการศึกษาอิทธิพลของความเค้นแบบแกนเดี่ยวต่อสมบัติไดอิเล็กตริกของสารเซรามิกเฟร์โรอิเล็กตริกที่สำคัญ กล่าวคือ BT PT PZT PZN PMN PIN PZT-BT PMN-PT PZN-PZT PIN-PT และ PZTBT-PMNT โดยสามารถแบ่งผลงานที่ได้จากโครงการวิจัยนี้ออกเป็น 3 กลุ่มใหญ่ กล่าวคือ 1. กระบวนการเตรียมผงและเซรามิก 2. สมบัติไดอิเล็กตริกและทางไฟฟ้าอื่นๆของสารเซรามิก และ 3. อิทธิพลของความเค้นแบบแกนเดี่ยวต่อสมบัติไดอิเล็กตริกและทางไฟฟ้าอื่นๆของสารเซรามิกทั้งหมดที่กล่าวมาข้างต้น ซึ่งกลุ่มผู้วิจัยได้ประสบความสำเร็จในการเตรียมผงและเซรามิกด้วยการใช้เทคนิคผสมออกไซด์ร่วมกับเทคนิคการบดย่อยละเอียด โดยได้ทราบถึงเงื่อนไขที่เหมาะสมต่อการเตรียมผงให้มีความบริสุทธิ์สูง และพบเงื่อนไขในการเผาที่เหมาะสมต่อการเตรียมเซรามิกแต่ละชนิดที่กล่าวมาเหล่านี้ให้มีความบริสุทธิ์และความหนาแน่นสูง และจากการตรวจสอบคุณลักษณะเฉพาะและคุณสมบัติทางไฟฟ้าต่างๆของเซรามิกที่เตรียมได้ก็พบว่าสารเซรามิกที่เตรียมได้นั้นแสดงคุณลักษณะเฉพาะเป็นสารเซรามิกเฟร์โรอิเล็กตริกแบบปกติ หรือสารเซรามิกเฟร์โรอิเล็กตริกกลุ่มรีแลกเซอร์ หรือสารเซรามิกที่แสดงลักษณะผสมกันระหว่างเซรามิกเฟร์โรอิเล็กตริกแบบปกติและสารเซรามิกเฟร์โรอิเล็กตริกกลุ่มรีแลกเซอร์ ทั้งนี้ขึ้นกับชนิดของสารเซรามิกและอัตราส่วนผสม และจากการศึกษาอิทธิพลของความเค้นแบบแกนเดี่ยวต่อสมบัติไดอิเล็กตริกและทางไฟฟ้าอื่นๆของสารเซรามิกก็พบว่าความเค้นมีผลอย่างชัดเจนในการเปลี่ยนแปลงสมบัติต่างๆในสารเซรามิกทุกระบบ โดยมีทิศทางและอัตราการเปลี่ยนแปลงที่ขึ้นอยู่กับชนิดของสารเซรามิกและอัตราส่วนผสม ท้ายที่สุดนั้นผลการศึกษาในโครงการวิจัยนี้ได้นำไปสู่ผลงานการตีพิมพ์ในระดับนานาชาติแล้วกว่า 40 เรื่อง

**คำหลัก:** ความเค้นแบบแกนเดี่ยว; สมบัติไดอิเล็กตริก; สารเซรามิกเฟร์โรอิเล็กตริก

# Abstract

**Project Code :** RSA4780002

**Project Title :** Effects of Uniaxial Stress on Dielectric Properties of Ferroelectric Ceramics

**Investigators :** Asst. Prof. Dr. Rattikorn Yimnirun

Department of Physics, Faculty of Science, Chiang Mai University

**E-mail Address :** rattikornyimnirun@yahoo.com

**Project Period :** August 31, 2004 to August 30, 2007

In this study, effects of uniaxial stress on the dielectric properties of important ceramics in BT PT PZT PZN PMN PIN PZT-BT PMN-PT PZN-PZT PIN-PT และ PZTBT-PMNT systems were investigated. The outputs of this project can be divided into 3 main groups; namely, 1. powder and ceramic fabrication, 2. dielectric and other electrical properties, and 3. effects of uniaxial stress on dielectric and other electrical properties of all the prepared ceramics. We have successfully prepared powders and ceramics by using the mixed-oxide technique in conjunction with the vibro-milling technique and found suitable conditions for preparing high purity powders and for fabricating each ceramic to high purity and density. From the characterization and electrical properties measurements, the prepared ceramics exhibit either normal or relaxor or mixed ferroelectric characteristics, depending upon the type of ceramics and composition ratio. Similarly, the uniaxial stress studies also indicate that the applied stress impose significant influence on the electrical properties with the direction and rate of change depending on the type of ceramics and composition ratio. Finally, the results from this project has resulted in more than 40 international publications.

**Keywords :** Uniaxial Stress; Dielectric Properties; Ferroelectric Ceramics

# Executive Summary

สารเซรามิกเฟร์โรอิเล็กตริก (ferroelectrics) เช่น แบเรียมไทเทเนต ($BaTiO_3$) หรือ BT เลดไทเทเนต ($PbTiO_3$) หรือ PT เลดเซอร์โคเนตไทเทเนต ($Pb(Zr,Ti)O_3$) หรือ PZT เลดซิงค์ไนโอเบต ($Pb(Zn_{1/3}Nb_{2/3})O_3$) หรือ PZN เลดแมกนีเซียมไนโอเบต ($Pb(Mg_{1/3}Nb_{2/3})O_3$) หรือ PMN และ เลดอินเดียมไนโอเบต ($Pb(In_{1/2}Nb_{1/2})O_3$) หรือ PIN ล้วนแล้วแต่เป็นสารที่ถูกพัฒนาขึ้นมาเพื่อใช้ประโยชน์ในอุปกรณ์อิเล็กทรอนิกส์ประเภทต่างๆ อย่างไรก็ตามโดยทั่วไปแล้ว ในสภาวะการใช้งานจริงของอุปกรณ์อิเล็กทรอนิกส์ที่ผลิตจากสารเซรามิกเฟร์โรอิเล็กตริกดังที่กล่าวมาแล้วนั้น สารเซรามิกมักจะอยู่สภาวะภายใต้ความเค้น ซึ่งอาจจะเกิดจากความเค้นเชิงกลภายนอกระหว่างการใช้งาน หรือความเค้นเชิงกลภายในอันเกิดจากการที่สารเซรามิก เหล่านี้ ดังนั้นข้อมูลเกี่ยวกับสมบัติไดอิเล็กตริกภายใต้อิทธิพลของความเค้น จึงมีความสำคัญอย่างมากต่อการออกแบบ การจัดสร้างและการใช้งานของอุปกรณ์อิเล็กทรอนิกส์ที่ผลิตจากสารเซรามิกเฟร์โรอิเล็กตริกเหล่านี้ ดังนั้นผู้วิจัยจึงทำการศึกษาอย่างเป็นระบบถึงอิทธิพลของความเค้นต่อสมบัติไดอิเล็กตริกของสารเซรามิกเฟร์โรอิเล็กตริกที่สำคัญ กล่าวคือ BT PT PZT PZN PMN PIN PZT-BT PMN-PT PZN-PZT PIN-PT และ PZTBT-PMNT โดยสามารถแบ่งผลงานที่ได้จากโครงการวิจัยนี้ออกเป็น 3 กลุ่มใหญ่ กล่าวคือ 1. กระบวนการเตรียมผงและเซรามิก 2. สมบัติไดอิเล็กตริกและทางไฟฟ้าอื่นๆของสารเซรามิก และ 3. อิทธิพลของความเค้นแบบแกนเดี่ยวต่อสมบัติไดอิเล็กตริกและทางไฟฟ้าอื่นๆของสารเซรามิกทั้งหมดที่กล่าวมาข้างต้น ซึ่งกลุ่มผู้วิจัยได้ประสบความสำเร็จในการเตรียมผงและเซรามิกด้วยการใช้เทคนิคผสมออกไซด์ร่วมกับเทคนิคการบดย่อยละเอียด โดยได้ทราบถึงเงื่อนไขที่เหมาะสมต่อการเตรียมผงให้มีความบริสุทธิ์สูง และพบเงื่อนไขในการเผาที่เหมาะสมต่อการเตรียมเซรามิกแต่ละชนิดที่กล่าวมาเหล่านี้ให้มีความบริสุทธิ์และความหนาแน่นสูง และจากการตรวจสอบคุณลักษณะเฉพาะและคุณสมบัติทางไฟฟ้าต่างๆของเซรามิกที่เตรียมได้ก็พบว่าสารเซรามิกที่เตรียมได้นั้นแสดงคุณลักษณะเฉพาะเป็นสารเซรามิกเฟร์โรอิเล็กตริกแบบปกติ หรือสารเซรามิกเฟร์โรอิเล็กตริกกลุ่มรีแลกเซอร์ หรือสารเซรามิกที่แสดงลักษณะผสมกันระหว่างเซรามิกเฟร์โรอิเล็กตริกแบบปกติและสารเซรามิกเฟร์โรอิเล็กตริก กลุ่มรีแลกเซอร์ ทั้งนี้ขึ้นกับชนิดของสารเซรามิกและอัตราส่วนผสม และจากการศึกษาอิทธิพลของความเค้นแบบแกนเดี่ยวต่อสมบัติไดอิเล็กตริกและทางไฟฟ้าอื่นๆของสารเซรามิกก็พบว่าความเค้นมีผลอย่างชัดเจนในการเปลี่ยนแปลงสมบัติต่างๆในสารเซรามิกทุกระบบ โดยมีทิศทางและอัตราการเปลี่ยนแปลงที่ขึ้นอยู่กับชนิดของสารเซรามิกและอัตราส่วนผสม

# เนื้อหางานวิจัย

ปรากฏการณ์พิโซอิเล็กตริก (piezoelectric effect) เป็นปรากฏการณ์ที่วัสดุสามารถเปลี่ยนพลังงานกลไปเป็นพลังงานไฟฟ้าหรือเปลี่ยนพลังงานไฟฟ้าไปเป็นพลังงานกลในผลึกเชิงเดี่ยว (single crystal compounds) และในสารประเภทเฟร์โรอิเล็กตริก ความเป็นเฟร์โรอิเล็กตริกของวัสดุจะขึ้นอยู่กับสมบัติของหน่วยเซลล์ (unit cell) พื้นฐานของโครงสร้างพื้นฐานของวัสดุจากการแบ่งกลุ่มผลึกเป็น 32 คลาส (class) ตามสมมาตร (symmetry) มี 21 คลาสเป็นประเภทที่ไม่มีศูนย์กลางสมมาตร (non-centrosymmetry) แต่มีเพียง 20 คลาส ที่มีสมบัติพิโซอิเล็กตริก และมี 10 คลาสที่เป็นเฟร์โรอิเล็กตริก

สารเซรามิกเฟร์โรอิเล็กตริกสามารถแบ่งได้เป็น 2 ประเภทใหญ่ๆ จากลักษณะของการเปลี่ยนแปลงเฟสและการตอบสนองต่อความถี่ คือ สารเซรามิกเฟร์โรอิเล็กตริกแบบปกติ (normal ferroelectrics) และสารเซรามิกเฟร์โรอิเล็กตริกกลุ่มรีแลกเซอร์ (relaxor ferroelectrics) ซึ่งในกลุ่มแรกนั้นการเปลี่ยนเฟสจะเกิดขึ้นอย่างรวดเร็ว (sharp transition) บริเวณอุณหภูมิคูรี (Curie temperature: $T_C$) และมีสมบัติไดอิเล็กตริกที่ไม่ค่อยขึ้นกับความถี่ ในขณะที่สารเซรามิกในกลุ่มที่สองนั้นจะเกิดการเปลี่ยนเฟสแบบช้าๆ (diffuse phass transition) และมีสมบัติไดอิเล็กตริกที่เปลี่ยนแปลงกับความถี่อย่างชัดเจน ตัวอย่างสารเซรามิกเฟร์โรอิเล็กตริกแบบปกติที่สำคัญได้แก่ แบเรียมไทเทเนต ($BaTiO_3$) หรือ BT เลดไทเทเนต ($PbTiO_3$) หรือ PT และเลดเซอร์โคเนตไทเทเนต ($Pb(Zr,Ti)O_3$) หรือ PZT ในขณะตัวอย่างของสารเซรามิกเฟร์โรอิเล็กตริกกลุ่มรีแลกเซอร์ ที่สำคัญประกอบด้วย เลดแมกนีเซียมไนโอเบต ($Pb(Mg_{1/3}Nb_{2/3})O_3$) หรือ PMN เลดซิงค์ไนโอเบต ($Pb(Zn_{1/3}Nb_{2/3})O_3$) หรือ PZN และ เลดอินเดียมไนโอเบต ($Pb(In_{1/2}Nb_{1/2})O_3$) หรือ PIN

**1. ที่มาและความสำคัญของปัญหา**

สืบเนื่องจากนโยบายของรัฐบาลที่ต้องการที่จะพัฒนาประเทศให้เป็นศูนย์กลางของภูมิภาคในด้านอุตสาหกรรมอิเล็กทรอนิกส์ อุตสาหกรรมยานยนต์และการแพทย์ รวมทั้งการพัฒนาด้านการเกษตรอันเป็นอาชีพหลักของประชาชนส่วนใหญ่ของประทศให้มีความก้าวหน้าและสามารถเพิ่มผลผลิตให้ได้ตามความต้องการ เพื่อนำประเทศไปสู่การเป็นครัวของโลก ซึ่งการพัฒนาด้านต่างๆเหล่านี้จะเป็นพื้นฐานในการพัฒนาประเทศอย่างยั่งยืนต่อไป อย่างไรก็ตาม เป็นที่ทราบกันดีว่า ในอุตสาหกรรมทุกด้านที่กล่าวมานั้น ช่วงที่ผ่านมาประเทศของเราได้มีการพัฒนาไปได้ค่อนข้างช้าและส่วนใหญ่เป็นไปในลักษณะของการนำชิ้นส่วนเข้ามาจากประเทศผู้ผลิตหลักโดยผู้ประกอบการต่างชาติมาประกอบเป็นอุปกรณ์และขายในประเทศหรือส่งออกไปขายยังประเทศอื่น ซึ่งลักษณะเช่นนี้คงไม่สามารถที่จะทำให้เกิดการพัฒนาประเทศอย่างยั่งยืนได้ ดังนั้นจึงควรต้องมีการพัฒนาอุตสาหกรรมเหล่านั้นขึ้นมาในประเทศโดยให้มีลักษณะแบบครบวงจร ถึงกระนั้น ในความเป็นจริงแล้วในอุตสาหกรรมบางประเภท ยกตัวอย่างเช่น อุตสาหกรรมทางด้านชิ้นส่วนอิเล็กทรอนิกส์ เช่น ตัวต้านทานและตัวเก็บประจุที่ใช้ทั่วไปในวงจรไฟฟ้าและ

อิเล็กทรอนิกส์นั้น การแข่งขันค่อนข้างสูงและโอกาสค่อนข้างต่ำที่ประเทศของเราจะประสพความสำเร็จในตลาดโลก ในขณะที่อุตสาหกรรมที่เน้นตลาดเฉพาะทางนั้นยังมีโอกาสที่เปิดกว้าง (niche market) ยกตัวอย่างเช่น ตัวเก็บประจุไฟฟ้าและตัวต้านทานที่ใช้ในวงจรควบคุมในรถยนต์ เทอร์มิสเตอร์ที่ใช้ควบคุมอุณหภูมิในรถยนต์ เซนเซอร์ที่สามารถใช้ตรวจวัดความชื้นในอาหารหรือผลไม้ หรือเซนเซอร์ที่ใช้ควบคุมการเผาไหม้ของเชื้อเพลิงในรถยนต์ แอกทัวเอเทอร์ที่ใช้ในการผลิตทางอุปกรณ์อิเล็กทรอนิกส์ที่ต้องการความละเอียดสูง ทรานสดิวเซอร์ที่สามารถใช้ในการตรวจหาฝูงปลาในทะเลและในอุปกรณ์ตรวจสอบตำหนิหรือรอยร้าวในวัสดุแบบไม่ทำลาย หม้อแปลงไฟฟ้า บัซเซอร์ในลำโพง ตัวบังคับการสั่นของหัวเข็มในเครื่องมือขูดหินปูน อุปกรณ์ทำความสะอาดเครื่องมือทางการแพทย์ด้วยอัลตร้าโซนิกส์ หัวตรวจวัดอัลตร้าซาวด์ หัวตรวจวัดความดันโลหิต และหุ่นยนต์ขนาดจิ๋วสำหรับใช้ในการตรวจอวัยวะภายในแบบไร้สาย เป็นต้น

วัสดุที่เป็นพื้นฐานในการผลิตอุปกรณ์ที่กล่าวมาทั้งหมดนั้นคือสารเซรามิกเฟร์โรอิเล็กตริก (ferroelectrics) เช่น แบเรียมไทเทเนต ($BaTiO_3$) หรือ BT เลดไทเทเนต ($PbTiO_3$) หรือ PT เลดเซอร์โคเนตไทเทเนต ($Pb(Zr,Ti)O_3$) หรือ PZT เลดซิงค์ไนโอเบต ($Pb(Zn_{1/3}Nb_{2/3})O_3$) หรือ PZN เลดแมกนีเซียมไนโอเบต ($Pb(Mg_{1/3}Nb_{2/3})O_3$) หรือ PMN และ เลดอินเดียมไนโอเบต ($Pb(In_{1/2}Nb_{1/2})O_3$) หรือ PIN ล้วนแล้วแต่เป็นสารที่ถูกพัฒนาขึ้นมาเพื่อใช้ประโยชน์ในอุปกรณ์อิเล็กทรอนิกส์ประเภทต่างๆ ที่กล่าวมาข้างต้น [1-9] ซึ่งโดยหลักการพื้นฐานแล้ววัสดุที่มีศักยภาพเหมาะสมสำหรับการนำมาประยุกต์ใช้ในงานต่างๆเหล่านี้นั้น จะต้องมีคุณลักษณะที่สำคัญอันได้แก่ การมีค่าสภาพยอมสัมพัทธ์ที่เหมาะสม ในช่วงของอุณหภูมิและความถี่สำหรับการทำงานของอุปกรณ์ มีค่าสัมประสิทธิ์ไพฟ้าเชิงกลคู่ควบสูง สามารถทำการจัดเรียงไดโพลภายในเนื้อสารได้ง่าย มีการสูญเสียของพลังงานในระหว่างการใช้งานที่ต่ำ มีอายุการใช้งานนาน และที่สำคัญต้องสามารถทำการเตรียมได้ง่าย โดยมีค่าใช้จ่ายไม่มากและปลอดภัย สามารถหาวัตถุดิบได้ง่าย และต้องการอุณหภูมิเผาที่ไม่สูงมากนัก เป็นต้น [1-9] ซึ่งโดยทั่วไปแล้วนั้น การผสมผสานของคุณสมบัติที่ดีต่างๆเหล่านี้ไม่สามารถพบได้ในวัสดุเดี่ยวๆตัวใดตัวหนึ่งที่กล่าวมาในข้างต้นได้ เนื่องจากวัสดุแต่ละชนิดต่างก็มีข้อดีและข้อเสียที่แตกต่างกันไปในลักษณะที่มีความเฉพาะตัวมาก ดังนั้นการศึกษาวิจัยเพื่อค้นหาวัสดุชนิดใหม่ๆ ที่อาศัยหลักการนำเอาวัสดุหลักๆที่มีอยู่เดิมมารวมเข้าด้วยกัน ที่สามารถจะผสมผสานข้อดีและช่วยบรรเทาข้อเสียของแต่ละวัสดุที่เป็นองค์ประกอบหลักได้อย่างลงตัว จึงเป็นวิธีการหนึ่งที่ได้รับความสนใจอย่างมากทั้งในแวดวงวิชาการและในวงการอุตสาหกรรม ทำให้ในปัจจุบันมีสารเซรามิกเฟร์โรอิเล็กตริกชนิดใหม่ๆที่มีความสลับซับซ้อนยิ่งขึ้นจำนวนมากเกิดขึ้นมาเช่น BT-PT, BT-PZT, PZT-PZN, PMN-PT, PMN-PZN, PMN-PZT, PIN-PT, PIN-PMN, PIN-PZN, BT-PMN-PZN, PT-PMN-PZN, PMN-PT-BT, PZT-PZN-PMN และ PMN-PT-PIN เป็นต้น [1-3,10-20] และงานวิจัยทางด้านนี้ส่วนใหญ่เน้นถึงการศึกษาถึงอิทธิพลของปัจจัยหลักในกระบวนการผลิตที่มีต่อพฤติกรรมการเกิดเฟส โครงสร้างจุลภาคและสมบัติไดอิเล็กตริกและสมบัติไพฟ้าเชิงกลของสารเซรามิกที่ผลิตขึ้น [10-24]

อย่างไรก็ตามโดยทั่วไปแล้ว ในสภาวะการใช้งานจริงของอุปกรณ์อิเล็กทรอนิกส์ที่ผลิตจากสารเซรามิกเฟร์โรอิเล็กตริกดังที่กล่าวมาแล้วนั้น สารเซรามิกมักจะอยู่สภาวะภายใต้ความเค้น ซึ่งอาจจะเกิดจากความเค้นเชิงกลภายนอกระหว่างการใช้งาน เช่น แอกทัวเอเทอร์และทรานสดิวเซอร์ เป็นต้น หรือความเค้นเชิงกลภายในอันเกิดจากการที่สารเซรามิกเหล่านี้ซึ่งมีสมบัติพิโซอิเล็กตริกจะเกิดการเปลี่ยนแปลงรูปร่างภายใต้อิทธิพลของสนามไฟฟ้าซึ่งส่งผลให้เกิดความเค้นกระทำต่อสารเซรามิก เช่น ตัวเก็บประจุไฟฟ้า เทอร์มิสเตอร์ เซนเซอร์ หม้อแปลงไฟฟ้า และหัวตรวจวัดอัลตร้าซาวด์ เป็นต้น ดังนั้นข้อมูลเกี่ยวกับสมบัติต่างๆ เช่น สมบัติไดอิเล็กตริกและสมบัติไฟฟ้าเชิงกล ภายใต้อิทธิพลของความเค้น จึงมีความสำคัญอย่างมากต่อการออกแบบ การจัดสร้างและการใช้งานของอุปกรณ์อิเล็กทรอนิกส์ที่ผลิตจากสารเซรามิกเฟร์โรอิเล็กตริกเหล่านี้ ซึ่งการศึกษาเหล่านี้นอกจากจะช่วยเสริมข้อมูลที่จำเป็นในการพัฒนาและการนำไปประยุกต์ใช้ของสารเซรามิกเฟร์โรอิเล็กตริกแล้ว ยังสามารถเสริมองค์ความรู้พื้นฐานในเรื่องโครงสร้างของโดเมน (domain structure) และการเคลื่อนที่ของโดเมน (domain motion) [25,26] ซึ่งเป็นกลไกที่สำคัญที่มีอิทธิพลต่อสมบัติไดอิเล็กตริกและสมบัติไฟฟ้าเชิงกลในสารเซรามิกเฟร์โรอิเล็กตริก ส่งผลให้ในช่วงที่ผ่านมาได้เริ่มมีการศึกษาถึงอิทธิพลของความเค้นต่อสมบัติทางไดอิเล็กตริกและไฟฟ้าเชิงกลของสารเซรามิกในระบบต่างๆ เช่น PZT PMN-PT และ PMN-PZT เป็นต้น แต่ยังคงอยู่ในวงที่จำกัดเมื่อเปรียบเทียบกับจำนวนของสารเซรามิกเฟร์โรอิเล็กตริกใหม่ๆที่ได้รับการพัฒนาขึ้นมา ทำให้งานวิจัยที่เป็นระบบในประเด็นของอิทธิพลของความเค้นต่อสมบัติต่างๆของสารเซรามิกเฟร์โรอิเล็กตริกที่สำคัญที่ปรากฏในวารสารงานวิจัยในระดับนานาชาติยังมีจำนวนที่ค่อนข้างน้อย [20,25-33]

ด้วยเหตุผลดังกล่าวมาข้างต้น ดังนั้นทางผู้วิจัยจึงได้เกิดแนวคิดที่จะทำการศึกษาอย่างเป็นระบบถึงอิทธิพลของความเค้นต่อสมบัติทางไฟฟ้าของสารเซรามิกเฟร์โรอิเล็กตริกที่สำคัญกล่าวคือ สารเซรามิกเฟร์โรอิเล็กตริกระบบเดี่ยว เช่น BT PT PZT PZN PMN PIN เป็นต้น สารเซรามิกเฟร์โรอิเล็กตริกระบบคู่ที่สำคัญที่เกิดจากการผสมสารในระบบเดี่ยว เช่น PZT-BT PMN-PT PZN-PZT PIN-PT เป็นต้น และ สารเซรามิกเฟร์โรอิเล็กตริกที่มีความซับซ้อนมากและไม่เป็นที่ปรากฏมาก่อน คือ PZTBT-PMNT โดยในเบื้องต้นโครงการวิจัยนี้จะมุ่งเน้นความสำคัญไปที่การศึกษาถึงสมบัติไดอิเล็กตริกของสารเหล่านี้ภายใต้อิทธิพลของความเค้นแบบแกนเดี่ยว ซึ่งการศึกษานี้มีความสำคัญในแง่ของการสร้างองค์ความรู้พื้นฐานใหม่ที่จำเป็นสำหรับการทำความเข้าใจในธรรมชาติของสมบัติไดอิเล็กตริกของสารเซรามิกเฟร์โรอิเล็กตริกระบบเดี่ยวภายใต้ความเค้น และอิทธิพลของสมบัติดังกล่าวของแต่ละองค์ประกอบต่อสมบัติไดอิเล็กตริกของสารเซรามิกในระบบที่มีความซับซ้อนมากขึ้น เพื่อเป็นแนวทางในการนำองค์ความรู้ที่ได้รับจากการวิจัยนี้ไปใช้ในภาคปฏิบัติเพื่อพัฒนาการออกแบบ การจัดสร้างและการใช้งานของอุปกรณ์อิเล็กทรอนิกส์ที่ผลิตจากสารเซรามิกเฟร์โรอิเล็กตริกเหล่านี้ให้มีประสิทธิภาพสูงขึ้น นอกจากนี้แล้ว โครงการวิจัยนี้ยังเป็นการสร้างผลงานวิจัยแบบต่อเนื่องซึ่งมุ่งเน้นการใช้องค์ความรู้ที่ได้รับจากโครงการวิจัยจากทุนส่งเสริมนักวิจัยรุ่นใหม่ของผู้วิจัยซึ่งได้ทำการศึกษาเกี่ยวกับอิทธิพลของความเค้นแบบ

แกนเดี่ยวต่อสมบัติไดอิเล็กตริกและไฟฟ้าเชิงกลของสารเซรามิกในระบบ PMN-PZT มาประยุกต์ใช้ ซึ่งโครงการดังกล่าวได้รับความสำเร็จเป็นอย่างดีและได้รับความสนใจและยอมรับโดยสามารถตีพิมพ์ผลงานทั้งในระดับชาติและนานาชาติ [20,36-40] และโครงการวิจัยนี้ยังเป็นการส่งเสริมให้เกิดการเชื่อมโยงด้านการวิจัยระหว่างนักวิจัยในประเทศโดยการนำผลการวิจัยจากนักวิจัยที่ได้รับทุนพัฒนานักวิจัยมาใช้ประโยชน์ [24,35] ซึ่งโครงการดังกล่าวนั้นได้มุ่งเน้นไปที่การการศึกษาถึงอิทธิพลของปัจจัยหลักในกระบวนการผลิตที่มีต่อพฤติกรรมการเกิดเฟสโครงสร้างจุลภาคและสมบัติไดอิเล็กตริกของสารเซรามิกในระบบ PZBT-PMNT โดยได้ศึกษารายละเอียดของสารเซรามิกเฟร์โรอิเล็กตริกระบบเดี่ยว BT PT PZT PZN PMN สารเซรามิกเฟร์โรอิเล็กตริกระบบคู่ PZT-BT PMN-PT และสารเซรามิกเฟร์โรอิเล็กตริกที่มีความซับซ้อนมาก PZTBT-PMNT ซึ่งผลการศึกษาเหล่านี้สามารถนำมาใช้โดยตรงในการเลือกเงื่อนไขที่เหมาะสมในการเตรียมสารเซรามิกที่มีความบริสุทธิ์และความหนาแน่นสูง รวมทั้งสมบัติไดอิเล็กตริกที่ดีมาใช้ในการศึกษาในโครงการวิจัยนี้ต่อไป นอกจากนี้โดยอาศัยความรู้เบื้องต้นจากระบบพื้นฐาน PT และ PZT ที่ศึกษามาก่อน ผู้วิจัยยังจะได้ขยายขอบเขตของงานวิจัยไปศึกษาสารเซรามิกเฟร์โรอิเล็กตริกระบบเดี่ยว PIN และ PZN รวมทั้งสารเซรามิกเฟร์โรอิเล็กตริกระบบคู่ PIN-PT และ PZN-PZTที่มีความสำคัญมากและในช่วง 5 ปีที่ผ่านมานี้ได้รับความสนใจอย่างแพร่หลายเนื่องจากมีสมบัติไดอิเล็กตริก สมบัติพิโซอิเล็กตริกและสมบัติเฟร์โรอิเล็กตริกที่โดดเด่นมากและกำลังได้รับการพัฒนาทางการค้าอย่างจริงจัง [8,9,14,15,17,41-43] จะเห็นได้ว่าโครงการวิจัยนี้นอกจากจะให้องค์ความรู้ที่สามารถนำไปใช้ในภาคปฏิบัติแล้ว ยังจะนำไปสู่ความรู้ความเข้าใจพื้นฐานใหม่ๆเกี่ยวกับสารเซรามิกเฟร์โรอิเล็กตริกที่สำคัญอันจะเป็นพื้นฐานในการพัฒนาประเทศและผลงานที่ได้ยังสามารถที่จะตีพิมพ์ในวารสารวิชาการระดับนานาชาติได้

**2. วัตถุประสงค์ของการวิจัย**

1. เพื่อศึกษากระบวนการเตรียมสารเซรามิกในระบบ BT PT PZT PZN PMN PIN PZT-BT PMN-PT PZN-PZT PIN-PT และ PBZT-PMNT
2. เพื่อศึกษาอิทธิพลของความเค้นแบบแกนเดี่ยวต่อสมบัติไดอิเล็กตริกของสารเซรามิก ระบบเดี่ยว BT PT PZT PZN PMN และ PIN
3. เพื่อศึกษาอิทธิพลของความเค้นแบบแกนเดี่ยวต่อสมบัติไดอิเล็กตริกของสารเซรามิก ระบบคู่ PZT-BT PMN-PT PZN-PZT และ PIN-PT
4. เพื่อศึกษาอิทธิพลของความเค้นแบบแกนเดี่ยวต่อสมบัติไดอิเล็กตริกของสารเซรามิกระบบ PBZT-PMNT
5. เพื่อศึกษาความสัมพันธ์ระหว่างสมบัติไดอิเล็กตริกภายใต้ความเค้นแบบแกนเดี่ยวของแต่ละองค์ประกอบและสมบัติดังกล่าวของสารเซรามิกระบบคู่
6. เพื่อศึกษาความสัมพันธ์ระหว่างสมบัติไดอิเล็กตริกภายใต้ความเค้นแบบแกนเดี่ยวของแต่ละองค์ประกอบและสมบัติดังกล่าวของสารเซรามิกระบบ PBZT-PMNT

**3. ระเบียบวิธีวิจัย**

ขั้นตอนการวิจัยในโครงการนี้ถูกแบ่งออกเป็น 3 ส่วนหลัก คือ 1) การศึกษาอิทธิพลอิทธิพลของความเค้นแบบแกนเดี่ยวต่อสมบัติไดอิเล็กตริกของสารเซรามิกระบบเดี่ยว BT PT PZT และ PMN สารเซรามิกระบบคู่ PZT-BT และ PMN-PT และสารเซรามิกระบบ PBZT-PMNT โดยใช้องค์ความรู้พื้นฐานในส่วนของเงื่อนไขในการเตรียมสารเซรามิกที่มีความบริสุทธิ์และความหนาแน่นสูงที่ได้จากการศึกษาอย่างละเอียดในโครงการวิจัยที่ได้รับทุนพัฒนานักวิจัยของรองศาสตราจารย์ ดร. สุพล อนันตา 2) การศึกษาการเตรียมเซรามิกในระบบ PZN PIN PZN-PZT และ PIN-PT ด้วยการใช้เทคนิคผสมออกไซด์ และ 3) การศึกษาอิทธิพลอิทธิพลของความเค้นแบบแกนเดี่ยวต่อสมบัติไดอิเล็กตริกของสารเซรามิกระบบเดี่ยว PZN และ PIN และสารเซรามิกระบบคู่ PZN-PZT และ PIN-PT ที่เตรียมขึ้นได้

ดังนั้นเพื่อให้เกิดความต่อเนื่องของการดำเนินการวิจัยที่สอดคล้องกับโครงการวิจัยทุนพัฒนานักวิจัยของรองศาสตราจารย์ ดร. สุพล อนันตา จึงต้องมีการวางแผนงานการวิจัยโดยมีรายละเอียดของระเบียบวิธีวิจัยดังนี้

**ปีที่ 1**

1. ศึกษาค้นคว้ารวบรวมข้อมูลจากผลงานวิจัยและเอกสารทางวิชาการที่เกี่ยวข้อง
2. ทำการติดตั้งและตรวจสอบเครื่องมืออัดแรงแบบแกนเดี่ยวเพื่อใช้ในการวัดสมบัติไดอิเล็กตริกของสารเซรามิกภายใต้ความเค้นแบบแกนเดี่ยว โดยชุดเครื่องมือดังกล่าวได้รับการพัฒนาและทดสอบแล้วจากโครงการวิจัยทุนส่งเสริมนักวิจัยรุ่นใหม่ (2545) และทำการติดตั้งและตรวจสอบอุปกรณ์อื่นๆที่จะใช้งานให้มีความพร้อม
3. เตรียมผงและเซรามิกในระบบ $BaTiO_3$ (BT) และ $Pb(Zr_{0.52}Ti_{0.48})O_3$ ด้วยการใช้เทคนิคผสมออกไซด์
4. ทำการตรวจสอบคุณลักษณะเฉพาะและคุณสมบัติของเซรามิกที่เตรียมได้
5. ทดสอบอิทธิพลของความเค้นแบบแกนเดี่ยวต่อสมบัติไดอิเล็กตริก (ค่าคงที่ไดอิเล็กตริก ($\varepsilon_r$) และการสูญเสียทางไดอิเล็กตริก ($\tan\delta$)) ของสารเซรามิกระบบเดี่ยว BT และ PZT ด้วยเครื่องมืออัดแรงแบบแกนเดี่ยว
6. เตรียมผงและเซรามิกในระบบ $PbTiO_3$ (PT) และ $Pb(Mg_{1/3}Nb_{2/3})O_3$ (PMN) ด้วยการใช้เทคนิคผสมออกไซด์
7. ทำการตรวจสอบคุณลักษณะเฉพาะและคุณสมบัติของเซรามิกที่เตรียมได้

8. ทดสอบอิทธิพลของความเค้นแบบแกนเดี่ยวต่อสมบัติไดอิเล็กตริก (ค่าคงที่ไดอิเล็กตริก ($\varepsilon_r$) และการสูญเสียทางไดอิเล็กตริก (tan $\delta$)) ของสารเซรามิกระบบเดี่ยว PT และ PMN ด้วยเครื่องมืออัดแรงแบบแกนเดี่ยว
9. อภิปรายผลการศึกษาและสรุปผลการวิจัย ตลอดจนข้อเสนอแนะในรูปแบบการเขียนรายงานความก้าวหน้า และการเตรียมผลงานเพื่อการตีพิมพ์

**ปีที่ 2**

10. เตรียมผงและเซรามิกในระบบ (1-x)PZT-xBT และ (1-x)PMN-xPT เมื่อ x มีค่าเป็น 0.1, 0.2, 0.3, 0.4, 0.5, 0.6, 0.7, 0.8 และ 0.9 ด้วยเทคนิคมิกซ์ออกไซด์โดยใช้สารที่เตรียมได้จาก ข้อ 8.3 และ 8.6 ที่มีความบริสุทธิ์สูงเป็นสารตั้งต้น
11. ทำการตรวจสอบคุณลักษณะเฉพาะและคุณสมบัติของเซรามิกที่เตรียมได้
12. ทดสอบอิทธิพลของความเค้นแบบแกนเดี่ยวต่อสมบัติไดอิเล็กตริก (ค่าคงที่ไดอิเล็กตริก ($\varepsilon_r$) และการสูญเสียทางไดอิเล็กตริก (tan $\delta$)) ของสารเซรามิกระบบคู่ PZT-BT และ PMN-PT ด้วยเครื่องมืออัดแรงแบบแกนเดี่ยว
13. สรุปความสัมพันธ์ระหว่างสมบัติไดอิเล็กตริกภายใต้ความเค้นแบบแกนเดี่ยวของ BT PZT PT และ PMN และสมบัติดังกล่าวของสารเซรามิกระบบ PZT-BT และ PMN-PT
14. ศึกษาการเตรียมผงและเซรามิกในระบบ $Pb(Zn_{1/3}Nb_{2/3})O_3$ (PZN) และ $Pb(In_{1/2}Nb_{1/2})O_3$ (PIN) ด้วยการใช้เทคนิคผสมออกไซด์ โดยศึกษาหาเงื่อนไขที่เหมาะสมต่อการเตรียมผงให้มีความบริสุทธิ์สูง และศึกษาหาเงื่อนไขในการเผาที่เหมาะสมต่อการเตรียมเซรามิกเหล่านี้ให้มีความบริสุทธิ์และความหนาแน่นสูง
15. ทำการตรวจสอบคุณลักษณะเฉพาะและคุณสมบัติของเซรามิกที่เตรียมได้
16. เตรียมเซรามิกในระบบ PZBT-PMNT ด้วยเทคนิคมิกซ์ออกไซด์โดยใช้สารที่เตรียมได้จาก ข้อ 8.10 ที่มีความบริสุทธิ์สูงเป็นสารตั้งต้น
17. ทำการตรวจสอบคุณลักษณะเฉพาะและคุณสมบัติของเซรามิกที่เตรียมได้
18. ทดสอบอิทธิพลของความเค้นแบบแกนเดี่ยวต่อสมบัติไดอิเล็กตริก (ค่าคงที่ไดอิเล็กตริก ($\varepsilon_r$) และการสูญเสียทางไดอิเล็กตริก (tan $\delta$)) ของสารเซรามิกระบบ PZBT-PMNT ด้วยเครื่องมืออัดแรงแบบแกนเดี่ยว

19. สรุปความสัมพันธ์ระหว่างสมบัติไดอิเล็กตริกภายใต้ความเค้นแบบแกนเดี่ยวของ PZBT และ PMNT และสมบัติดังกล่าวของสารเซรามิกระบบ PZBT-PMNT
20. อภิปรายผลการศึกษาและสรุปผลการวิจัย ตลอดจนข้อเสนอแนะในรูปแบบการเขียนรายงานความก้าวหน้า และการเตรียมผลงานเพื่อการตีพิมพ์

**ปีที่ 3**

21. ทดสอบอิทธิพลของความเค้นแบบแกนเดี่ยวต่อสมบัติไดอิเล็กตริก (ค่าคงที่ไดอิเล็กตริก ($\varepsilon_r$) และการสูญเสียทางไดอิเล็กตริก (tan $\delta$)) ของสารเซรามิกระบบเดี่ยว PZN และ PIN ด้วยเครื่องมืออัดแรงแบบแกนเดี่ยว
22. ศึกษาการเตรียมผงและเซรามิกในระบบ (1-x)PZN-xPZT และ (1-x)PIN-xPT เมื่อ x มีค่าเป็น 0.1, 0.2, 0.3, 0.4, 0.5, 0.6, 0.7, 0.8 และ 0.9 ด้วยเทคนิคมิกซ์ออกไซด์ โดยใช้สารที่เตรียมได้จาก ข้อ 8.14 ที่มีความบริสุทธิ์สูงเป็นสารตั้งต้น ด้วยการใช้เทคนิคผสมออกไซด์ โดยศึกษาหาเงื่อนไขที่เหมาะสมต่อการเตรียมผงให้มีความบริสุทธิ์สูง และศึกษาหาเงื่อนไขในการเผาที่เหมาะสมต่อการเตรียมเซรามิกเหล่านี้ให้มีความบริสุทธิ์และความหนาแน่นสูง
23. ทำการตรวจสอบคุณลักษณะเฉพาะและคุณสมบัติของเซรามิกที่เตรียมได้
24. ทดสอบอิทธิพลของความเค้นแบบแกนเดี่ยวต่อสมบัติไดอิเล็กตริก (ค่าคงที่ไดอิเล็กตริก ($\varepsilon_r$) และการสูญเสียทางไดอิเล็กตริก (tan $\delta$)) ของสารเซรามิกระบบ PZN-PZT และ PIN-PT ด้วยเครื่องมืออัดแรงแบบแกนเดี่ยว
25. สรุปความสัมพันธ์ระหว่างสมบัติไดอิเล็กตริกภายใต้ความเค้นแบบแกนเดี่ยวของ PT PZT PZN และ PIN และสมบัติดังกล่าวของสารเซรามิกระบบ PZN-PZT และ PIN-PT
26. อภิปรายผลการศึกษาและสรุปผลการวิจัย ตลอดจนข้อเสนอแนะในรูปแบบการเขียนรายงานฉบับสมบูรณ์ และการเตรียมผลงานเพื่อการตีพิมพ์

**4. ประโยชน์ที่ได้รับจากโครงการวิจัยนี้**

1. องค์ความรู้ใหม่ในเรื่องกระบวนการเตรียมเซรามิกในระบบ BT PT PZT PZN PMN PIN PZT-BT PMN-PT PZN-PZT PIN-PT และ PBZT-PMNT
2. องค์ความรู้ใหม่ในเรื่องของอิทธิพลของความเค้นแบบแกนเดี่ยวต่อสมบัติไดอิเล็กตริกของสารเซรามิกระบบเดี่ยว BT PT PZT PZN PMN และ PIN
3. องค์ความรู้ใหม่ในเรื่องของอิทธิพลของความเค้นแบบแกนเดี่ยวต่อสมบัติไดอิเล็กตริกของสารเซรามิกระบบคู่ PZT-BT PMN-PT PZN-PZT และ PIN-PT
4. ความรู้ความเข้าใจถึงความสัมพันธ์ระหว่างสมบัติไดอิเล็กตริกภายใต้ความเค้นแบบแกนเดี่ยวของแต่ละองค์ประกอบและสมบัติดังกล่าวของสารเซรามิกระบบคู่
5. องค์ความรู้ใหม่ในเรื่องของอิทธิพลของความเค้นแบบแกนเดี่ยวต่อสมบัติไดอิเล็กตริกของสารเซรามิกระบบ PBZT-PMNT
6. ความรู้ความเข้าใจถึงความสัมพันธ์ระหว่างสมบัติไดอิเล็กตริกภายใต้ความเค้นแบบแกนเดี่ยวของ PZT-BT และ PMN-PTและสมบัติดังกล่าวของสารเซรามิกระบบ PBZT-PMNT
7. ผลงานวิจัยในรูปของสิ่งตีพิมพ์ ได้แก่สิ่งตีพิมพ์ในวารสารทางวิชาการต่างๆ การนำเสนอผลงานในการประชุมวิชาการและสัมมนา หรือหนังสือตำราวิชาการเฉพาะด้าน กล่าวคือ ตำราเรื่อง สมบัติทางไฟฟ้าของเซรามิกเฟร์โรอิเล็กทริก
8. องค์ความรู้ใหม่ที่จะนำไปใช้ประกอบการเรียนการสอนและการปรับปรุงกระบวนวิชาในหลักสูตรวัสดุศาสตร์ทั้งในระดับปริญญาตรีและระดับบัณฑิตศึกษาที่ผู้วิจัยรับผิดชอบอยู่ต่อไป
9. นักวิจัยรุ่นใหม่และรุ่นกลางที่มีความรู้ทางด้านสารเซรามิกเฟร์โรอิเล็กตริกกลุ่มเพอรอพสไกต์และแนวทางในการกำหนดหัวข้อวิทยานิพนธ์สำหรับการพัฒนาบุคลากรทางด้านวัสดุศาสตร์ที่เกี่ยวข้องทั้งในระดับปริญญาโท และเอก สาขาวัสดุศาสตร์อย่างต่อเนื่อง
10. แนวทางการพัฒนาชุดโครงการวิจัยและการสร้างความร่วมมือของกลุ่มนักวิจัยภายในสถาบันต้นสังกัดและระหว่างกลุ่มวิจัยต่างๆที่สนใจในเรื่องที่เกี่ยวข้องกันทั้งในและต่างประเทศ

**5. สรุปผลที่ได้จากโครงการวิจัยนี้**

โดยสรุปแล้วสามารถแบ่งองค์ความรู้ใหม่ที่ได้จากโครงการวิจัยนี้ออกเป็น 3 กลุ่มใหญ่ กล่าวคือ

1. องค์ความรู้ใหม่ในเรื่องกระบวนการเตรียมผงและเซรามิกในระบบ BT PT PZT PZN PMN PIN PZT-BT PMN-PT PZN-PZT PIN-PT และ PBZT-PMNT
2. องค์ความรู้ใหม่ในเรื่องของสมบัติไดอิเล็กตริกและทางไฟฟ้าอื่นๆของสารเซรามิก ในระบบ BT PT PZT PZN PMN PIN PZT-BT PMN-PT PZN-PZT PIN-PT และ PBZT-PMNT
3. องค์ความรู้ใหม่ในเรื่องของอิทธิพลของความเค้นแบบแกนเดี่ยวต่อสมบัติไดอิเล็กตริกและทางไฟฟ้าอื่นๆของสารเซรามิกในระบบ BT PT PZT PZN PMN PIN PZT-BT PMN-PT PZN-PZT PIN-PT และ PBZT-PMNT

ซึ่งผลงานที่ได้ใน 3 กลุ่มในเบื้องต้นนั้น ถือเป็นผลงานที่เกี่ยวข้อง*โดยตรง*กับโครงการวิจัยนี้ ดังจะได้กล่าวถึงในรายละเอียดต่อไป

**ส่วนที่ 1:** สำหรับองค์ความรู้ใหม่ในเรื่องกระบวนการเตรียมผงและเซรามิกในระบบ BT PT PZT PZN PMN PIN PZT-BT PMN-PT PZN-PZT PIN-PT และ PBZT-PMNT นั้น กลุ่มผู้วิจัยได้ประสบความสำเร็จในการเตรียมผงและเซรามิกในระบบ $BaTiO_3$(BT) $Pb(Zr_{0.52}Ti_{0.48})O_3$ $PbTiO_3$(PT) $Pb(Mg_{1/3}Nb_{2/3})O_3$(PMN) $Pb(Zn_{1/3}Nb_{2/3})O_3$(PZN) และ $Pb(In_{1/2}Nb_{1/2})O_3$(PIN) ด้วยการใช้เทคนิคผสมออกไซด์ โดยศึกษาหาเงื่อนไขที่เหมาะสมต่อการเตรียมผงให้มีความบริสุทธิ์สูง และศึกษาหาเงื่อนไขในการเผาที่เหมาะสมต่อการเตรียมเซรามิก เหล่านี้ให้มีความบริสุทธิ์และความหนาแน่นสูง นอกจากนี้ก็ได้เตรียมผงและเซรามิกในระบบ (1-x)PZT-xBT (1-x)PMN-xPT (1-x)PZN-xPZT และ (1-x)PIN-xPT เมื่อ x มีค่าเป็น 0.1, 0.2, 0.3, 0.4, 0.5, 0.6, 0.7, 0.8 และ 0.9 และทำการเตรียมเซรามิกในระบบ PZBT-PMNT ด้วยการใช้เทคนิคผสมออกไซด์เช่นกัน ผลงานที่ได้รับนั้นได้ถูกนำไปตีพิมพ์ในวารสารทางวิชาการต่างๆ ดังต่อไปนี้ (ทั้งนี้ รายละเอียดได้ถูกนำเสนอในแต่ละผลงานแล้ว)

1. R. Wongmaneerung, **R. Yimnirun** and S. Ananta, “Effects of Vibro-Milling Time on Phase Formation and Particle Size of Lead Titanate Nanopowders”, *Materials Letters,* 60(12), pp 1447-1452 (2006).
2. R. Wongmaneerung, T. Sarnkonsri, **R. Yimnirun** and S. Ananta “Effects of milling method and calcination condition on phase and morphology characteristics of $Mg_4Nb_2O_9$ powders”, *Materials Science and Engineering B*, 130(1-3), pp 246-253 (2006).

3. R. Wongmaneerung, **R. Yimnirun** and S. Ananta, “Effects of Milling Time and Calcination Condition on Phase Formation and Particle Size of Lead Titanate Nanopowders Prepared by Vibro-milling”, *Materials Letters*, 60, pp 2666-2671 (2006)
4. R. Wongmaneerung, T. Sarnkonsri, **R. Yimnirun** and S. Ananta “Effects of magnesium niobate precursor and calcination condition on phase formation and morphology of lead magnesium niobate powders”, *Materials Science and Engineering B,* 132, pp 292-299 (2006).
5. A. Ngamjarurojana, O. Khamman, **R. Yimnirun** and S. Ananta, “Effect of Calcination Conditions on Phase Formation and Particle Size of Zinc Niobate Powders Synthesized by Solid-State Reaction”, *Materials Letters*, 60, pp 2867-2872 (2006).
6. S. Wongsaenmai, **R. Yimnirun** and S. Ananta, “Effects of Calcination Conditions on Phase Formation and Particle Size of Indium Niobate Powders Synthesized by the Solid-State Reaction”, *Materials Letters* (2007) *in press.*
7. O. Khamman, **R. Yimnirun** and S. Ananta,”Effect of Vibro-Milling Time on Phase Formation and Particle Size of Lead Zirconate Nanopowders” *Materials Letters* (2007) *in press.*
8. A. Prasatkhetragarn, **R. Yimnirun** and S. Ananta, “Effect of calcination conditions on phase formation and particle size of $Zn_3Nb_2O_8$ powders synthesized by solid-state reaction”, *Materials Letters* (2007) *in press*
9. S. Wongsaenmai, **R. Yimnirun** and S. Ananta, “Influence of Calcination Conditions on Phase Formation and Particle Size of Indium Niobate Powders Synthesized by the Solid-State Reaction”, *Journal of Materials Science* (2007) *in press*
10. W. Chaisan, O. Khamman, **R. Yimnirun** and S. Ananta,, “Effects of Calcination Conditions on Phase and Morphology Evolution of Lead Zirconate Powders Synthesized by Solid-State Reaction”, *Journal of Materials Science* (2007) *in press*
11. Orawan Khamman, Rewadee Wongmaneerung, Wanwilai Chaisan, **Rattikorn Yimnirun** and Supon Ananta, “Potential of Vibro-Milling Technique for Preparation of Electroceramic Nanopowders” *Journal of Alloys and Compounds* (2007) *in press.*

12. Athipong Ngamjarurojana, Orawan Khamman, Supon Ananta, and **Rattikorn Yimnirun**, “Synthesis and Characterizations of Lead Zinc Niobate-Lead Zirconate Titanate Powders” *Journal of Electroceramics* (2007) *accepted.*
13. Supattra Wongsaenmai, Orawan Khamman, Supon Ananta, and **Rattikorn Yimnirun**, “Synthesis and Characterizations of Lead Indium Niobate-Lead Titanate Powders” *Journal of Electroceramics* (2007) *accepted.*
14. Rewadee Wongmaneerung, Orawan Khamman, **Rattikorn Yimnirun**, and Supon Ananta, “Synthesis and Characterizations of Lead Titanate Powders” *Journal of Electroceramics* (2007) *accepted.*
15. O. Khamman, **R. Yimnirun** and S. Ananta,”Effect of Vibro-Milling Time and Calcination n Phase Formation and Particle Size of Lead Zirconate Nanopowders” *Ferroelectrics (2007) accepted*
16. A. Prasatkhetragarn, **R. Yimnirun** and S. Ananta, “Effects of Calcination Conditions on Phase Formation of Zirconium Titanate Powders Synthesized by the Solid-State Reaction”, *Ferroelectrics* (2007) *accepted*
17. W. Chaisan, A. Prasatkhetragarn**, R. Yimnirun**, S. Ananta, *“*Two-Stage Solid-State Reaction of Lead Zirconate Titanate Powders” *Ferroelectrics (2007) accepted*
18. O. Khamman, T. Sarakonsri, A. Rujiwatra, Y. Laosiritaworn, **R. Yimnirun**, and S. Ananta. “Effects of Milling Time and Calcination Condition on Phase Formation and Particle Size of Lead Zirconate Nanopowders Prepared by Vibro-milling“ *Journal of Materials Science* (2007) *accepted.*

**ส่วนที่ 2:** ในส่วนขององค์ความรู้ใหม่ในเรื่องของสมบัติไดอิเล็กตริกและทางไฟฟ้าอื่นๆ ของสารเซรามิกในระบบ BT PT PZT PZN PMN PIN PZT-BT PMN-PT PZN-PZT PIN-PT และ PBZT-PMNT นั้น ได้รับโดยตรงจากการทำการตรวจสอบคุณลักษณะเฉพาะและคุณสมบัติต่างๆของเซรามิกที่เตรียมได้ และผลงานที่ได้นั้นก็ได้ถูกนำไปตีพิมพ์ในวารสารทางวิชาการต่างๆ ดังต่อไปนี้ (รายละเอียดได้ถูกนำเสนอในแต่ละผลงานแล้ว)

1. W. Chaisan, **R. Yimnirun**, S. Ananta and D.P. Cann, “Dielectric properties of solid solutions in the lead zirconate titanate-barium titanate system prepared by a modified mixed-oxide method ,” *Materials Letters,* 59(28), pp 3732-3737 (2005).
2. **Rattikorn Yimnirun**, Rungnapa Tipakontitikul and Supon Ananta, “Effect of Sintering Temperature on Densification and Dielectric Properties of

$Pb(Zr_{0.44}Ti_{0.56})O_3$ Ceramics" *International Journal of Modern Physics B*, 20(16), pp 2415-2424 (2006).

3. W. Chaisan, **R. Yimnirun**, S. Ananta and D.P. Cann, "Phase Development and Dielectric Properties of $(1-x)Pb(Zr_{0.52}Ti_{0.48})O_3–xBaTiO_3$ ceramics ," *Materials Science and Engineering B,*132, pp 300-306 (2006).
4. R. Wongmaneerung, **R. Yimnirun**, S. Ananta, R. Guo, and A.S. Bhalla, "Polarization Behavior in the Two Stage Sintered Lead Titanate Ceramics" *Ferroelectric Letters*, 33(5-6), pp 137-146 (2006).
5. **Rattikorn Yimnirun**, Yongyut Laosiritaworn, Supattra Wongsaenmai and Supon Ananta, "Scaling Behavior of Dynamic Hysteresis in Soft PZT Bulk Ceramics", *Applied Physics Letters,* 89(16), pp 162901-3 (2006)
6. R. Wongmaneerung, **R. Yimnirun** and S. Ananta, "Effects of Sintering Condition on Phase Formation, Microstructure and Dielectric Properties of Lead Titanate Ceramics", *Applied Physics A*, 86(2), pp 249-255 (2007).
7. **R. Yimnirun**, R. Wongmaneerung, S. Wongsaenmai, A. Ngamjarurojana, S. Ananta, and Y. Laosiritaworn, "Temperature Scaling of Dynamic Hysteresis in Soft Lead Zirconate Titanate Bulk Ceramic" *Applied Physics Letters*, 90(11), pp 112906 (2007).
8. **R. Yimnirun**, R. Wongmaneerung, S. Wongsaenmai, A. Ngamjarurojana, S. Ananta, and Y. Laosiritaworn, "Dynamic Hysteresis and Scaling Behavior of Hard Lead Zirconate Titanate Bulk Ceramic" *Applied Physics Letters*, 90(11), pp 112908 (2007).
9. Supattra Wongsaenmai, Xiaoli Tan, Supon Ananta, and **Rattikorn Yimnirun**, "Dielectric and Ferroelectric Properties of Fine Grains $Pb(In_{1/2}Nb_{1/2})O_3–PbTiO_3$ Ceramics" *Journal of Alloys and Compounds* (2007) *in press*
10. W. Chaisan, **R. Yimnirun**, S. Ananta, "Two-Stage Sintering of Barium Titanate and Resulting Characteristics" *Ferroelectrics (2007) in press*
11. **Rattikorn Yimnirun**, Xiaoli Tan, Supon Ananta, and Supattra Wongsaenmai, "Preparation of Fine-Grain Lead Indium Niobate Ceramics with Wolframite Precursor Method and Resulting Electrical Properties" *Applied Physics A* (2007) *in press*
12. W. Chaisan, **R. Yimnirun**, S. Ananta and D.P. Cann, "Dielectric and Ferroelectric Properties of Ceramics in PZT-BT System," *Materials Chemistry and Physics* (2007) *in press.*

13. **R. Yimnirun** “Dielectric Properties of PMN-PT Prepared by Mixed Oxide Method” *International Journal of Modern Physics B* (2007) *accepted*
14. P. Ketsuwan, Y. Laosiritaworn, S. Ananta, and **R. Yimnirun**, “Effect of Sintering Temperature on Phase Formation, Dielectric, Piezoelectric, and Ferroelectric Properties of Nb-doped $Pb(Zr_{0.52}Ti_{0.48})O_3$ Ceramics” *Ferroelectrics* (2007) *accepted.*
15. S. Wongsaenmai, A. Bhalla, R. Guo, S. Ananta, and **R. Yimnirun**, “Effect of Addition BT on Relaxor Behavior of PIN-PT Ceramics” *Integrated Ferroelectrics* (2007) *accepted*.
16. S. Wongsaenmai, A. Bhalla, X. Tan, S. Ananta, and **R. Yimnirun**, “Dielectric Properties and Relaxor Behavior of PIN-Based System” *Ferroelectrics Letters* (2007) *accepted.*

**ส่วนที่ 3:** ในส่วนนี้นั้นถือเป็นผลงานหลักของโครงการวิจัยนี้ โดยองค์ความรู้ใหม่ในเรื่องของอิทธิพลของความเค้นแบบแกนเดี่ยวต่อสมบัติไดอิเล็กตริกและทางไฟฟ้าอื่นๆของสารเซรามิกในระบบ BT PT PZT PZN PMN PIN PZT-BT PMN-PT PZN-PZT PIN-PT และ PBZT-PMNT นั้นได้จากการใช้เครื่องมืออัดแรงแบบแกนเดี่ยวประกอบในการวัดสมบัติไดอิเล็กตริก เช่น ค่าคงที่ไดอิเล็กตริก ($\varepsilon_r$) และการสูญเสียทางไดอิเล็กตริก (tan $\delta$) และสมบัติอื่นๆ เช่น สมบัติเฟร์โรอิเล็กทริกฮิสเทอรีซิส (วงวน P-E) ของสารเซรามิกในทุกระบบที่กล่าวมาภายใต้ความเค้นแบบแกนเดี่ยว และผลงานที่ได้นั้นก็ได้ถูกนำไปตีพิมพ์ในวารสารทางวิชาการต่างๆ ดังต่อไปนี้ (รายละเอียดได้ถูกนำเสนอในแต่ละผลงานแล้ว)

1. **Rattikorn Yimnirun**, Yongyut Laosiritaworn, and Supattra Wongsaenmai, “Effects of Uniaxial Compressive Pre-Stress on Ferroelectric Properties of Soft PZT Ceramic” *Journal of Physics D: Applied Physics*, 39, pp 759-764 (2006).
2. **R. Yimnirun**, S. Ananta, A. Ngamjarurojana, and S. Wongsaenmai, “Effects of Uniaxial Stress on Dielectric Properties of Ferroelectric Ceramics”, *Current Applied Physics,* 6(3), pp 520-524 (2006).
3. **Rattikorn Yimnirun**, Muangjai Unruan, Yongyut Laosiritaworn, and Supon Ananta, “Change of Dielectric Properties of Ceramics in Lead Magnesium Niobate-Lead Titanate System With Compressive Stress”, *J. Physics D: Applied Physics*, 39, pp 3097-3102 (2006)

4. **R. Yimnirun**, “Change in Dielectric Properties of Normal and Relaxor Ferroelectric Ceramic Composites in BT-PZT and PMN-PZT Systems by Uniaxial Compressive Stress” *Ferroelectrics,* 331, pp 9-18 (2006)
5. **Rattikorn Yimnirun**, “Contributions of Domain-Related Phenomena on Dielectric Constant of Lead-Based Ferroelectric Ceramics Under Uniaxial Compressive Pre-Stress” *International Journal of Modern Physics B*, 20(23), pp 3409-3417 (2006).
6. **Rattikorn Yimnirun**, Supattra Wongsaenmai, Supon Ananta, and Yongyut Laosiritaworn “Stress-Dependent Scaling Behavior of Dynamic Hysteresis in Bulk Soft Ferroelectric Ceramics”, *Applied Physics Letters*, 89(24), pp 242901-3 (2006).
7. **R. Yimnirun**, S. Ananta, and S. Chamunglap, “Dielectric Properties of (1-x)PZT-xBT Ceramics Under Uniaxial Compressive Pre-Stress” *Materials Chemistry and Physics*, 102(2-3), pp 165-170 (2007).
8. Narit Triumnak, Muangjai Unruan, Supon Ananta, and **Rattikorn Yimnirun**, “Uniaxial Stress Dependence of Dielectric Properties of 0.9PMN-0.1PT Ceramics” *Journal of Electroceramics* (2007) *accepted.*
9. **R. Yimnirun,** A. Ngamjarurojana, Y. Laosiritaworn, Supon Ananta, and Narit Triamnak, “Dielectric Properties of PZT-PZN Ceramics Under Compressive Stress” *Ferroelectrics* (2007) *accepted.*

# หนังสืออ้างอิง


1. B. Jaffe, W.R. Cook Jr., and H. Jaffe, *Piezoelectric Ceramics*, Academic Press, 1971.
2. Y. Xu, *Ferroelectric Materials and Their Applications*, North-Holland, 1991.
3. A.J. Moulson and J.M. Herbert, *Electroceramics*, Chapman and Hall, 1993.
4. R.E. Newnham and G.R. Ruschau, *Am. Ceram. Soc. Bull*. **75**[10] 51 (1996).
5. K. Uchino, *Piezoelectric Actuators and Ultrasonic Motors*, Kluwer Academic, 1997.
6. J.F. Scott, *Ferroelectrics*, **206/207**, 365 (1998).
7. G.H. Haertling, *J. Am. Ceram. Soc.* **82**[4] 797 (1999).
8. A.S. Bhalla, R. Guo and R. Roy, Mat. Res. Innovat. **4**, 3 (2000)
9. S.E.E Park and W. Hackenberger, *Current Opinion Sol. State Mat. Sci.* **6**, 11 (2002).
10. H. Chen, X. Guo and Z. Meng, *Mater. Chem.Phys.* **75**, 202 (2002).
11. R. Zuo, L. Li, X. Hu and Z. Gui, *Mater. Lett*. **54**, 185 (2002).
12. Y. H. Chen, K. Uchino, M. Shen and D. Viehland, *J. Appl. Phys.* **90(3)**, 1455 (2001).
13. H. Chen, J. Long and Z. Meng, *Mater. Sci. Eng*. **B99**, 433 (2003).
14. S. Priya, K. Uchino and D. Viehland, *Appl. Phys. Lett*. **81(13)**, 2430 (2002).
15. N. Yasuda, H. Ohwa, M. Kume, K. Hayashi, Y. Hosono and Y. Yamashita, *J. Cryst. Growth*. **229**, 299 (1999).
16. E. F. Alberta and A. S. Bhalla, *Mater. Lett*. **40**, 114 (1999).
17. E. F. Alberta and A. S. Bhalla, *Mater. Lett*. **29**, 127 (1996).
18. H. Ouchi, *J. Am. Ceram. Soc.* **51** 169 (1968).
19. C.H. Wang, *J. Eur. Ceram. Soc*. **22** 2033 (2002).
20. R. Yimnirun, S. Ananta, E. Meechoowas and S. Wongsaenmai, *J. Phys. D: Appl. Phys*. **36** 1615 (2003).
21. R. Yimnirun, S. Ananta and P. Laoratanakul, *J. Eur. Ceram. Soc.* **25** 3225 (2005).
22. W. Chaisan, S. Ananta and T. Tunkasiri, *Curr. Appl. Phys*. **4** 182 (2004).
23. S. Ananta, R. Tipakorntitikul and T. Tunkasiri, *Mater. Lett.* **57** 2637 (2003).
24. สุพล อนันตา, การพัฒนากระบวนการเตรียมสาร PZT โดยวิธีการประยุกต์กระบวนการผสมออกไซด์แบบ 2 ขั้นตอน, รายงานฉบับสมบูรณ์โครงการทุนวิจัยหลังปริญญาเอก, สนับสนุนโดยสำนักงานกองทุนสนับสนุนการวิจัย (สกว.) พ.ศ. 2545.
25. S. Sherrit, D.B. Van Nice, J.T. Graham, B.K. Mukherjee and H.D. Wiederick, *Proc. IEEE ISAF* 167 (1992).
26. Q.M. Zhang, J. Zhao, K. Uchino and J. Zheng, *J. Mater. Res.* **12[1]** 226 (1997).

27. D. Viehland, J.F. Li, E. McLaughlin, J. Powers, R. Janus and H. Robinson, *J. Appl. Phys.* **95(4)**, 1969 (2004).
28. I.J. Fritz, *J. Appl. Phys.* **49(9)**, 4922 (1978).
29. D. Viehland and J. Powers, *Appl. Phys. Lett.* **78(20)**, 3112 (2001).
30. D. Viehland, F. Tito, E. McLaughlin, H. Robinson, R. Janus, L Ewart and J. Powers, and, *J. Appl. Phys.* **90(3)**, 1496 (2001).
31. J. Zhao, A.E. Glazounov and Q.M. Zhang, *Appl. Phys. Lett.* **74(3)**, 4362 (1999).
32. D. Viehland, L. Ewart, J. Powers, and L.F. Li, *J. Appl. Phys.* **90(5)**, 2479 (2001).
33. D. Audigier, C. Richard, C. Descamps, M. Troccaz and L. Eyraud, *Ferroelectrics,* **154** 219 (1994).
34. รัตติกร ยิ้มนิรัญ, อิทธิพลของความเค้นแบบแกนเดี่ยวต่อสมบัติไดอิเล็กตริกและไฟฟ้าเชิงกลของสารเซรามิกในระบบ PMN-PZT, รายงานฉบับสมบูรณ์โครงการทุนส่งเสริมนักวิจัยรุ่นใหม่, สนับสนุนโดยสำนักงานกองทุนสนับสนุนการวิจัย (สกว.) พ.ศ. 2547.
35. สุพล อนันตา, อิทธิพลของปัจจัยในกระบวนการเตรียมต่อการเกิดเฟส โครงสร้างจุลภาค และสมบัติไดอิเล็กตริกของสารเซรามิก PBZT-PMNT, รายงานฉบับสมบูรณ์โครงการทุนพัฒนานักวิจัย, สนับสนุนโดยสำนักงานกองทุนสนับสนุนการวิจัย (สกว.) พ.ศ. 2549.
36. R. Yimnirun, S. Ananta, E. Meechoowas, S. Wongsaenmai, *Chiang Mai J. Sci.* **30**, 81 (2003).
37. S. Wongsaenmai, S. Ananta and R. Yimnirun, *Chiang Mai J. Sci.*, *in press* (2004).
38. สุพัตรา วงศ์แสนใหม่, สุพล อนันตา และ **รัตติกร ยิ้มนิรัญ,** *วารสารสงขลานครินทร์วิทยาศาสตร์และเทคโนโลยี***, 25(5)**, 629 (2546).
39. สุพัตรา วงศ์แสนใหม่, สุพล อนันตา และ **รัตติกร ยิ้มนิรัญ,** *วารสารวิทยาศาสตร์ มข***, 31(2)**, 73 (2546).
40. สุพัตรา วงศ์แสนใหม่, สุพล อนันตา และ **รัตติกร ยิ้มนิรัญ,** *วารสารเทคโนโลยีสุรนารี***, 10(3)**, (2546).
41. Y.D. Hou, M.K. Zhu, H. Wang, B. Wang, H. Yan and C.S. Tian, *Mater. Lett.*, *In Press* (2003).
42. S. Priya and K. Uchino, *J. Appl. Phys*. **91(7)**, 4515 (2002).
43. T. Bove, W. Wolny, E. Ringgaard and A. Pedersen, *J. Eur. Ceram. Soc*. **21**, 1469 (2001).

# Output จากโครงการวิจัยที่ได้รับทุนจาก สกว.

**1. ผลงานตีพิมพ์ในวารสารวิชาการนานาชาติ จำนวนทั้งสิ้น 70 เรื่องได้แก่**

**1.1 ผลงานวิจัยโดยตรงที่ได้ตีพิมพ์แล้ว 44 เรื่อง (รายละเอียดในภาคผนวก)**

1. W. Chaisan, **R. Yimnirun**, S. Ananta and D.P. Cann, “Dielectric properties of solid solutions in the lead zirconate titanate-barium titanate system prepared by a modified mixed-oxide method ,” *Materials Letters,* 59(28), pp 3732-3737 (2005).
2. **Rattikorn Yimnirun**, Yongyut Laosiritaworn, and Supattra Wongsaenmai, “Effects of Uniaxial Compressive Pre-Stress on Ferroelectric Properties of Soft PZT Ceramic” *Journal of Physics D: Applied Physics*, 39, pp 759-764 (2006).
3. R. Wongmaneerung, **R. Yimnirun** and S. Ananta, “Effects of Vibro-Milling Time on Phase Formation and Particle Size of Lead Titanate Nanopowders”, *Materials Letters,* 60(12), pp 1447-1452 (2006).
4. **R. Yimnirun**, S. Ananta, A. Ngamjarurojana, and S. Wongsaenmai, “Effects of Uniaxial Stress on Dielectric Properties of Ferroelectric Ceramics”, *Current Applied Physics,* 6(3), pp 520-524 (2006).
5. R. Wongmaneerung, T. Sarnkonsri, **R. Yimnirun** and S. Ananta “Effects of milling method and calcination condition on phase and morphology characteristics of $Mg_4Nb_2O_9$ powders”, *Materials Science and Engineering B*, 130(1-3), pp 246-253 (2006).
6. **Rattikorn Yimnirun**, Muangjai Unruan, Yongyut Laosiritaworn, and Supon Ananta, “Change of Dielectric Properties of Ceramics in Lead Magnesium Niobate-Lead Titanate System With Compressive Stress”, *J. Physics D: Applied Physics*, 39, pp 3097-3102 (2006)
7. **R. Yimnirun**, “Change in Dielectric Properties of Normal and Relaxor Ferroelectric Ceramic Composites in BT-PZT and PMN-PZT Systems by Uniaxial Compressive Stress” *Ferroelectrics,* 331, pp 9-18 (2006)
8. R. Wongmaneerung, **R. Yimnirun** and S. Ananta, “Effects of Milling Time and Calcination Condition on Phase Formation and Particle Size of Lead Titanate Nanopowders Prepared by Vibro-milling”, *Materials Letters*, 60, pp 2666-2671 (2006)

9. **Rattikorn Yimnirun**, Rungnapa Tipakontitikul and Supon Ananta, "Effect of Sintering Temperature on Densification and Dielectric Properties of $Pb(Zr_{0.44}Ti_{0.56})O_3$ Ceramics" *International Journal of Modern Physics B*, 20(16), pp 2415-2424 (2006).
10. R. Wongmaneerung, T. Sarnkonsri, **R. Yimnirun** and S. Ananta "Effects of magnesium niobate precursor and calcination condition on phase formation and morphology of lead magnesium niobate powders", *Materials Science and Engineering B,* 132, pp 292-299 (2006).
11. W. Chaisan, **R. Yimnirun**, S. Ananta and D.P. Cann, "Phase Development and Dielectric Properties of $(1-x)Pb(Zr_{0.52}Ti_{0.48})O_3–xBaTiO_3$ ceramics ," *Materials Science and Engineering B,*132, pp 300-306 (2006).
12. A. Ngamjarurojana, O. Khamman, **R. Yimnirun** and S. Ananta, "Effect of Calcination Conditions on Phase Formation and Particle Size of Zinc Niobate Powders Synthesized by Solid-State Reaction", *Materials Letters*, 60, pp 2867-2872 (2006).
13. **Rattikorn Yimnirun**, "Contributions of Domain-Related Phenomena on Dielectric Constant of Lead-Based Ferroelectric Ceramics Under Uniaxial Compressive Pre-Stress" *International Journal of Modern Physics B*, 20(23), pp 3409-3417 (2006).
14. **Rattikorn Yimnirun**, Yongyut Laosiritaworn, Supattra Wongsaenmai and Supon Ananta, "Scaling Behavior of Dynamic Hysteresis in Soft PZT Bulk Ceramics", *Applied Physics Letters,* 89(16), pp 162901-3 (2006)
15. R. Wongmaneerung, **R. Yimnirun**, S. Ananta, R. Guo, and A.S. Bhalla, "Polarization Behavior in the Two Stage Sintered Lead Titanate Ceramics" *Ferroelectric Letters*, 33(5-6), pp 137-146 (2006).
16. **Rattikorn Yimnirun**, Supattra Wongsaenmai, Supon Ananta, and Yongyut Laosiritaworn "Stress-Dependent Scaling Behavior of Dynamic Hysteresis in Bulk Soft Ferroelectric Ceramics", *Applied Physics Letters*, 89(24), pp 242901-3 (2006).
17. R. Wongmaneerung, **R. Yimnirun** and S. Ananta, "Effects of Sintering Condition on Phase Formation, Microstructure and Dielectric Properties of Lead Titanate Ceramics", *Applied Physics A*, 86(2), pp 249-255 (2007).

18. **R. Yimnirun**, S. Ananta, and S. Chamunglap, “Dielectric Properties of (1-x)PZT-xBT Ceramics Under Uniaxial Compressive Pre-Stress” *Materials Chemistry and Physics*, 102(2-3), pp 165-170 (2007).
19. **R. Yimnirun**, R. Wongmaneerung, S. Wongsaenmai, A. Ngamjarurojana, S. Ananta, and Y. Laosiritaworn, “Temperature Scaling of Dynamic Hysteresis in Soft Lead Zirconate Titanate Bulk Ceramic” *Applied Physics Letters*, 90(11), pp 112906 (2007).
20. **R. Yimnirun**, R. Wongmaneerung, S. Wongsaenmai, A. Ngamjarurojana, S. Ananta, and Y. Laosiritaworn, “Dynamic Hysteresis and Scaling Behavior of Hard Lead Zirconate Titanate Bulk Ceramic” *Applied Physics Letters*, 90(11), pp 112908 (2007).
21. S. Wongsaenmai, **R. Yimnirun** and S. Ananta, “Effects of Calcination Conditions on Phase Formation and Particle Size of Indium Niobate Powders Synthesized by the Solid-State Reaction”, *Materials Letters* (2007) *in press.*
22. O. Khamman, **R. Yimnirun** and S. Ananta, ”Effect of Vibro-Milling Time on Phase Formation and Particle Size of Lead Zirconate Nanopowders” *Materials Letters* (2007) *in press.*
23. Supattra Wongsaenmai, Xiaoli Tan, Supon Ananta, and **Rattikorn Yimnirun**, “Dielectric and Ferroelectric Properties of Fine Grains $Pb(In_{1/2}Nb_{1/2})O_3$–$PbTiO_3$ Ceramics” *Journal of Alloys and Compounds* (2007) *in press*
24. A. Prasatkhetragarn, **R. Yimnirun** and S. Ananta, “Effect of calcination conditions on phase formation and particle size of $Zn_3Nb_2O_8$ powders synthesized by solid-state reaction”, *Materials Letters* (2007) *in press*
25. S. Wongsaenmai, **R. Yimnirun** and S. Ananta, “Influence of Calcination Conditions on Phase Formation and Particle Size of Indium Niobate Powders Synthesized by the Solid-State Reaction”, *Journal of Materials Science* (2007) *in press*
26. W. Chaisan, **R. Yimnirun**, S. Ananta, “Two-Stage Sintering of Barium Titanate and Resulting Characteristics” *Ferroelectrics (2007) in press*
27. W. Chaisan, O. Khamman, **R. Yimnirun** and S. Ananta,, “Effects of Calcination Conditions on Phase and Morphology Evolution of Lead

Zirconate Powders Synthesized by Solid-State Reaction", *Journal of Materials Science* (2007) *in press*

28. **Rattikorn Yimnirun**, Xiaoli Tan, Supon Ananta, and Supattra Wongsaenmai, "Preparation of Fine-Grain Lead Indium Niobate Ceramics with Wolframite Precursor Method and Resulting Electrical Properties" *Applied Physics A* (2007) *in press*
29. Orawan Khamman, Rewadee Wongmaneerung, Wanwilai Chaisan, **Rattikorn Yimnirun** and Supon Ananta, "Potential of Vibro-Milling Technique for Preparation of Electroceramic Nanopowders" *Journal of Alloys and Compounds* (2007) *in press.*
30. W. Chaisan, **R. Yimnirun**, S. Ananta and D.P. Cann, "Dielectric and Ferroelectric Properties of Ceramics in PZT-BT System," *Materials Chemistry and Physics* (2007) *in press.*
31. Narit Triumnak, Muangjai Unruan, Supon Ananta, and **Rattikorn Yimnirun**, "Uniaxial Stress Dependence of Dielectric Properties of 0.9PMN-0.1PT Ceramics" *Journal of Electroceramics* (2007) *accepted.*
32. Athipong Ngamjarurojana, Orawan Khamman, Supon Ananta, and **Rattikorn Yimnirun**, "Synthesis and Characterizations of Lead Zinc Niobate-Lead Zirconate Titanate Powders" *Journal of Electroceramics* (2007) *accepted.*
33. Supattra Wongsaenmai, Orawan Khamman, Supon Ananta, and **Rattikorn Yimnirun**, "Synthesis and Characterizations of Lead Indium Niobate-Lead Titanate Powders" *Journal of Electroceramics* (2007) *accepted.*
34. Rewadee Wongmaneerung, Orawan Khamman, **Rattikorn Yimnirun**, and Supon Ananta, "Synthesis and Characterizations of Lead Titanate Powders" *Journal of Electroceramics* (2007) *accepted.*
35. **R. Yimnirun** "Dielectric Properties of PMN-PT Prepared by Mixed Oxide Method" *International Journal of Modern Physics B* (2007) *accepted*
36. O. Khamman, **R. Yimnirun** and S. Ananta,"Effect of Vibro-Milling Time and Calcination n Phase Formation and Particle Size of Lead Zirconate Nanopowders" *Ferroelectrics (2007) accepted*

37. A. Prasatkhetragarn, **R. Yimnirun** and S. Ananta, “Effects of Calcination Conditions on Phase Formation of Zirconium Titanate Powders Synthesized by the Solid-State Reaction”, *Ferroelectrics* (2007) *accepted*
38. W. Chaisan, A. Prasatkhetragarn**, R. Yimnirun**, S. Ananta, *“*Two-Stage Solid-State Reaction of Lead Zirconate Titanate Powders” *Ferroelectrics (2007) accepted*
39. **R. Yimnirun,** A. Ngamjarurojana, Y. Laosiritaworn, Supon Ananta, and Narit Triamnak, “Dielectric Properties of PZT-PZN Ceramics Under Compressive Stress” *Ferroelectrics* (2007) *accepted.*
40. P. Ketsuwan, Y. Laosiritaworn, S. Ananta, and **R. Yimnirun**, “Effect of Sintering Temperature on Phase Formation, Dielectric, Piezoelectric, and Ferroelectric Properties of Nb-doped $Pb(Zr_{0.52}Ti_{0.48})O_3$ Ceramics” *Ferroelectrics* (2007) *accepted.*
41. **R. Yimnirun**, Y. Laosiritaworn, S. Ananta, and S. Wongsaenmai, “Scaling Behavior of Dynamic Ferroelectric Hysteresis in Soft PZT Ceramics: Stress Dependence” *Ferroelectrics* (2007) *accepted.*
42. S. Wongsaenmai, A. Bhalla, R. Guo, S. Ananta, and **R. Yimnirun**, “Effect of Addition BT on Relaxor Behavior of PIN-PT Ceramics” *Integrated Ferroelectrics* (2007) *accepted*.
43. S. Wongsaenmai, A. Bhalla, X. Tan, S. Ananta, and **R. Yimnirun**, “Dielectric Properties and Relaxor Behavior of PIN-Based System” *Ferroelectrics Letters* (2007) *accepted.*
44. O. Khamman, T. Sarakonsri, A. Rujiwatra, Y. Laosiritaworn, **R. Yimnirun**, and S. Ananta. “Effects of Milling Time and Calcination Condition on Phase Formation and Particle Size of Lead Zirconate Nanopowders Prepared by Vibro-milling“ *Journal of Materials Science* (2007) *accepted.*

### 1.2 ผลงานวิจัยที่อยู่ระหว่างการส่งไปเพื่อตีพิมพ์ 26 เรื่อง

1. **Rattikorn Yimnirun**, Muangjai Unruan, Rewadee Wongmaneerung, Orawan Khamman, Wanwilai Chaisan, and Supon Ananta, “Dielectric Properties of Complex Perovskite PZBT-PMNT Ceramic Under Compressive Stress” submitted to *International Journal of Modern Physics B* (2007)

2. S. Wongsaenmai, S. Ananta, **R. Yimnirun**, W. Qu, and X. Tan, "Ferroelectric Properties and Phase Transitions of PBINT Ceramics" submitted to *Applied Physics A* (2007)
3. **R. Yimnirun**, R. Wongmaneerung, S. Wongsaenmai, A. Ngamjarurojana, S. Ananta, and Y. Laosiritaworn, "Temperature Scaling of Dynamic Hysteresis in Hard Lead Zirconate Titanate Bulk Ceramic" submitted to *Applied Physics A* (2007)
4. R. Wongmaneerung, **R. Yimnirun**, S. Ananta, "Processing and Properties of $Pb(Mg_{1/3}Nb_{2/3})O_3$-$PbTiO_3$ Based Ceramics" submitted to *Current Applied Physics* (2007)
5. **Rattikorn Yimnirun**, Narit Triamnak, Muangjai Unruan, Athipong Ngamjarurojana, Yongyut Laosiritaworn, and Supon Ananta, "Ferroelectric Properties of $Pb(Zr_{1/2}Ti_{1/2})O_3$—$Pb(Zn_{1/3}Nb_{2/3})O_3$ Ceramics Under Compressive Stress" submitted to *Current Applied Physics* (2007)
6. N. Triamnak, S. Wongsaenmai, S. Ananta, **R. Yimnirun**, "Dielectric Properties of PIN-PT Ceramics Under Compressive Stress" submitted to *Current Applied Physics* (2007)
7. N. Wongdamnern, N. Triamnak, A. Ngamjarurojana, Y. Laosiritaworn, S. Ananta, and **R. Yimnirun**, "Effects of Temperature and Stress on Ferroelectric Properties of Hard and Soft PZT Ceramics" submitted to *Current Applied Physics* (2007)
8. S. Wongsaenmai, A. Bhalla, R. Guo, S. Ananta, and **R. Yimnirun**, "Thermal Expansion Measurement in the Relaxor Ferroelectric PIN-PT System" submitted to *Materials Letters* (2007)
9. **Rattikorn Yimnirun**, Narit Triamnak, Muangjai Unruan, Athipong Ngamjarurojana, Yongyut Laosiritaworn, and Supon Ananta, "Stress-Dependent Ferroelectric Properties of $Pb(Zr_{1/2}Ti_{1/2})O_3$—$Pb(Zn_{1/3}Nb_{2/3})O_3$ Ceramic Systems" submitted to *Ceramics International* (2007)
10. Supattra Wongsaenmai, Supon Ananta, Xiaoli Tan, **Rattikorn Yimnirun**, "Dielectric and Ferroelectric Properties of Lead Indium Niobate Ceramic Prepared by Wolframite Method" submitted to *Ceramics International* (2007)

11. N. Wongdamnern, N. Triamnak, A. Ngamjarurojana, Y. Laosiritaworn, S. Ananta, and **R. Yimnirun**, "Comparative Studies of Dynamic Hysteresis Responses in Hard and Soft PZT Ceramics" submitted to *Ceramics International* (2007)
12. R. Wongmaneerung, A. Rittidech, O. Khamman, **R. Yimnirun** and S. Ananta, "Processing and Properties of $Pb(Mg_{1/3}Nb_{2/3})O_3$-$PbTiO_3$ Based Ceramics" submitted to *Ceramics International* (2007)
13. A. Ngamjarurojana, S. Ural, S. Ananta, **R. Yimnirun**, and K. Uchino, "Effects of Mn-Doping on PZN-PZT Ceramics" submitted to *Ceramics International* (2007)
14. A. Ngamjarurojana, S. Ural, S. Ananta, **R. Yimnirun**, and K. Uchino, "Low Sintering Temperature PZN-PZT Based-Ceramics" submitted to *Ceramics International* (2007)
15. W. Chaisan, **R. Yimnirun**, and S. Ananta, "Synthesis and Properties of PZT-BT Nanocomposites" submitted to *Ceramics International* (2007)
16. W. Chaisan, **R. Yimnirun**, and S. Ananta, "Synthesis of BT Nanopowders" submitted to *Ceramics International* (2007)
17. R. Wongmaneerung, O. Khamman, **R. Yimnirun** and S. Ananta, "Potential of Vibro-Milling in Nanopowders Production" submitted to *Ceramics International* (2007)
18. P. Ketsuwan, S. Ananta, **R. Yimnirun**, and Y. Laosiritaworn, "Effect of Porosity on Hysteresis Properties of Ferroelectrics" submitted to *Ceramics International* (2007)
19. Y. Laosiritaworn, S. Ananta, and **R. Yimnirun**, " Monte-Carlo Simulation on Stress Dependence on Ferroelectric Properties" submitted to *Ceramics International* (2007)
20. W. Suktomya, S. Ananta, **R. Yimnirun**, and Y. Laosiritaworn, "Neural Network Approach to Prediction of Powder Processing" submitted to *Ceramics International* (2007)
21. Piyachon Ketsuwan , Yongyut Laosiritaworn , Supon Ananta, and **Rattikorn Yimnirun**, "Effect of Nb-Doping on Electrical Properties of $Pb(Zr_{0.52}Ti_{0.48})O_3$ Ceramics" submitted to *Ceramics International* (2007)

22. N. Triamnak, S. Wongsaenmai, S. Ananta, **R. Yimnirun**, “Effects of Compressive Stress on the Dielectric Properties of PIN-PT Ceramics” submitted to *Ceramics International* (2007)
23. W. Chaisan, **R. Yimnirun**, and S. Ananta, “Synthesis and Properties of PZT-BT Nanocomposites” submitted to *J. Materials Science* (2007)
24. W. Chaisan, **R. Yimnirun**, and S. Ananta, “Synthesis of BT Nanopowders” submitted to *J. Materials Science* (2007)
25. **R. Yimnirun**, S. Wongsaenmai, R. Wongmaneerung, N. Wongdamnern, A. Ngamjarurojana, S. Ananta, and Y. Laosiritaworn, “ Stress- and Temperature-Dependent Scaling Behavior of Dynamic Hysteresis in Soft PZT Bulk Ceramics” submitted to *Physica Scripta* (2007)
26. **R. Yimnirun**, N. Triamnak, M. Unruan, S. Wongsaenmai, A. Ngamjarurojana, Y. Laosiritaworn, and S. Ananta, “Dielectric and Ferroelectric Properties of Complex Perovskite Ceramics Under Compressive Stress” submitted to *Physica Scripta* (2007)

## 2. การนำผลงานวิจัยไปใช้ประโยชน์

### 2.1 เชิงพาณิชย์

ในการวิจัยนี้ถึงแม้ไม่ได้มุ่งหวังในด้านการนำผลงานไปใช้ประโยชน์ในเชิงพาณิชย์ แต่มุ่งเน้นในการสร้างองค์ความรู้ใหม่ แต่อุปกรณ์ที่ถูกพัฒนาขึ้นมาใช้ประกอบการศึกษา ซึ่งได้แก่ ชุดอุปกรณ์ในการวัดสมบัติไดอิเล็กตริกภายใต้ความเค้นนั้น สามารถนำไปประยุกต์ใช้ในการวัดสมบัติดังกล่าวทั้งในกรณีที่ไม่มีความเค้นและกรณีที่มีความเค้นในวัสดุตัวอื่นๆได้ ซึ่งสามารถที่จะลดการสั่งซื้ออุปกรณ์ที่มีความคล้ายคลึงจากต่างประเทศได้

### 2.2 เชิงนโยบาย

ผลการวิจัยที่ได้จากโครงการนี้ได้ถูกนำไปใช้ในการกำหนดแผนและทิศทางการวิจัยของผู้วิจัยที่ชัดเจนขึ้น ดังจะเห็นได้จากการเสนอหัวข้อวิจัยเพื่อขอรับทุนพัฒนาศักยภาพการทำงานวิจัยของอาจารย์รุ่นกลาง ประจำปี 2550 จากสำนักงานกองทุนสนับสนุนการวิจัยและสำนักงานคณะกรรมการการอุดมศึกษา ซึ่งเป็นการวิจัยต่อเนื่องจากโครงการวิจัยนี้ เพื่อเป็นการส่งเสริมให้เกิดการวิจัยแบบมีทิศทางมากขึ้น

**2.3 เชิงสาธารณะ**

โครงการวิจัยนี้ได้ก่อให้เกิดเครือข่ายความร่วมมือในการวิจัยมากขึ้นระหว่างนักวิจัยรุ่นกลางและนักวิจัยรุ่นใหม่ทั้งในและต่างประเทศ เช่นความร่วมมืออย่างใกล้ชิดในการวิจัยกับ รศ. ดร. สุพล อนันตา ภาควิชาฟิสิกส์ คณะวิทยาศาสตร์ มหาวิทยาลัยเชียงใหม่ ซึ่งเน้นการวิจัยด้านกระบวนการผลิตเซรามิก ในขณะที่ผู้วิจัยได้มีส่วนร่วมในการวัดสมบัติทางไฟฟ้าของเซรามิกที่ผลิตขึ้น นอกจากนี้ก็มีความร่วมมือกับ ผศ. ดร. ยงยุทธ เหล่าศิริถาวร ภาควิชาฟิสิกส์ คณะวิทยาศาสตร์ มหาวิทยาลัยเชียงใหม่ ที่นำความรู้เรื่องฟิสิกส์คณานามาประกอบการคำนวณหลายๆอย่าง นอกจากนี้ยังได้มีการสร้างความร่วมมือด้านการวิจัยกับนักวิจัยในต่างประเทศคือ Prof. David Cann แห่ง Oregon State University และ Prof. Xiaoli Tan แห่ง Iowa State University สหรัฐอเมริกา และที่สำคัญที่สุดผู้วิจัยได้รับความรู้ในการวิจัยจากนักวิจัยอาวุโสจากทั้งในประเทศและต่างประเทศคือ ศ. ดร. ทวี ตันฑศิริ แห่งภาควิชาฟิสิกส์ คณะวิทยาศาสตร์ มหาวิทยาลัยเชียงใหม่ และ Prof. Robert Newnham Prof. Kenji Uchino และ Prof. Amar Bhalla แห่ง The Pennsylvania State University สหรัฐอเมริกา

**2.4 เชิงวิชาการ (พัฒนาการเรียนการสอน/สร้างนักวิจัยใหม่)**

ผลงานที่ได้จากการวิจัยนี้ได้ถูกนำไปใช้ประกอบการเรียนการสอนในหลายๆ กระบวนวิชาของสาขาวิชาวัสดุศาสตร์ ทั้งในระดับปริญญาตรีและระดับบัณฑิตศึกษา เช่น MATS 743 Electroceramics MATS 701 Characterization and Properties of Materials MATS 703 Fabrication Processes of Materials และ MATS 723 Ferroelectric Materials นอกจากนี้ผู้วิจัยยังนำผลงานบางส่วนไปประกอบการเขียนตำราเรื่อง สมบัติทางไฟฟ้าของเซรามิกเฟร์โรอิเล็กทริก (Electrical Properties of Ferroelectric Ceramics) สำหรับในส่วนของการสร้างนักวิจัยใหม่นั้น นอกจากประโยชน์โดยตรงที่เกิดกับผู้วิจัยเองแล้ว โครงการวิจัยนี้ได้มีส่วนในการฝึกฝนทักษะการวิจัยและการเผยแพร่ผลงานให้กับนักศึกษาทั้งในระดับปริญญาตรีและระดับบัณฑิตศึกษาในฐานะผู้ช่วยวิจัยร่วมกับหัวหน้าโครงการ และผลงานวิจัยที่ได้สามารถนำไปตีพิมพ์ในวารสารทางวิชาการทั้งในและต่างประเทศ รวมทั้งการนำเสนอผลงานในที่ประชุมทางวิชาการระดับนานาชาติ (ดังแสดงใน output และผลงานอื่นๆ) ซึ่งมีผลให้เกิดการพัฒนานักวิจัยรุ่นใหม่มากขึ้น

**3. อื่น ๆ (ผลงานตีพิมพ์ในวารสารวิชาการและการเสนอผลงานในที่ประชุมวิชาการนานาชาติ)**

**3.1 ผลงานตีพิมพ์ในวารสารวิชาการในประเทศจำนวนทั้งสิ้น 9 เรื่องได้แก่**

1. S. Chamunglap, S. Ananta and **R. Yimnirun**, "Effect of Uniaxial Stress on Dielectric Properties of PZT, BT and 0.55PZT-0.45BT Ceramics," *Naresuan University Science Journal*, 2004, 1(2), 15-21.
2. A. Ngamjarurojana, S. Wongsaenmai, O. Khamman, S. Ananta and **R. Yimnirun**, "Hysteresis Properties of Lead Zirconate Titanate Ceramic Under Uniaxial compressive Pre-Stress," *Chiang Mai Journal of Science*, 2005, 32(3), 355-359.
3. R. Tipakontitikul, S. Ananta and **R. Yimnirun**, "Effect of Sintering Conditions on Densification and Dielectric Properties of PZT Ceramics," *Chiang Mai Journal of Science*, 2005, 32(3), 323-329.
4. S. Chamunglap, S. Ananta and **R. Yimnirun**, "Uniaxial Stress Dependence of Dielectric Properties of PZT and 0.95PZT-0.05BT Ceramics," *Chiang Mai Journal of Science*, 2005, 32(3), 337-342.
5. R. Wongmaneerung, **R. Yimnirun** and S. Ananta, "Synthesis and Characterizations of Lead Titanate Nano-Sized Powders via a Rapid Vibro-milling," *Chiang Mai Journal of Science*, 2005, 32(3), 399-404.
6. A. Ngnamjarurojana, Y. Laosiritaworn, S. Ananta, and **R. Yimnirun**, " Synthesis and Characterization of Zinc Niobate Nanopowder via a Vibro-Milling Method" *Chiang Mai University Journal*, 2005, 4(1), 47-52.
7. R. Wongmaneerung, Y. Laosiritaworn, **R. Yimnirun** and S. Ananta, "A Mixed Oxide Synthetic Route to $Mg_4Nb_2O_9$ Nanopowders in a Corundum-Like Phase," *Chiang Mai University Journal*, 2005, 4(1), 41-46.
8. R. Wongmaneerung, S. Ananta, **R. Yimnirun** and Y. Laosiritaworn, "Monte Carlo Simulation of Nano-Powder from Mechanical Milling," *Chiang Mai University Journal*, 2005, 4(1), 169-175.
9. **R. Yimnirun**, "Roles of Nano-Domains on Uniaxial Stress Dependence of Dielectric Properties of Ferroelectric Ceramics", *Chiang Mai University Journal*, 2006 *in press*

**3.2 การเสนอผลงานในที่ประชุมวิชาการนานาชาติจำนวนทั้งสิ้น 34 เรื่องได้แก่**

1. **R. Yimnirun**, S. Ananta, A. Ngamjarurojana, and S. Wongsaenmai, “Effects of Uniaxial Stress on Dielectric Properties of Ferroelectric Ceramics”, *The 2nd International Conference on Advanced Materials and Nanotechnology*, Queenstown, New Zealand (February 2005)
2. Rungnapa Tipakontitikul, Supon Ananta, **Rattikorn Yimnirun**, “Formation and Transitions in Lead Zirconate Titanate-Lead Magnesium Niobate System” *The 2nd International Conference on Advanced Materials and Nanotechnology*, Queenstown, New Zealand (February 2005)
3. A. Ngamjarurojana, S. Wongsaenmai, R. Tipakontitikul, S. Ananta and **R. Yimnirun**, “Hysteresis Properties of Lead Zirconate Titanate Ceramic Under Uniaxial compressive Pre-Stress,” *The International Conference on Smart Materials: Smart/Intelligent Materials and Nanotechnology*, 1-3 Dec. 2004, Chiang Mai, Thailand.
4. R. Tipakontitikul, S. Ananta and **R. Yimnirun**, “Effect of Sintering Conditions on Densification and Dielectric Properties of PZT Ceramics,” *The International Conference on Smart Materials: Smart/Intelligent Materials and Nanotechnology*, 1-3 Dec. 2004, Chiang Mai, Thailand.
5. S. Chamunglap, S. Ananta and **R. Yimnirun**, “Uniaxial Stress Dependence of Dielectric Properties of PZT and 0.95PZT-0.05BT Ceramics,” *The International Conference on Smart Materials: Smart/Intelligent Materials and Nanotechnology*, 1-3 Dec. 2004, Chiang Mai, Thailand.
6. R. Wongmaneerung, **R. Yimnirun** and S. Ananta, “Synthesis and Characterizations of Lead Titanate Nano-Sized Powders via a Rapid Vibro-milling”, *The International Conference on Smart Materials: Smart/Intelligent Materials and Nanotechnology*, 1-3 Dec. 2004, Chiang Mai, Thailand.
7. Narit Triumnak, Supon Ananta, and **Rattikorn Yimnirun**, “Uniaxial Stress Dependence of Dielectric Properties of 0.9PMN-0.1PT Ceramics” *The 4th Asian Meeting on Electroceramics,* Hangzhou, China (June 2005)
8. Athipong Ngamjarurojana, Supon Ananta, and **Rattikorn Yimnirun**, “Synthesis and Characterizations of Lead Zinc Niobate-Lead Zirconate

Titanate Powders" *The 4th Asian Meeting on Electroceramics,* Hangzhou, China (June 2005)

9. Supattra Wongsaenmai, Supon Ananta, and **Rattikorn Yimnirun**, "Synthesis and Characterizations of Lead Indium Niobate-Lead Titanate Powders" *The 4th Asian Meeting on Electroceramics,* Hangzhou, China (June 2005)
10. Rewadee Wongmaneerung, **Rattikorn Yimnirun**, and Supon Ananta, "Synthesis and Characterizations of Lead Titanate Powders" *The 4th Asian Meeting on Electroceramics,* Hangzhou, China (June 2005)
11. O. Khamman, **R. Yimnirun** and S. Ananta,"Effect of Vibro-Milling Time and Calcination n Phase Formation and Particle Size of Lead Zirconate Nanopowders" AMF-5, Japan (September 2006)
12. A. Prasatkhetragarn, **R. Yimnirun** and S. Ananta, "Effects of Calcination Conditions on Phase Formation of Zirconium Titanate Powders Synthesized by the Solid-State Reaction", AMF-5, Japan (September 2006)
13. W. Chaisan, A. Prasatkhetragarn**, R. Yimnirun**, S. Ananta, "Two-Stage Solid-State Reaction of Lead Zirconate Titanate Powders" AMF-5, Japan (September 2006)
14. **R. Yimnirun,** A. Ngamjarurojana, Y. Laosiritaworn, Supon Ananta, and Narit Triamnak, "Dielectric Properties of PZT-PZN Ceramics Under Compressive Stress" AMF-5, Japan (September 2006)
15. P. Ketsuwan, Y. Laosiritaworn, S. Ananta, and R. Yimnirun, "Effect of Sintering Temperature on Phase Formation, Dielectric, Piezoelectric, and Ferroelectric Properties of Nb-doped $Pb(Zr_{0.52}Ti_{0.48})O_3$ Ceramics" AMF-5, Japan (September 2006)
16. **R. Yimnirun**, Y. Laosiritaworn, S. Ananta, and S. Wongsaenmai, "Scaling Behavior of Dynamic Ferroelectric Hysteresis in Soft PZT Ceramics: Stress Dependence" AMF-5, Japan (September 2006)
17. **Rattikorn Yimnirun**, Supattra Wongsaenmai, Yongyut Laosiritaworn and Supon Ananta , "Uniaxial Stress Dependence and Scaling Behavior of Dynamic Hysteresis Responses in Soft PZT Ceramics" ISAF-2006, North Carolina, USA (August 2006)

18. Wanwilai Chaisan**, Rattikorn Yimnirun**, and Supon Ananta , “Two-Stage of Barium Titanate” ISAF-2006, North Carolina, USA (August 2006)
19. Rewadee Wongmaneerung, Amar Bhalla, Ryan Guo, Supon Ananta, and **Rattikorn Yimnirun**, “Thermal Expansion Investigation of PMN-PT Ceramics” ISAF-2006, North Carolina, USA (August 2006)
20. Supattra Wongsaenmai, Xiaoli Tan, Supon Ananta, and Rattikorn Yimnirun, “Investigation of New PBINT Ceramic Systems” ISAF-2006, North Carolina, USA (August 2006)
21. **Rattikorn Yimnirun**, Narit Triamnak, Muangjai Unruan, Athipong Ngamjarurojana, Yongyut Laosiritaworn, and Supon Ananta, “Stress-Dependent Ferroelectric Properties of $Pb(Zr_{1/2}Ti_{1/2})O_3$—$Pb(Zn_{1/3}Nb_{2/3})O_3$ Ceramic Systems” *The 5th Asian Meeting on Electroceramics,* Bangkok, Thailand (December 2006)
22. Supattra Wongsaenmai, Supon Ananta, Xiaoli Tan, **Rattikorn Yimnirun**, “Dielectric and Ferroelectric Properties of Lead Indium Niobate Ceramic Prepared by Wolframite Method” *The 5th Asian Meeting on Electroceramics,* Bangkok, Thailand (December 2006)
23. N. Wongdamnern, N. Triamnak, A. Ngamjarurojana, Y. Laosiritaworn, S. Ananta, and **R. Yimnirun**, “Comparative Studies of Dynamic Hysteresis Responses in Hard and Soft PZT Ceramics” *The 5th Asian Meeting on Electroceramics,* Bangkok, Thailand (December 2006)
24. R. Wongmaneerung, A. Rittidech, O. Khamman, **R. Yimnirun** and S. Ananta, “Processing and Properties of $Pb(Mg_{1/3}Nb_{2/3})O_3$-$PbTiO_3$ Based Ceramics” *The 5th Asian Meeting on Electroceramics,* Bangkok, Thailand (December 2006)
25. A. Ngamjarurojana, S. Ural, S. Ananta, **R. Yimnirun**, and K. Uchino, “Effects of Mn-Doping on PZN-PZT Ceramics” *The 5th Asian Meeting on Electroceramics,* Bangkok, Thailand (December 2006)
26. A. Ngamjarurojana, S. Ural, S. Ananta, **R. Yimnirun**, and K. Uchino, “Low Sintering Temperature PZN-PZT Based-Ceramics” *The 5th Asian Meeting on Electroceramics,* Bangkok, Thailand (December 2006)
27. W. Chaisan, **R. Yimnirun**, and S. Ananta, “Synthesis and Properties of PZT-BT Nanocomposites” *The 5th Asian Meeting on Electroceramics,* Bangkok, Thailand (December 2006)

28. W. Chaisan, **R. Yimnirun**, and S. Ananta, “Synthesis of BT Nanopowders” *The 5th Asian Meeting on Electroceramics,* Bangkok, Thailand (December 2006)
29. R. Wongmaneerung, O. Khamman, **R. Yimnirun** and S. Ananta, “Potential of Vibro-Milling in Nanopowders Production” *The 5th Asian Meeting on Electroceramics,* Bangkok, Thailand (December 2006)
30. P. Ketsuwan, S. Ananta, **R. Yimnirun**, and Y. Laosiritaworn, “Effect of Porosity on Hysteresis Properties of Ferroelectrics” *The 5th Asian Meeting on Electroceramics,* Bangkok, Thailand (December 2006)
31. Y. Laosiritaworn, S. Ananta, and **R. Yimnirun**, “ Monte-Carlo Simulation on Stress Dependence on Ferroelectric Properties” *The 5th Asian Meeting on Electroceramics,* Bangkok, Thailand (December 2006)
32. W. Suktomya, S. Ananta, **R. Yimnirun**, and Y. Laosiritaworn, “Neural Network Approach to Prediction of Powder Processing” *The 5th Asian Meeting on Electroceramics,* Bangkok, Thailand (December 2006)
33. Piyachon Ketsuwan , Yongyut Laosiritaworn , Supon Ananta, and **Rattikorn Yimnirun**, “Effect of Nb-Doping on Electrical Properties of $Pb(Zr_{0.52}Ti_{0.48})O_3$ Ceramics” *The 5th Asian Meeting on Electroceramics,* Bangkok, Thailand (December 2006)
34. N. Triamnak, S. Wongsaenmai, S. Ananta, **R. Yimnirun**, “Effects of Compressive Stress on the Dielectric Properties of PIN-PT Ceramics” *The 5th Asian Meeting on Electroceramics,* Bangkok, Thailand (December 2006)

# ภาคผนวก

**Re-Print หรือ Pre-Print หรือ Accepted Manuscript**

**ของ**

**ผลงานตีพิมพ์ในวารสารวิชาการนานาชาติ**

Available online at www.sciencedirect.com
SCIENCE DIRECT
ELSEVIER
Materials Letters 59 (2005) 3732 – 3737
materials letters
www.elsevier.com/locate/matlet

# Dielectric properties of solid solutions in the lead zirconate titanate–barium titanate system prepared by a modified mixed-oxide method

Wanwilai Chaisan [a,*], Rattikorn Yimnirun [a], Supon Ananta [a], David P. Cann [b]

[a] *Department of Physics, Faculty of Science, Chiang Mai University, Chiang Mai, Thailand*
[b] *Materials Science and Engineering Department, Iowa State University, Ames, IA, USA*

Received 13 January 2005; accepted 30 June 2005
Available online 22 July 2005

**Abstract**

Ceramic solid solutions within the system $(1-x)Pb(Zr_{0.52}Ti_{0.48})O_3-xBaTiO_3$, where $x$ ranged from 0.0 to 1.0, were prepared by a modified mixed-oxide method. The crystal structure, microstructure and dielectric properties of the ceramics were investigated as a function of composition via X-ray diffraction (XRD), scanning electron microscopy (SEM) and dielectric spectroscopy. While pure BT and PZT ceramics exhibited sharp phase transformation expected for normal ferroelectrics, the $(1-x)$PZT–$x$BT solid solutions showed that with increasing solute concentration (BT or PZT), the phase transformation became more diffuse. This was primarily evidenced by an increased broadness in the dielectric peak, with a maximum peak width occurring at $x=0.4$.


*Keywords:* Dielectric properties; Barium titanate (BT); Lead zirconate titanate (PZT)

## 1. Introduction

Currently lead-based perovskite ferroelectric ceramics are widely applied in multilayer capacitors and sensors because of their excellent electrical properties [1]. Many of these applications require materials with superior dielectric and piezoelectric properties. Both $BaTiO_3$ (BT) and $Pb(Zr,Ti)O_3$ (PZT) are among the most common ferroelectric materials and have been studied extensively since the late 1940s [2,3]. These two ceramics have distinct characteristics that make each ceramic suitable for different applications. The compound $Pb(Zr_{0.52}Ti_{0.48})O_3$ (PZT) has great piezoelectric properties which can be applied in transducer applications. Furthermore, it has a high $T_C$ of 390 °C which allows piezoelectric devices to be operated at relatively high temperatures. Barium titanate (BT) is a normal ferroelectric material which exhibits a high dielectric constant, a lower $T_C$ (~120 °C) and better mechanical properties [1–3]. However, sintering temperature of BT is higher than PZT. Thus, mixing PZT with BT is expected to decrease the sintering temperature of BT-based ceramics, a desirable move towards electrode of lower cost [4]. Moreover, since PZT–BT is not a pure-lead system, it is easier to prepare single phase ceramics with significantly lower amount of undesirable pyrochlore phases, usually associated with lead-based system [5,6]. With their complimentary characteristics, it is expected that excellent properties with preparation ease can be obtained from ceramics in PZT–BT system. In addition, the Curie temperature of PZT–BT system can be engineered over a wide range of temperature by varying the composition in this system. Therefore, this study is aimed at investigating dielectric properties of PZT–BT system over the whole composition range in hope to identify compositions with desirable properties.

* Corresponding author.
*E-mail address:* wanwilai_chaisan@yahoo.com (W. Chaisan).

0167-577X/$ - see front matter © 2005 Elsevier B.V. All rights reserved.
doi:10.1016/j.matlet.2005.06.045

BT has been mixed into solid solutions with $SrTiO_3$ (BST) and with $PbTiO_3$ (BPT) to adjust the Curie temperature and to optimize the dielectric and piezoelectric response [1,2,7,8]. PZT ceramics are always modified with other chemical constituents, such as Nb and La, to improve the physical properties for specific applications [2,3,9]. Moreover, solid solutions between normal and relaxor ferroelectric materials such as PZN–BT [10], PMN–PZT [11], PZT–PNN [12], PMN–PT [13] and PZN–PT [14] have been widely studied for dielectric applications and to examine the order–disorder behavior. However the superior dielectric properties of these relaxor systems have been associated with the presence of unwanted phase, densification behavior and microstructure development [15]. It is well known that the single phase of relaxor materials is very difficult to prepare and these systems always exhibit high dielectric loss and strong frequency dependence which is not suitable for some applications [2,16]. Even though there have been extensive work on PZT-based and BT-based solid solutions, there are only a few studies on PZT–BT solid solutions [5,6,17]. Chaisan et al. [5] prepared perovskite powders in the whole series of the solid solutions in PZT–BT system. The phase formation characteristics, cell parameters and the degree of tetragonality were examined as a function of composition. It was found that complete solid solutions of perovskite-like phase in the $(1-x)$PZT–$x$BT system occurred across the entire composition range. Lattice parameters of the tetragonal phase and of the rhombohedral phase were found to vary with chemical composition. The degree of tetragonality increased, while optimum firing temperatures decreased continuously with decreasing BT content. Moreover, pseudo-binary system of PZN–BT–PZT was previously studied and the effect of processing conditions on the piezoelectric and dielectric properties of this system was also discussed [17].

Thus far, from these literatures, there have been no systematic studies on the dielectric properties of the whole series of PZT–BT compositions. Therefore, as an extension of our earlier work on structural studies of the PZT–BT system [5], the overall purpose of this study is to investigate the dielectric properties of the solid solution between two normal ferroelectrics with the aim of identifying excellent electrical properties within this system. Although the conventional mixed-oxide method has attracted interest to prepare normal ferroelectric PZT and BT materials for many decades, several methods such as mechanical activation [6] and sol–gel-hydrothermal technique [18] still have been developed for better approach. A number of chemical routes has also been used as alternatives [19–21]. However these techniques are more complicated and expensive than the conventional mixed-oxide route, which limits its commercial applicability for mass powder synthesis. In this respect, it is desirable to develop a method based on the mixed-oxide method for preparation of PZT–BT ferroelectric materials. Therefore, this paper presents the dielectric properties of compositions in the PZT–BT binary system prepared via a modified mixed-oxide method, in which PZT powders are prepared through lead zirconate ($PbZrO_3$) precursor to eliminate pyrochlore phase usually found in powders from a conventional mixed-oxide method [5].

## 2. Experimental procedures

The compositions $(1-x)Pb(Zr_{0.52}Ti_{0.48})O_3-xBaTiO_3$ or $(1-x)$PZT–$x$BT, where $x=0.0$, 0.1, 0.3, 0.4, 0.5, 0.7, 0.9 and 1.0, were prepared by a modified mixed-oxide method [5]. Reagent grade PbO, $ZrO_2$, $TiO_2$ and $BaCO_3$ powders (Fluka, >99% purity) were used as starting materials. Powder of each end member (PZT and BT) was first formed in order to avoid unwanted pyrochlore phases. For the preparation of BT, $BaCO_3$ and $TiO_2$ powders were homogeneously mixed via ball-milling for 24 h with zirconia media in ethanol. The well-mixed powder was calcined at 1300 °C for 2 h in an alumina crucible. With a modified mixed-oxide method [5], the PZT powders were prepared by using a lead zirconate ($PbZrO_3$) as precursor in order to reduce the occurrence of undesirable phase. Pure $PbZrO_3$ phase was first formed by reacting PbO with $ZrO_2$ at 800 °C for 2 h. $PbZrO_3$ powder was then mixed with PbO and $TiO_2$ and milled, dried and calcined at 900 °C for 2 h to form single phase PZT. The $(1-x)$PZT–$x$BT powders were then formulated from the BT and PZT components by employing the similar mixed-oxide procedure and calcining at various

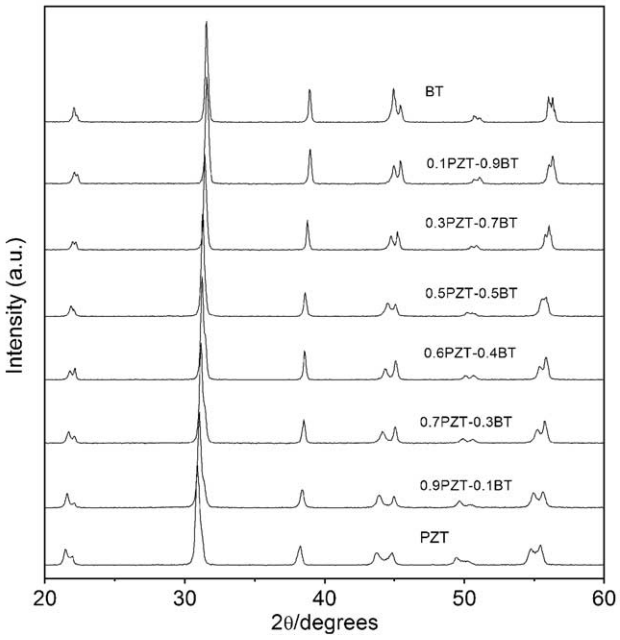


Fig. 1. XRD diffraction patterns of sintered $(1-x)$PZT–$x$BT ceramics.

Table 1
Characteristics of (1 − x)PZT–xBT ceramics with optimized processing conditions

| Compositions | Sintering temperature (°C) | Density (g/cm$^3$) | Average grain size (μm) |
|---|---|---|---|
| PZT | 1100 | 7.7 | 2.36 |
| 0.9PZT–0.1BT | 1200 | 7.6 | 2.86 |
| 0.7PZT–0.3BT | 1200 | 7.2 | 1.97 |
| 0.6PZT–0.4BT | 1250 | 6.9 | 2.31 |
| 0.5PZT–0.5BT | 1250 | 6.6 | 3.87 |
| 0.3PZT–0.7BT | 1250 | 5.7 | 3.71 |
| 0.1PZT–0.9BT | 1300 | 5.3 | 5.72 |
| BT | 1350 | 5.8 | 2.42 |

temperatures between 900 and 1300 °C for 2 h in order to obtain single phase $(1-x)$PZT–$x$BT powders [5].

The calcined $(1-x)$PZT–$x$BT powders were then isostatically cold-pressed into pellets with a diameter of 15 mm and a thickness of 2 mm at a pressure of 4 MPa and sintered for 2 h over a range of temperatures between 1050 and 1350 °C depending upon the composition. Densities of sintered ceramics were measured by Archimedes method and X-ray diffraction (XRD using $CuK_\alpha$ radiation) was employed to identify the phases formed. The grain morphology and size were directly imaged using scanning electron microscopy (SEM) and the average grain size was determined by using a mean

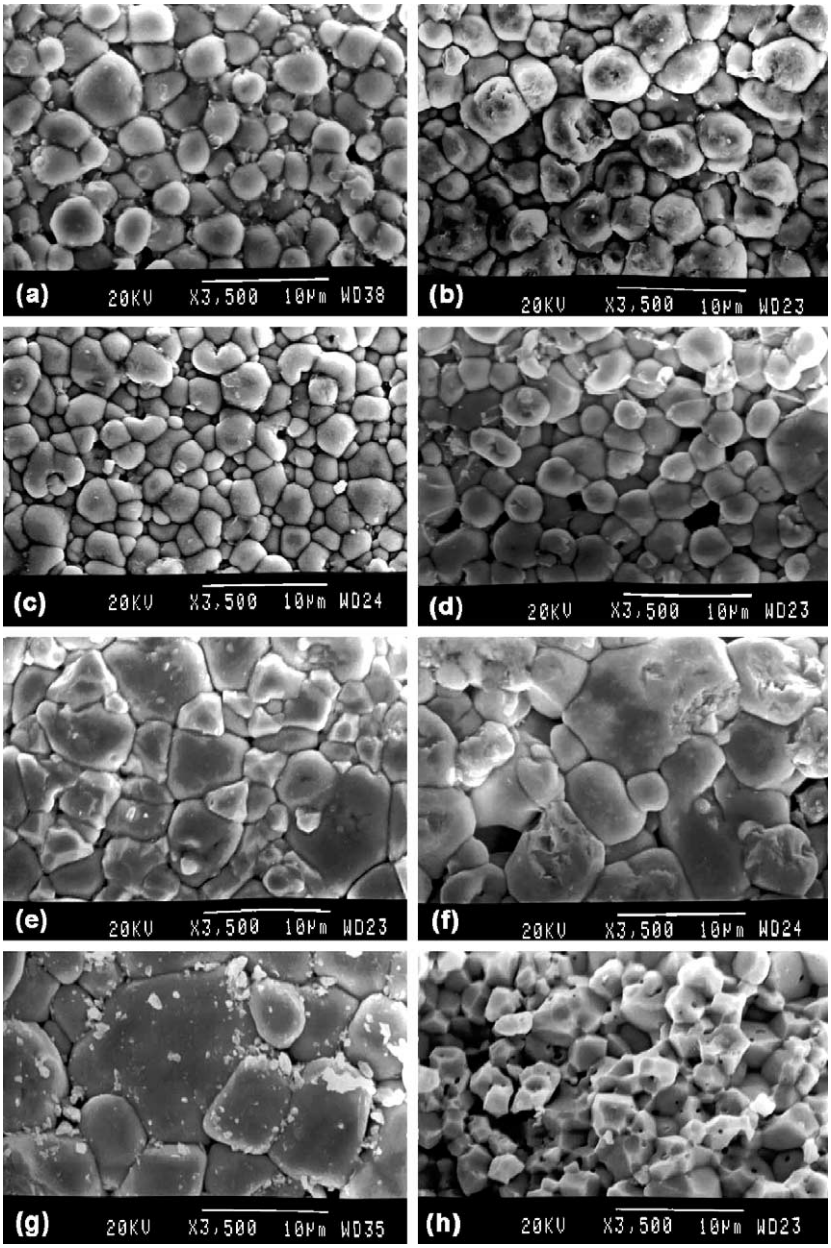


Fig. 2. SEM micrographs of $(1-x)$PZT–$x$BT ceramics: (a) PZT, (b) 0.9PZT–0.1BT, (c) 0.7PZT–0.3BT, (d) 0.6PZT–0.4BT, (e) 0.5PZT–0.5BT, (f) 0.3PZT–0.7BT, (g) 0.1PZT–0.9BT and (h) BT.

linear intercept method [22]. For electrical measurements, silver paste was fired on both sides of the polished samples at 550 °C for 30 min as the electrodes. A dimension of ceramics after sintered and polished is about 12.5 mm in diameter and 1 mm in thickness. Dielectric properties of the sintered ceramics were studied as a function of both temperature and frequency. The capacitance was measured with a HP4284A LCR meter in connection with a Delta Design 9023 temperature chamber and a sample holder (Norwegian Electroceramics) capable of high temperature measurement. Dielectric constant ($\varepsilon_r$) was calculated using the geometric area and thickness of the discs.

## 3. Results and discussion

The phase formation behavior of the sintered $(1-x)$PZT–$x$BT ceramics is revealed by XRD as shown in Fig. 1. The $BaTiO_3$ ceramic sintered at 1350 °C was identified as single phase perovskite having tetragonal symmetry. With increasing PZT content, the diffraction peaks shifted towards lower angle and the diffraction peak around $2\theta$ of 43°–46° was found to split at composition $x=0.5$. This observation suggests that this composition may lead to a diffuse MPB between the tetragonal and rhombohedral PZT phases [23]. In this case, the peak of tetragonal phase is much stronger than that of rhombohedral phase. However, the (200) peak splitting for the PZT–BT system exhibited more clearly in powders as reported in our earlier work [5]. Additionally, the PZT–BT ceramics showed single diffraction peaks which indicate good homogeneity and complete solid solution within the $(1-x)$PZT–$x$BT system [24]. The pure $Pb(Zr_{0.52}Ti_{0.48})O_3$ ceramic sintered at 1100 °C showed a co-existence of both tetragonal and rhombohedral phases which can be matched with the JCPDS file no. 33-0784 and 73-2022, respectively.

The optimized sintering temperatures at which ceramics with single phase and highest densification are obtained, densities, and average grain sizes of the sintered $(1-x)$PZT–$x$BT ceramics are listed in Table 1. Higher firing temperatures were necessary for compositions containing a large fraction of BT. Compositions with $x=0.7$ and $x=0.9$ could not be sintered to sufficient densities and the theoretical densities of ceramics in this range were about 86%–89%. It is possible that volatilization of PbO during firing is the main reason for the failure in preparing dense ceramics over this composition range [25,26]. As shown in Fig. 2, SEM micrographs reveal that the compositions with $0.0 \le x \le 0.4$ exhibit good densification and homogenous grain size. For the compositions with $0.5 \le x \le 0.9$, the grain size varies greatly from 1 to 15 μm and defective grains and some degree of porosity are clearly seen; these matched with the density data. The reason for the variation of grain sizes in this composition range is not clearly understood. However, it can be assumed that since sintering temperatures for highest

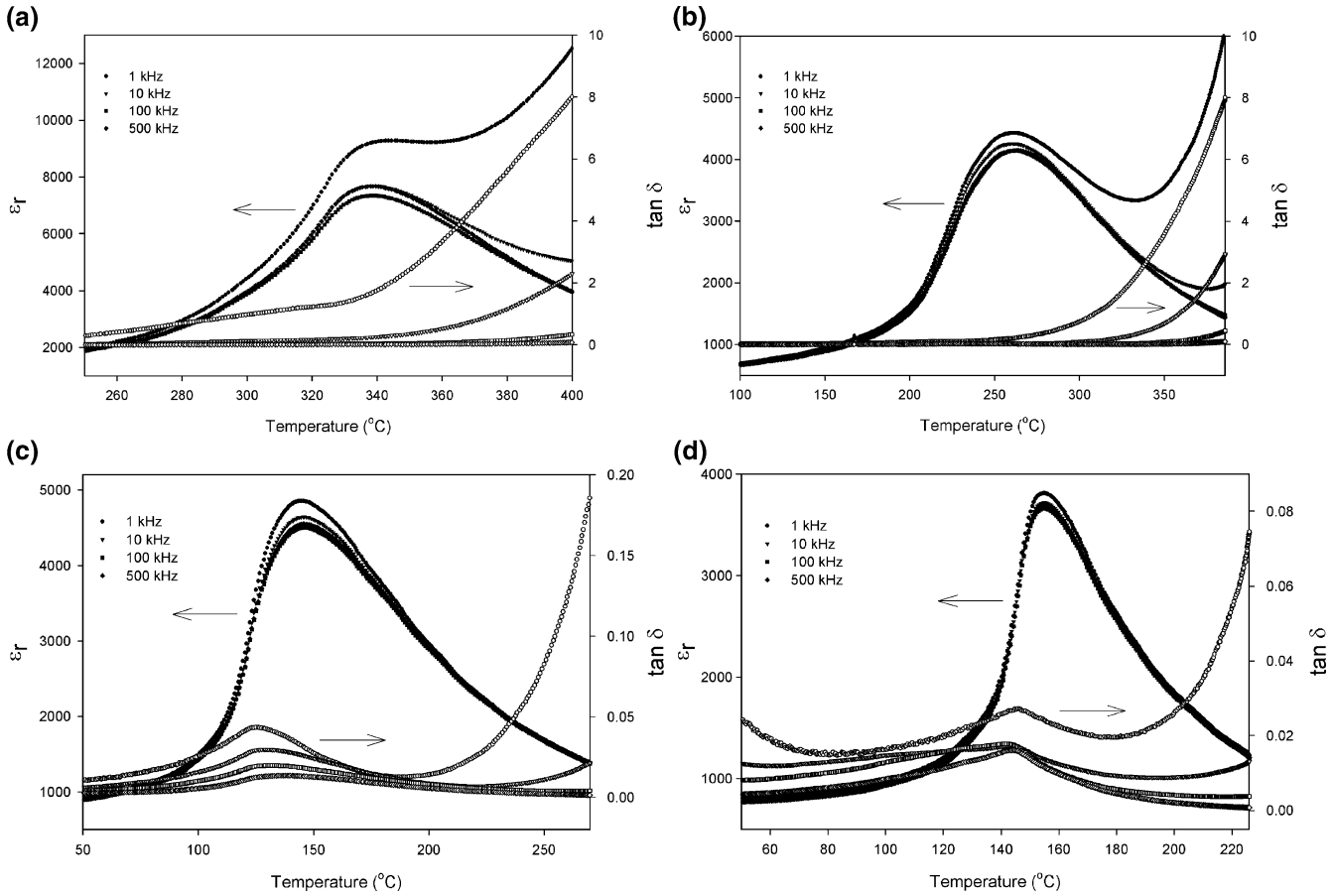


Fig. 3. Temperature and frequency dependence of dielectric properties of (a) 0.9PZT–0.1BT, (b) 0.7PZT–0.3BT, (c) 0.3PZT–0.7BT and (d) 0.1PZT–0.9BT ceramics.

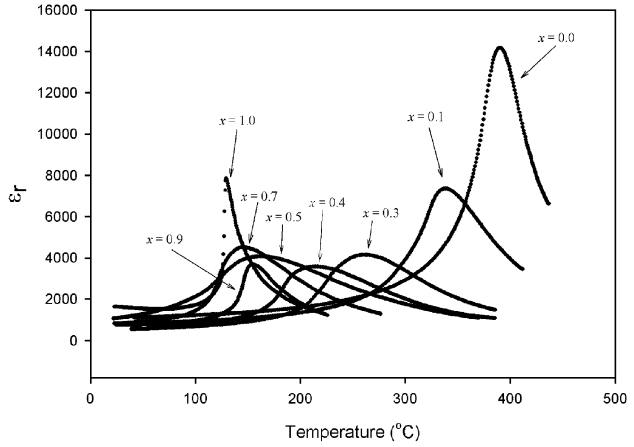


Fig. 4. Temperature dependence of dielectric constant ($\varepsilon_r$) of $(1-x)$PZT–$x$BT ceramics at 100 kHz.

densification of PZT and BT ceramics are very different (900 °C and 1300 °C, respectively), this could lead to different grain growth behaviors between two phases, hence heterogeneous microstructure [27].

Fig. 3 shows the temperature dependence of dielectric constant ($\varepsilon_r$) and dissipation factor (tan $\delta$) at various frequencies for compositions with $x=0.1$, 0.3, 0.7 and 0.9. All compositions show indication of a diffuse phase transition of dielectric constant with rather weak frequency dependence. In addition, Curie temperatures ($T_C$) are also noticeably frequency independent [28]. It should be noted that the dielectric loss tangent of all ceramics increases rapidly at high temperature as a result of thermally activated space charge conduction [11]. The representative temperature dependence of the dielectric constant ($\varepsilon_r$) measured at 100 kHz for $(1-x)$PZT–$x$BT samples with $0.0 \le x \le 1.0$ is shown in Fig. 4. The Curie temperatures and maximum dielectric constants of the pure PZT and BT ceramics in this work were, respectively, 390 °C and 14,200 for PZT, and 129 °C and 7800 for BT. Therefore, a solid solution between PZT and BT is expected to show a transition temperature between 390 and 129 °C. The variation of $T_C$ with compositions and dielectric data are listed in Table 2. The Curie temperature significantly decreases with increasing BT content up to 50 mol%. However, for the compositions $0.5 \le x \le 0.9$, $T_C$ is not clearly depending on composition and remains at a nearly constant value between 140 and 160 °C. Even though the presence of Pb is known to shift $T_C$ to higher temperatures [2,3], the nearly constant $T_C$ with increasing Pb content in the composition with $0.5 \le x \le 0.9$ is likely caused by PbO loss due to the high sintering temperatures required for these compositions [25,26]. For pure PZT, the $\varepsilon_r$ peak is sharp and approaches 15,000. However, the $\varepsilon_r$ peaks become broader with increasing BT content, and the broadest peak occurs at the $x=0.4$ composition. It is very interesting to observe that the $\varepsilon_r$ peak becomes more sharp as the BT content further increases.

Table 2
Dielectric properties of $(1-x)$PZT–$x$BT ceramics

| Compositions | $T_C$ (°C) | $\varepsilon_m$ | $\gamma$ | $\delta$ |
|---|---|---|---|---|
| PZT | 390 | 14,200 | 1.74 | 16.1 |
| 0.9PZT–0.1BT | 338 | 7300 | 1.76 | 16.2 |
| 0.7PZT–0.3BT | 262 | 4100 | 1.86 | 16.6 |
| 0.6PZT–0.4BT | 214 | 3600 | 1.97 | 17.1 |
| 0.5PZT–0.5BT | 162 | 4100 | 1.91 | 17.3 |
| 0.3PZT–0.7BT | 146 | 4500 | 1.74 | 15.9 |
| 0.1PZT–0.9BT | 155 | 3700 | 1.63 | 14.4 |
| BT | 129 | 7800 | 1.16 | 12.5 |

To understand the interesting dielectric behavior of the PZT–BT system, we look at the different behaviors of normal and relaxor ferroelectric. For a normal ferroelectric such as PZT and BT, above the Curie temperature the dielectric constant follows the Curie–Weiss law:

$$\varepsilon = \frac{c}{T - T_0} \tag{1}$$

where $c$ is the Curie constant and $T_0$ is the Curie–Weiss temperature [2,11,29]. For a ferroelectric with a diffuse phase transition, the following equation:

$$\frac{1}{\varepsilon} \approx (T - T_m)^2 \tag{2}$$

has been shown to be valid over a wide temperature range instead of the normal Curie–Weiss law (Eq. (1)) [10,30]. In Eq. (2), $T_m$ is the temperature at which the dielectric constant is maximum. If the local Curie temperature distribution is Gaussian, the reciprocal permittivity can be written in the form [10,12]:

$$\frac{1}{\varepsilon} = \frac{1}{\varepsilon_m} + \frac{(T - T_m)^\gamma}{2\varepsilon_m \delta^2} \tag{3}$$

where $\varepsilon_m$ is maximum permittivity, $\gamma$ is diffusivity, and $\delta$ is diffuseness parameter. For $(1-x)$PZT–$x$BT compositions, the diffusivity ($\gamma$) and diffuseness parameter ($\delta$) can be estimated from the slope and intercept of the dielectric data shown in Fig. 5, and tabulated in Table 2.

For the PZT-rich ceramics, the values of $\gamma$ and $\delta$ increase with increasing BT content, confirming the diffuse phase transitions in PZT–BT solid solutions. It is clear that the addition of BT raises the degree of disorder in $(1-x)$PZT–$x$BT over the compositional range $0.1 \le x \le 0.5$. The highest degree of diffuseness is exhibited in the 0.5PZT–0.5BT ceramic. Similarly, from the BT end member, the values of both $\gamma$ and $\delta$ exhibit the same trend with

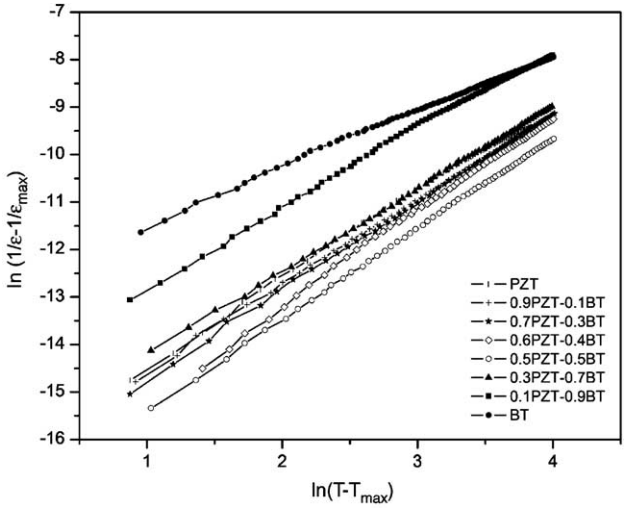


Fig. 5. Plots of $\ln\left(\frac{1}{\varepsilon} - \frac{1}{\varepsilon_m}\right)$ vs. $\ln(T - T_m)$ for $(1-x)$PZT–$x$BT ceramics.

increasing PZT content. This observation indicates that PZT addition also induces disorder in BT-rich compositions. It should also be mentioned here that different dielectric behaviors could also be caused by grain size variation [11]. However, the grain size, as shown in Table 1, in this study does not differ significantly enough to cause such a variation in the dielectric properties. Finally, it should be noted here that with comparison to other solid solution systems, such as PMN–PT, PZN–PT, PZT–PNN [12–14], ceramics in PZT–BT are much easier to prepare with minimized pyrochlore phases, lower dielectric loss and weak frequency dependence.

## 4. Conclusions

The dielectric properties of solid solutions in the $(1-x)$PZT–$x$BT system prepared via the mixed-oxide method are reported. All compositions in this study were single phase perovskite with tetragonal symmetry. The results indicated that the dielectric behavior of pure PZT and BT follows a Curie–Weiss law, while solid solutions of $(1-x)$PZT–$x$BT ($0.1 \leq x \leq 0.9$) exhibited a diffuse phase transition behavior with a Curie temperature ranging between 390 °C to 129 °C. In $(1-x)$PZT–$x$BT solid solutions, the degree of diffuseness increased with increased solute content up to a maximum at $x=0.5$.

## Acknowledgements

This work was supported by the Thailand Research Fund (TRF), Graduate School of Chiang Mai University and the Ministry of University Affairs.

## References

[1] A.J. Moulson, J.M. Herbert, Electroceramics: Materials, Properties, Applications, 2nd edition, John Wiley & Sons, Ltd., 2003, p. 243.
[2] G.H. Haertling, J. Am. Ceram. Soc. 82 (1999) 797–818.
[3] B. Jaffe, W.R. Cook, Piezoelectric Ceramics, R.A.N. Publishers, 1971, p. 317.
[4] J. Chen, Z. Shen, F. Liu, X. Liu, J. Yun, Scr. Mater. 49 (2003) 509–514.
[5] W. Chaisan, S. Ananta, T. Tunkasiri, Cur. Appl. Phys. 4 (2004) 182–185.
[6] B.K. Gan, J.M. Xue, D.M. Wan, J. Wang, Appl. Phys., A 69 (1999) 433–436.
[7] K. Uchino, Acta Mater. 46 (1998) 3745–3753.
[8] A.D. Polli, F.F. Lange, C.G. Levi, J. Am. Ceram. Soc. 83 (2000) 873–881.
[9] H. Jaffe, D.A. Berlincourt, Proc. IEEE 53 (1965) 1372–1386.
[10] A. Halliyal, U. Kumar, R.E. Newnham, L.E. Cross, Am. Ceram. Soc. Bull. 66 (1987) 671–676.
[11] R. Yimnirun, S. Ananta, P. Laoratanakul, Mater. Sci. Eng., B, Solid-State Mater. Adv. Technol. 112 (2004) 79–86.
[12] N. Vittayakorn, G. Rujijanagul, X. Tan, M.A. Marquardt, D.P. Cann, J. Appl. Phys. 96 (2004) 5103–5109.
[13] K. Babooram, H. Tailor, Z.-G. Ye, Ceram. Int. 30 (2004) 1411–1417.
[14] J.J. Lima-Silva, I. Guedes, J.M. Filho, A.P. Ayala, M.H. Lente, J.A. Eiras, D. Garcia, Solid State Commun. 131 (2004) 111–114.
[15] J.P. Guha, J. Eur. Ceram. Soc. 23 (2003) 133–139.
[16] L.E. Cross, Ferroelectrics 151 (1994) 305–320.
[17] F. Xia, X. Yao, J. Mater. Sci. 34 (1999) 3341–3343.
[18] J. Zeng, M. Zhang, Z. Song, L. Wang, J. Li, K. Li, C. Lin, Appl. Surf. Sci. 148 (1999) 137–141.
[19] R.N. Das, R.K. Pati, P. Pramanik, Mater. Lett. 45 (2000) 743–748.
[20] A. Abreu, S.M. Zanetti, M.A.S. Oliveira, G.P. Thim, J. Eur. Ceram. Soc. 25 (2005) 743–748.
[21] R.N. Das, P. Pramanik, Mater. Lett. 40 (1999) 251–254.
[22] D.G. Brandon, W.D. Kaplan, Microstructural Characterization of Materials, John Wiley & Sons, Ltd., 1999, p. 409.
[23] A.K. Arora, R.P. Tandon, A. Mansingh, Ferroelectrics 132 (1992) 9.
[24] B.D. Cullity, Elements of X-ray Diffraction, Addison-Wesley Publishing Company, Inc., 1978, p. 32.
[25] A. Garg, D.C. Agrawal, Mater. Sci. Eng., B, Solid-State Mater. Adv. Technol. 56 (1999) 46–50.
[26] C.H. Wang, S.J. Chang, P.C. Chang, Mater. Sci. Eng., B, Solid-State Mater. Adv. Technol. 111 (2004) 124–130.
[27] Y.-M. Chiang, D.P. Birnie, W.D. Kingery, Physical Ceramics, John Wisley & Sons, Inc., 1997, p. 522.
[28] T.R. Shrout, J. Fielding, Proc. IEEE Ultrasonics Symposium, 1990, pp. 711–720.
[29] L.E. Cross, Mater. Chem. Phys. 43 (1996) 108–115.
[30] R.D. Shannon, C.T. Prewitt, Acta Crystallogr., B Struct. Crystallogr. Cryst. Chem. 25 (1969) 925–945.

INSTITUTE OF PHYSICS PUBLISHING JOURNAL OF PHYSICS D: APPLIED PHYSICS
J. Phys. D: Appl. Phys. **39** (2006) 759–764 doi:10.1088/0022-3727/39/4/025

# Effect of uniaxial compressive pre-stress on ferroelectric properties of soft PZT ceramics

**Rattikorn Yimnirun, Yongyut Laosiritaworn and Supattra Wongsaenmai**

Department of Physics, Faculty of Science, Chiang Mai University, Chiang Mai 50200, Thailand

Received 21 October 2005, in final form 11 January 2006
Published 3 February 2006
Online at stacks.iop.org/JPhysD/39/759

**Abstract**
The effect of uniaxial compressive pre-stress on the ferroelectric properties of commercial soft PZT ceramics is investigated. The ferroelectric properties under the uniaxial compressive pre-stress of the ceramics are observed at stress up to 24 MPa using a compressometer in conjunction with a modified Sawyer–Tower circuit. The results show that the ferroelectric characteristics, i.e. the area of the ferroelectric hysteresis ($P$–$E$) loops, the saturation polarization ($P_{sat}$), the remanent polarization ($P_r$), and the loop squareness ($R_{sq}$) decrease with increasing compressive pre-stress, while the coercive field ($E_c$) is virtually unaffected by the applied stress. The stress-induced domain wall motion suppression and non-180° ferroelectric domain switching processes are responsible for the changes observed. In addition, a significant decrease in these parameters after a full cycle of stress application has been observed and attributed to the stress-induced decrease in the switchable part of the spontaneous polarization at high stress. Furthermore, the permittivity calculated from the $P$–$E$ loops is found to decrease with increasing applied pre-stress. This finding differs considerably from the results in the low-field experimental condition. Finally, this study clearly shows that the applied stress has a significant influence on the ferroelectric properties of soft PZT ceramics.

(Some figures in this article are in colour only in the electronic version)

## 1. Introduction

Lead zirconate titanate ($Pb(Zr_{1-x}Ti_x)O_3$ or PZT) ceramics are among the lead-based complex perovskites that have been investigated extensively, from both the academic and commercial viewpoints. They are employed extensively in sensor and actuators applications, as well as smart systems [1–6]. The most widely studied and used PZT compositions are in the vicinity of the morphotropic phase boundary (MPB) between the tetragonal and rhombohedral ferroelectric phases [1, 4, 6–8]. However, to meet the requirements for specific applications, PZT ceramics are usually modified with dopants [1, 4, 9–12]. Generally, donor (higher-valency) additives induce 'soft' piezoelectric behaviours with higher dielectric and piezoelectric activities suitable for sensor and actuator applications. On the other hand, acceptor (lower-valency) additives result in 'hard' piezoelectric behaviours particularly suitable for ultrasonic motor applications [1, 2, 4–6].

However, in these applications PZT ceramics are often subjected to mechanical loading, either deliberately in the design of the device itself or because the device is used to changing shapes as in many smart structure applications or the device is used under environmental stresses [1–7]. A prior knowledge of how the material properties change under different load conditions is therefore crucial for proper design of a device and for suitable selection of materials for a specific application. Despite that fact, material constants used in many design calculations are often obtained from a stress-free measuring condition, which in turn may lead to incorrect or inappropriate actuator and transducer designs. It is therefore important to determine the properties of these materials as

  

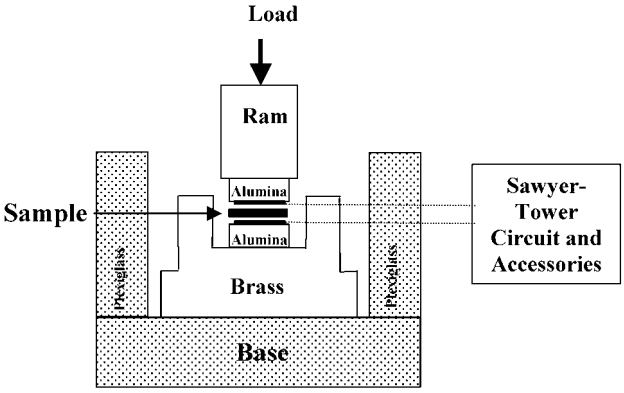


**Figure 1.** A schematic of the experimental set-up.

a function of applied stress. Previous investigations on the stress-dependence of dielectric and electrical properties of many ceramic systems, such as undoped-PZT, PLZT, BT, PMN-PT, PZT-BT and PMN-PZT, have clearly emphasized the importance of the subject [13–21]. The present study is aimed at studying technically important and commercially available soft PZT ceramics. Many investigations have already revealed interesting results on the dielectric and piezoelectric properties of the soft PZT ceramics under applied stress [15–17, 21]. However, there has been no work on the stress dependence of the ferroelectric properties of the ceramics. Therefore, this study is undertaken to investigate the influences of the uniaxial compressive pre-stress on the ferroelectric properties of the soft PZT ceramics.

## 2. Experiments and measurements

A commercially available soft PZT ceramic (PKI-552, Piezo Kinetics Inc., USA) was used in this study. Denoted as Navy Type VI, this ceramic is designed for applications that require high electromechanical activity and high dielectric constant. Its properties are (measured by the supplier) longitudinal charge coefficient $d_{33} = 550\,\mathrm{pm\,V^{-1}}$; planer coupling factor $k_p = 0.63$, dielectric constant (1 kHz) $\varepsilon_r = 3400$, Curie temperature $T_C = 200\,^{\circ}\mathrm{C}$ and bulk density $= 7.6\,\mathrm{g\,cm^{-3}}$. The disc-shaped samples with diameter of 10 mm and thickness of 1 mm were pre-poled by the supplier.

The ferroelectric hysteresis ($P$–$E$) loops were characterized by using a computer controlled modified Sawyer–Tower circuit. The electric field was applied to a sample by a high voltage ac amplifier (Trek, model 610D) with the input sinusoidal signal with a frequency of 100 Hz from a signal generator (Goodwill, model GAG-809). The detailed descriptions of this system are explained elsewhere [22, 23]. To study the effects of the uniaxial stress on the ferroelectric properties, the uniaxial compressometer was constructed [24]. As shown in figure 1, the compressometer was developed for simultaneous applications of the mechanical stress and the electric field. The compressometer cell consisting of a cylindrical brass cell with a heavy brass base, a brass ram and a precisely guided loading platform provides true uniaxial stress during mechanical loading. The prepared specimen was carefully placed between the two alumina blocks and the electric field was applied to the specimen via the copper shims attached to the alumina blocks. With this setting, the uniaxial compressive stress was applied parallel to the electric field direction. During the measurements, the specimen was immersed in silicone oil to prevent high-voltage arcing during electric loading. The uniaxial compressive stress was supplied by the servohydraulic load frame and the applied stress was monitored with the pressure gauge of the load frame. Measurements were performed as a function of mechanical pre-stress applied discretely between 0 and 24 MPa. During the measurements, a desired pre-stress was first applied to the sample and then the electric field was applied. The ferroelectric hysteresis ($P$–$E$) loop was recorded at room temperature (25 °C) for both loading and unloading conditions. The parameters obtained from the loops were the saturation polarization ($P_{sat}$), the remanent polarization ($P_r$) and the coercive field ($E_c$), which are defined as the points where the loops reach the maximum polarization, cross the zero field and cross the zero polarization, respectively. The measurements reported were for the samples during their first mechanical stress cycle. It should also be noted that the reported ferroelectric parameters were obtained after a total of 10 cycles of the electric field were applied to the sample at each constant pre-stress.

## 3. Results and discussion

The polarization versus electric field ($P$–$E$) hysteresis loops of the soft PZT ceramics under different compressive pre-stress during loading and unloading are shown in figures 2 and 3, respectively. It should first be noticed that the area of the $P$–$E$ loops decreases steadily with increasing the pre-stress (figure 2) and then increases when the stress is gradually removed (figure 3). The $P$–$E$ loop area indicates the polarization dissipation energy of a ferroelectric material subjected to one full cycle of electric field application [25]. This amount of energy loss is directly related to volume involved in the switching process during the application of electric field [21]. Therefore, the decrease in the loop area with increasing pre-stress is a result of the stress-induced domain wall motion suppression [21]. The polarization dissipation energy is consequently found to decrease non-linearly with increasing applied pre-stress, as plotted in figure 4, indicating that the sample volume contributing to polarization reversal decreases with the increasing pre-stress. In the stress-free state, the dissipation energy is $\sim 8.1 \times 10^5\,\mathrm{J\,m^{-3}}$; while at 24 MPa, the dissipation energy decreases to $3.8 \times 10^5\,\mathrm{J\,m^{-3}}$ ($< 50\%$ of the stress-free state). A similar observation has also been found in previous investigations [13, 14, 21, 26–28]. In addition, even though the $P$–$E$ loop expands when the stress is being removed, the loop does not return to its original form after the stress cycle, as shown in figure 3. Correspondingly, the dissipation energy increases at a slower rate during the unloading, and eventually the stress-free value of the dissipation energy after a full stress cycle drops to $\sim 5.6 \times 10^5\,\mathrm{J\,m^{-3}}$, as displayed in figure 4. The difference in the dissipation energy during stress loading and unloading is believed to be caused by the decrease in the switchable part of spontaneous polarization of the ceramic after being subjected to the high pre-stress, as will be supported by the following discussions [17, 29].

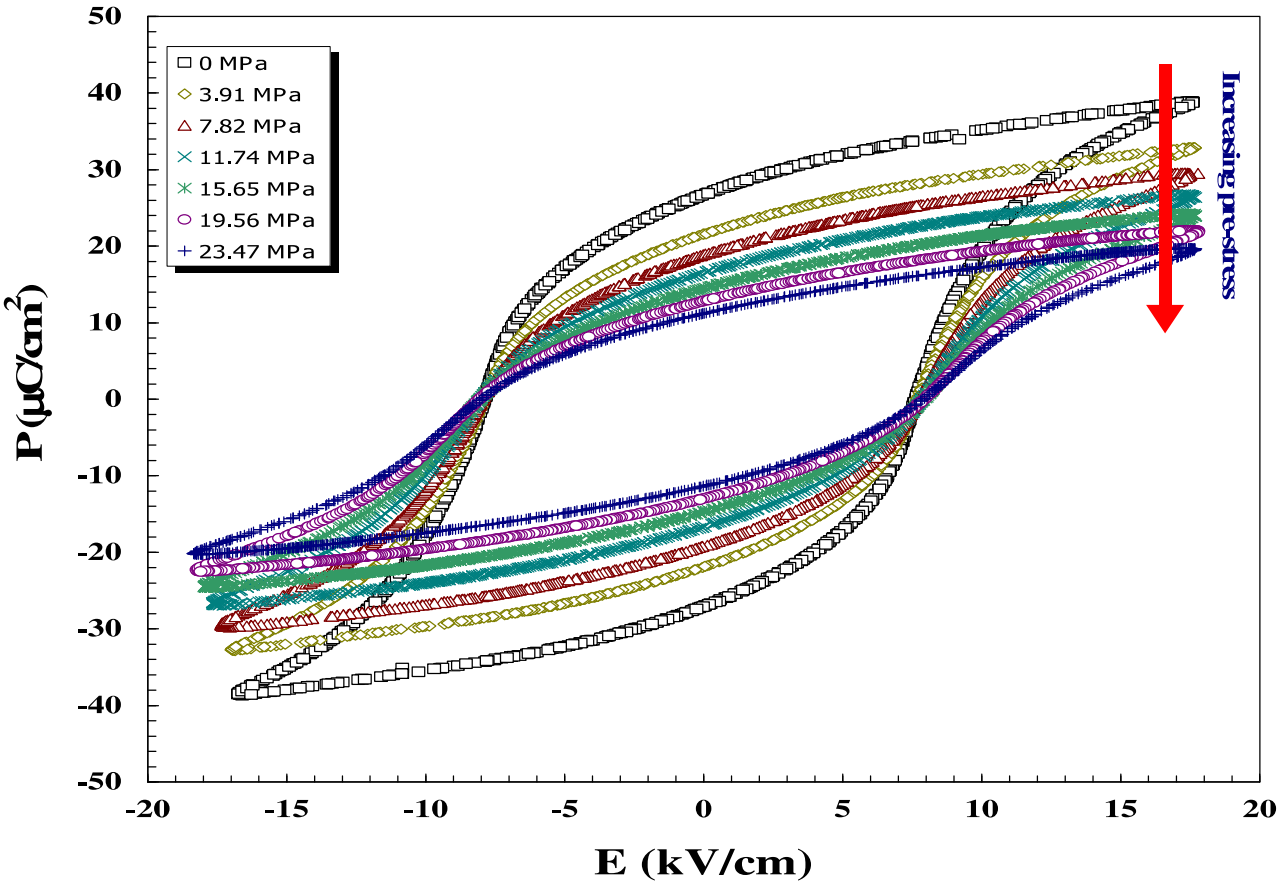


**Figure 2.** Polarization versus electric field ($P$–$E$) hysteresis loops as a function of compressive pre-stress for soft PZT ceramic during loading.

The changes in the saturation polarization ($P_{sat}$), the remanent polarization ($P_r$), and the coercive field ($E_c$) with the uniaxial compressive pre-stress are plotted in figures 5–7, respectively. Similarly to the trend observed in the dissipation energy, figures 5 and 6 clearly show that both the saturation and remanent polarizations decrease as the compressive pre-stress increases. The decrease is very pronounced with the polarization values at 24 MPa being approximately 50% of the stress-free values. In addition, a significant decrease in the polarization values of the ceramic is also observed after a mechanical stress cycle. The $P_{sat}$ value before the stress cycle is recorded as 39 $\mu$C cm$^{-2}$, while the value is reduced to 23 $\mu$C cm$^{-2}$ after the sample is exposed to a complete cycle of the mechanical stress. A similar drop is also observed for the $P_r$ values, with the values before and after the stress cycle being 26.5 and 17, in the units of $\mu$C cm$^{-2}$, respectively. This suggests a significant stress-induced decrease in the switchable part of the spontaneous polarization of the soft PZT ceramic resulting in the observed decrease in the polarization values, as well as the dissipation energy, under high stress [17, 29]. In contrast, the applied pre-stress shows little or no influence on the coercive field ($E_c$), as demonstrated in figure 7. These results clearly indicate that soft PZT ceramics are not suitable for high stress applications. It should also be noted that previous investigations on other ceramic systems, such as BT, PLZT, PMN-PT and PMN-PZT, showed a similar tendency [13, 14, 21, 26–28, 30].

The ferroelectric characteristics of the soft PZT ceramic can also be assessed with the hysteresis loop squareness ($R_{sq}$), which can be calculated from the empirical expression

$$R_{sq} = (P_r/P_s) + (P_{1.1E_c}/P_r), \quad (1)$$

where $P_r$ is the remanent polarization, $P_s$ is the saturated polarization obtained at some finite field strength below the dielectric breakdown and $P_{1.1E_c}$ is the absolute value of the polarization at the field equal to 1.1 $E_c$ [31]. For the ideal square loop, $R_{sq}$ is equal to 2.00. As depicted in figure 8, the $R_{sq}$ values generally decrease with increasing pre-stress and the values during the loading are slightly larger than those during the unloading. This observation is clearly a result of the decrease in the polarizations under the pre-stress. The observations in figures 2–8 clearly indicate that the ferroelectric characteristics of the soft PZT ceramic decrease considerably under the application of the compressive pre-stress.

To understand, at least qualitatively, these experimental results on the soft PZT ceramic, one can interpret the changes in terms of domain-reorientation processes [15–21]. When the uniaxial compressive stress is applied in the direction parallel to the poling direction, the applied stress tends to keep the ferroelectric domains aligned with their polar axes away from the stress direction through the non-180° ferroelectric domain switching processes. Therefore, it takes a larger than usual applied electric field to reorient the domains along the stress direction, resulting in a lower value of the saturated

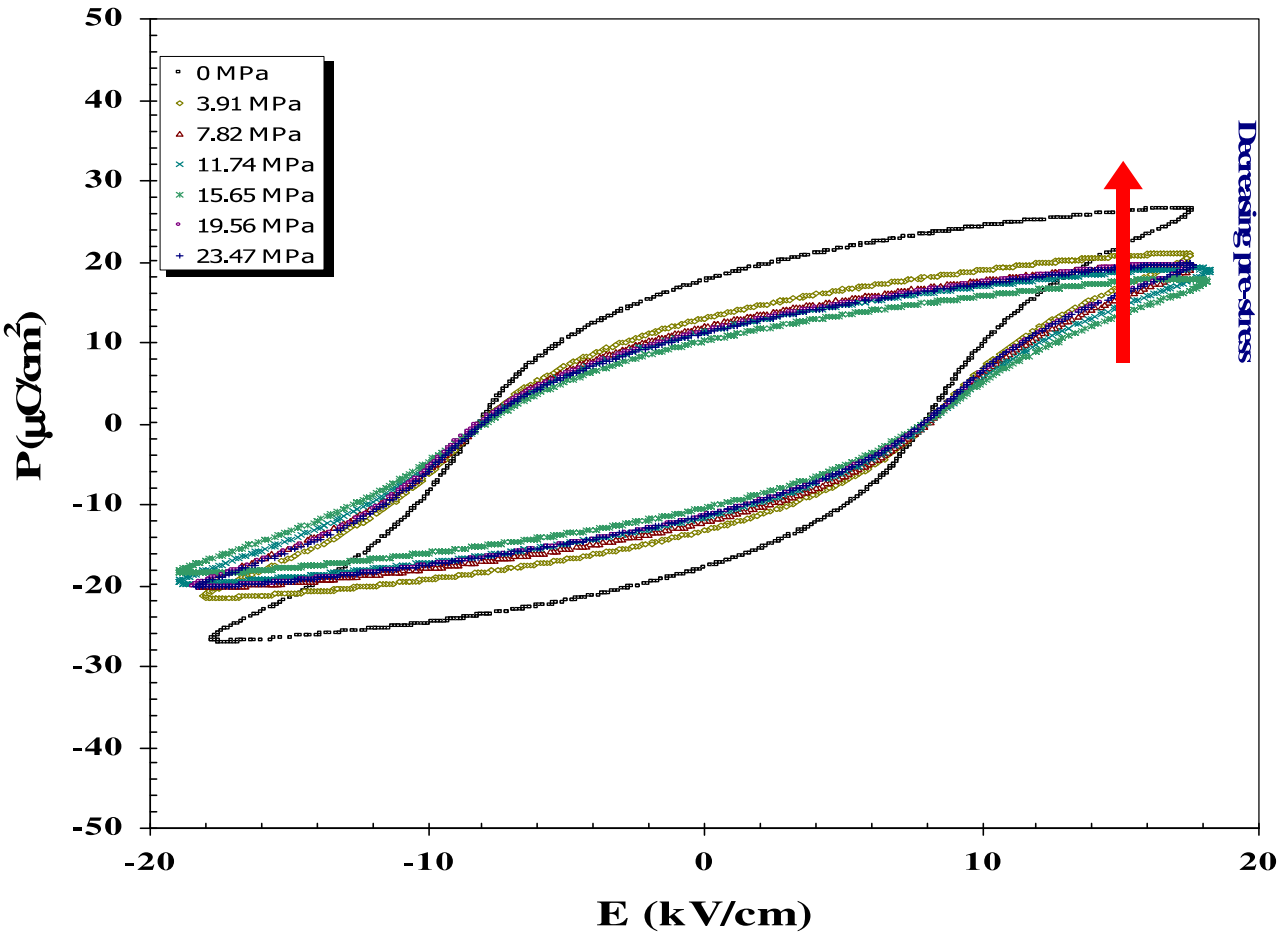


**Figure 3.** Polarization versus electric field ($P$–$E$) hysteresis loops as a function of compressive pre-stress for soft PZT ceramic during unloading.

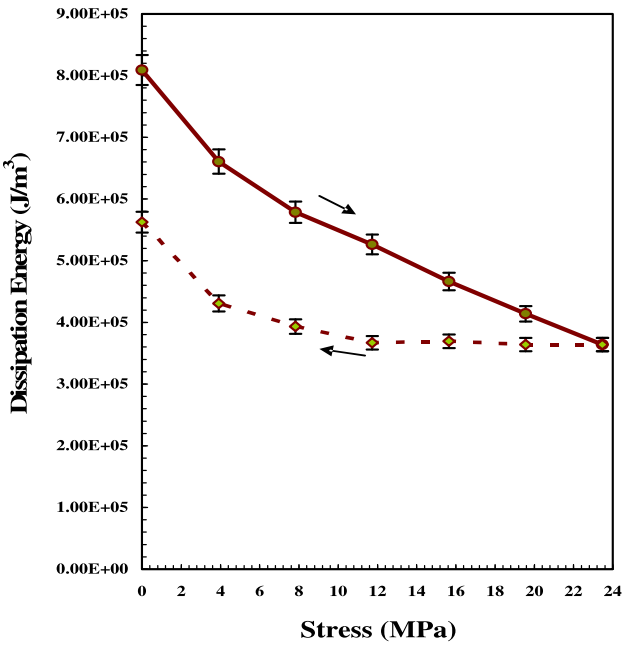


**Figure 4.** Changes in dissipation energy (hysteresis loop area) with compressive pre-stress for soft PZT ceramic.

polarization ($P_{sat}$), as shown in figure 5. When the electric field is reduced to zero the domains tend to rotate back away from the pre-stress direction, resulting in a lower than usual remanent polarization ($P_r$), as depicted in figure 6 [13, 21]. Furthermore, the decrease in the dissipation energy with increasing compressive pre-stress indicates that more and more ferroelectric domains are constrained by the pre-stress and cannot be re-oriented by the electric field so as to participate in the polarization reversal. Consequently, both the saturation and remanent polarizations become lower with increasing compressive pre-stress [21]. In addition, the decrease in the switchable part of spontaneous polarization at the high pre-stress causes the difference in the above-mentioned parameters during stress loading and unloading. The results of the changes in the ferroelectric characteristics of the soft PZT ceramic with increasing compressive pre-stress are in agreement with the previous investigations of many ferroelectric ceramics [13, 14, 20, 21, 26–28].

Furthermore, from the $P$–$E$ loops the dielectric permittivity can be evaluated from the relation

$$\varepsilon = \frac{\Delta P}{\Delta E}, \tag{2}$$

where $\Delta P$ is the polarization difference between +1 and $-1\,\mathrm{kV\,cm^{-1}}$. The calculated dielectric permittivity can be called differential permittivity, which includes the reversible

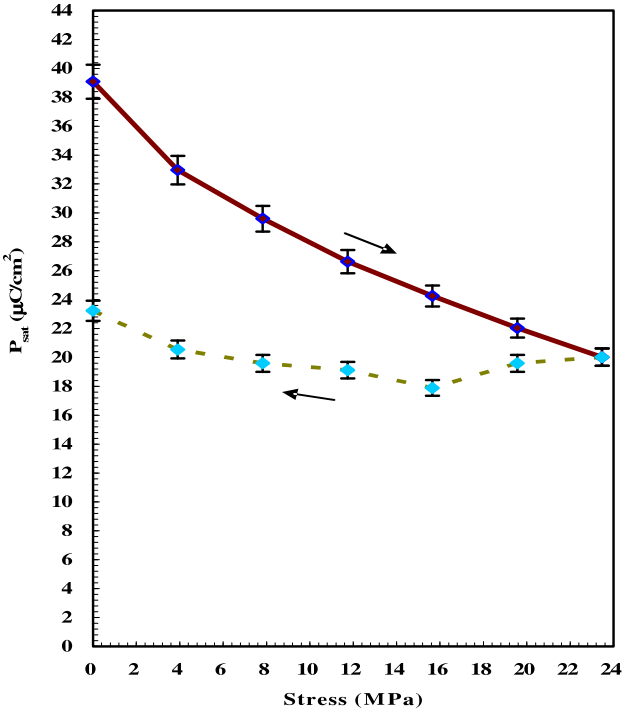


**Figure 5.** Changes in saturated polarization ($P_{sat}$) with compressive pre-stress for soft PZT ceramic.

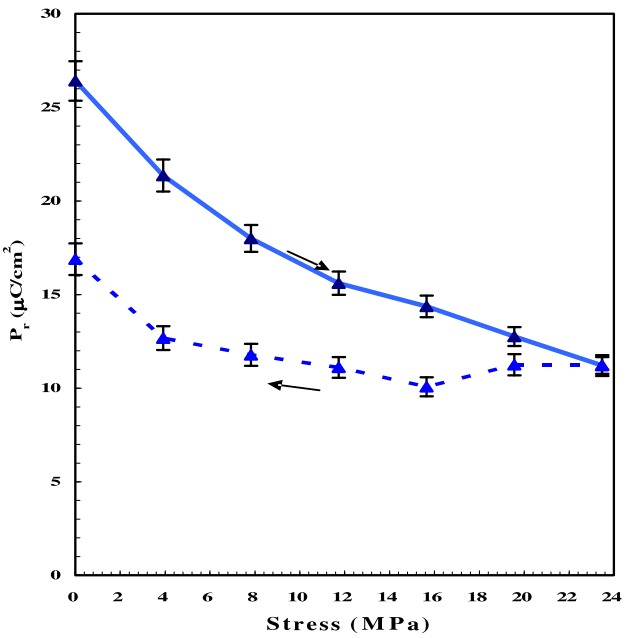


**Figure 6.** Changes in remanent polarization ($P_r$) with compressive pre-stress for soft PZT ceramic.

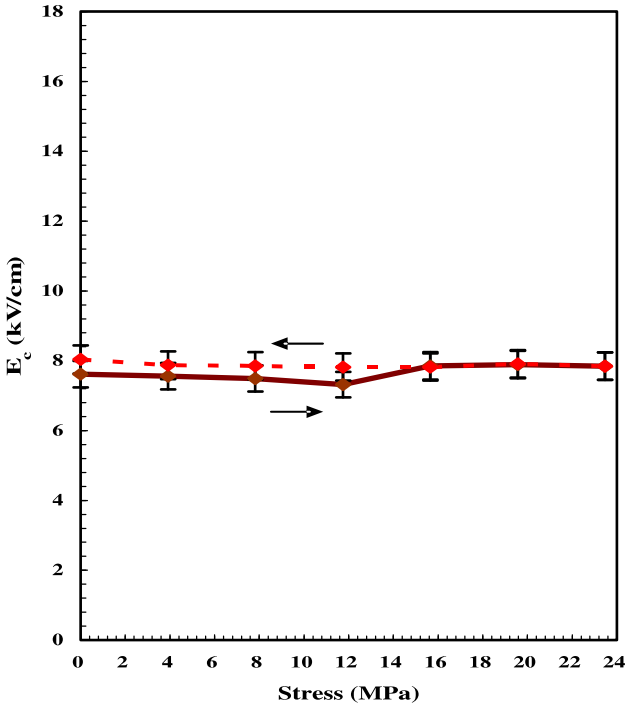


**Figure 7.** Changes in coercive field ($E_c$) with compressive pre-stress for soft PZT ceramic.

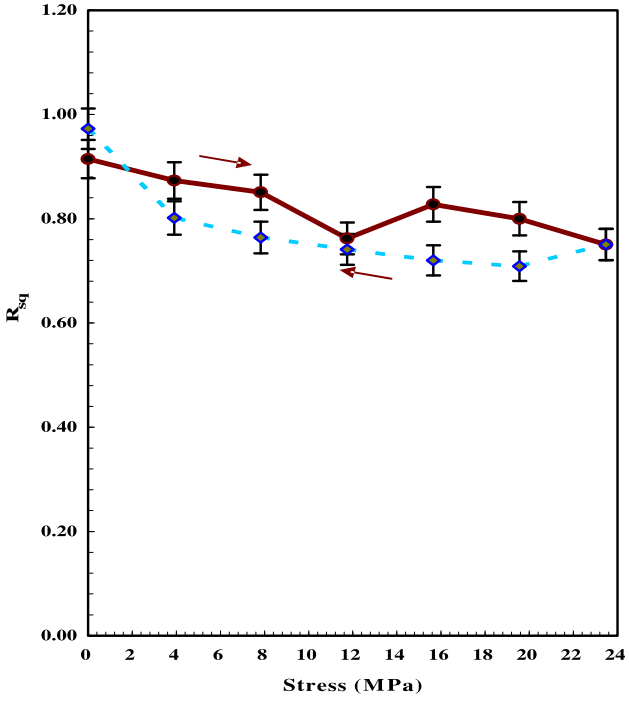


**Figure 8.** Changes in loop squareness ($R_{sq}$) with compressive pre-stress for soft PZT ceramic.

(intrinsic dielectric property) and irreversible (extrinsic domain switching related property) contributions of the materials [21]. Therefore, the stress-free value of the differential permittivity of ∼16 000 is significantly larger than that of the reported low-field permittivity of 3 400, which is largely governed by the reversible contributions [17, 21]. The study on another type of soft PZT reported the same order of dielectric permittivity enhancement under high-field measurement [26]. The change in the differential permittivity is illustrated in figure 9 as a function of the pre-stress. The differential permittivity of the soft PZT ceramic decreases with increasing applied pre-stress. This differs considerably from the results described in previous investigations [19, 29], in which the stress dependence of the dielectric properties was measured at a much lower field strength (1 V mm$^{-1}$). In those studies, the dielectric permittivity of the soft PZT was found

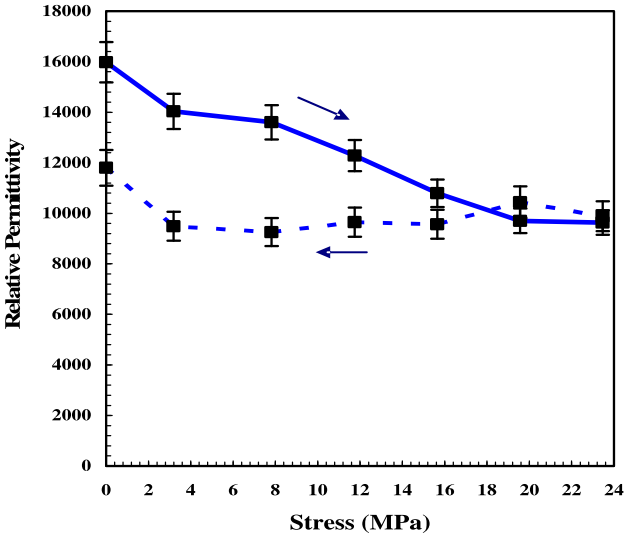


**Figure 9.** Changes in the differential permittivity (measured from the slope of $P$–$E$ curves as the field passes through 0 kV cm$^{-1}$) with compressive pre-stress for soft PZT ceramic.

to increase slightly with the applied compressive stress up to 30 MPa.

## 4. Conclusions

In this study, the effects of uniaxial compressive pre-stress on the ferroelectric properties of soft PZT ceramics are investigated. The ferroelectric properties under the uniaxial compressive pre-stress of the ceramics are observed up to 24 MPa using a compressometer in conjunction with a modified Sawyer–Tower circuit. The results show that the ferroelectric characteristics, i.e. the area of the ferroelectric hysteresis ($P$–$E$) loops, which corresponds to the energy dissipation, the saturation polarization ($P_{sat}$), the remanent polarization ($P_r$) and the loop squareness ($R_{sq}$), decrease with increasing compressive pre-stress, while the coercive field ($E_c$) is virtually unaffected by the applied stress. The non-180° ferroelectric domain switching and stress-induced domain wall suppression processes are responsible for the changes observed. In addition, a significant decrease in these parameters after a full cycle of stress application has been observed and attributed to the stress induced decrease in the switchable part of spontaneous polarization. Furthermore, the permittivity calculated from the hysteresis loops is found to decrease with increasing applied pre-stress. This finding differs considerably from the results in the low-field experimental condition, which clearly signifies the importance of the experimental conditions used to determine the dielectric properties under the applied stress. Finally, this study undoubtedly shows that the applied stress has significant influences on the ferroelectric properties of the soft PZT ceramics.

## Acknowledgment

Financial supports from the Thailand Research Fund (TRF) and Faculty of Science and Graduate School of Chiang Mai University are gratefully acknowledged.

## References

[1] Jaffe B, Cook W R and Jaffe H 1971 *Piezoelectric Ceramics* (New York: Academic)
[2] Haertling G H 1999 *J. Am. Ceram. Soc.* **82** 797
[3] Cross L E 1996 *Mater. Chem. Phys.* **43** 108
[4] Moulson A J and Herbert J M 2003 *Electroceramics* 2nd edn (New York: Wiley-Interscience)
[5] Uchino K 2000 *Ferroelectric Devices* (New York: Dekker)
[6] Xu Y H 1991 *Ferroelectric Materials and Their Applications* (Amsterdam: North Holland)
[7] Cross L E 1987 *Ferroelectrics* **76** 241
[8] Cao W and Cross L E 1993 *Phys. Rev.* B **47** 4825
[9] Takahashi S 1982 *Ferroelectrics* **41** 143
[10] Chu S Y, Chen T Y and Tsai I T 2003 *Integr. Ferroelectr.* **58** 1293
[11] Chen X M and Yang J S 1998 *J. Eur. Ceram. Soc.* **18** 1059
[12] Kulcsar F 1959 *J. Am. Ceram. Soc.* **42** 49
[13] Fritz I J 1978 *J. Appl. Phys.* **49** 4922
[14] Lynch C S 1996 *Acta Mater.* **44** 4137
[15] Zhang Q M, Zhao J, Uchino K and Zheng J 1997 *J. Mater. Res.* **12** 226
[16] Zhao J, Glazounov A E and Zhang Q M 1999 *Appl. Phys. Lett.* **74** 436
[17] Yang G, Liu S F, Ren W and Mukherjee B K 2000 *Symp. on Smart Structures and Materials, Proc. SPIE* **3992** 103
[18] Viehland D and Powers J 2001 *J. Appl. Phys.* **89** 1820
[19] Yimnirun R, Ananta S, Meechoowas E and Wongsaenmai S 2003 *J. Phys. D: Appl. Phys.* **36** 1615
[20] Viehland D, Li J F, McLaughlin E, Powers J, Janus R and Robinson H 2004 *J. Appl. Phys.* **95** 1969
[21] Zhou D, Kamlah M and Munz D 2005 *J. Eur. Ceram. Soc.* **25** 425
[22] Jiang Q 1992 *PhD Thesis* Pennsylvania State University
[23] Park S E and Shrout T R 1997 *J. Appl. Phys.* **82** 1804
[24] Yimnirun R, Moses P J, Meyer R J and Newnham R E 2003 *Rev. Sci. Instrum.* **74** 3429
[25] Lines M E and Glass A M 1977 *Principles and Applications of Ferroelectrics and Related Materials* (Oxford: Clarendon Press)
[26] Fang D and Li C 1999 *J. Mater. Sci.* **34** 4001
[27] Guillon O, Delobelle P, Thiebaud F, Walter V and Perreux D 2004 *Ferroelectrics.* **308** 95
[28] Zhao J and Zhang Q M 1996 *Proc. IEEE Int. Symp. on Applications of Ferroelectrics (ISAF)* **2** 971
[29] Yang G, Ren W, Liu S F, Masys A J and Mukherjee B K 2000 *Proc. IEEE Ultrasonic Symp.* **2** 1005
[30] Yimnirun R, Ananta S, Ngamjarurojana A and Wongsaenmai S 2005 *Appl. Phys.* A—*Mater.* **81** 1227
[31] Jin B M, Kim J and Kim S C 1997 *Appl. Phys.* A—*Mater.* **65** 53

Available online at www.sciencedirect.com
SCIENCE DIRECT
Materials Letters 60 (2006) 1447–1452
materials letters
www.elsevier.com/locate/matlet

# Effect of vibro-milling time on phase formation and particle size of lead titanate nanopowders

R. Wongmaneerung, R. Yimnirun, S. Ananta *

*Department of Physics, Faculty of Science, Chiang Mai University, Chiang Mai 50200, Thailand*

Received 5 August 2005; accepted 14 November 2005
Available online 1 December 2005

**Abstract**

A perovskite-like phase of lead titanate, $PbTiO_3$, nanopowder was synthesized by a solid-state reaction via a rapid vibro-milling technique. The effect of milling time on the phase formation and particle size of $PbTiO_3$ powder was investigated. Powder samples were characterized using TG-DTA, XRD, SEM and laser diffraction techniques. It was found that an average particle size of 17 nm was achieved at 25 h of vibro-milling after which a higher degree of particle agglomeration was observed on continuation of milling to 35 h. In addition, by employing an appropriate choice of the milling time, a narrow particle size distribution curve was also observed.


*Keywords:* Lead titanate; Milling; Nanopowders; Phase formation; Particle size

## 1. Introduction

Lead titanate, $PbTiO_3$ (PT), is one of the ferroelectric materials which exhibits a perovskite structure. It has a Curie temperature ~490 °C. The unique properties of the PT, i.e. the high transition temperature, pyroelectric coefficient and spontaneous polarization, make it useful for high frequency and high temperature applications in electronic devices [1,2]. When combined with other oxides, lead titanate can form a series of solid solutions such as $Pb(Zr_{1-x},Ti_x)O_3$ (PZT), $Pb(Mg_{1/3}Nb_{2/3})O_3$–$PbTiO_3$ (PMNT) and $Pb(Zn_{1/3}Nb_{2/3})O_3$–$PbTiO_3$ (PZN-PT) [2–4]. These ferroelectric alloys are widely used in ultrasonic transducers, nonvolatile memories, microactuators, multilayer capacitors and electro-optic devices [1,2]. To fabricate them, a fine powder of perovskite phase with a minimal degree of particle agglomeration is needed as the starting material in order to achieve a dense and uniform microstructure at a given sintering temperature. In order to improve the sintering behaviour of PT ceramics, a crucial focus of powder synthesis in recent years has been the formation of uniform-sized, single morphology particulates ranging in size from nanometer to micrometers [5–7].

The development of a method to produce nanopowders of precise stoichiometry and desired properties is complex, depending on a number of variables such as nature and purity of starting materials, processing history, temperature, etc. To obtain nanosized PT powders, many investigations have focused on several chemistry-based preparation routes, such as sol–gel [5], co-precipitation [6], hydrothermal reaction [7], besides the more conventional solid-state reaction of mixed oxides [8,9]. All these techniques are aimed at reducing the particle size and temperature of preparation of the compound even though they are more involved and complicated in approach than the solid-state reaction. Moreover, high-purity PT nanopowders are still not available in bulk quantity and also very expensive. The advantage of using mechanical milling for preparation of nanosized powders lies in its ability to produce mass quantities of powders in the solid state using simple equipment and low cost starting precursors [8,9]. Although some research has been done in the preparation of PT powders via a vibro-milling technique [10,11], to our knowledge a systematic study regarding the influence of milling time on the preparation of PT powders has not yet been reported.

* Corresponding author. Tel.: +66 53 943367; fax: +66 53 357512.
*E-mail address:* supon@chiangmai.ac.th (S. Ananta).

0167-577X/$ - see front matter © 2005 Elsevier B.V. All rights reserved.
doi:10.1016/j.matlet.2005.11.043

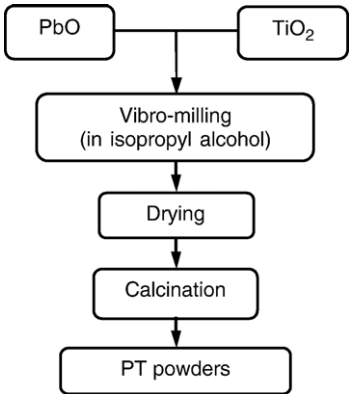


Fig. 1. Preparation route for PT powders.

Therefore, in this work, the effect of milling time on phase formation, and particle size of lead titanate powders was investigated in this connection. The potential of the vibro-milling technique as a simple and low-cost method to obtain usable quantities of single-phase lead titanate powders at low temperature and with nanosized particles was also examined.

## 2. Experimental procedure

Commercially available lead oxide, PbO (JCPDS file number 77-1971) and titanium oxide, $TiO_2$ (JCPDS file number 21-1272) (Fluka, >99% purity) were used in this study. The two oxide powders exhibited an average particle size in the range of 3 to 5 μm. $PbTiO_3$ powder was synthesized by the solid-state reaction of these raw materials. Powder-processing (Fig. 1) was carried out in a manner similar to that employed in the preparation of other materials, as described previously [12,13]. A vibratory laboratory mill (McCrone Micronizing Mill) powered by a 1/30 HP motor was employed for preparing the stoichiometric $PbTiO_3$ powders. The grinding vessel consists of a 125 ml capacity polypropylene jar fitted with a screw-capped, gasketless, polythene closure. The jar is packed with an ordered array of identical, cylindrical, grinding media of polycrystalline corundum. A total of 48 milling media cylinder with a powder weight of 20 g was kept constant in each batch. The milling operation was carried out in isopropanal inert to the polypropylene jar. Various milling times ranging from 0.5 to 35 h were selected in order to investigate the phase formation characteristic of lead titanate and the smallest particle size. After drying at 120 °C, the milled powders were calcined at 600 °C (inside a closed alumina crucible) for 1 h with heating/cooling rates of 20 °C $min^{-1}$ [11].

Table 1
Effect of milling time on the variation of particle size of PT powders measured by different techniques

| Milling time (h) | Per. phase (%) | XRD | | SEM | | Laser scattering | |
|---|---|---|---|---|---|---|---|
| | | *A* (nm) | *c*/*a* | *D* (nm) | *P* (nm) | *D* (nm) | *P* (nm) |
| 0.5 | 89.20 | 40 | 1.056 | 145 | 40–250 | 1090 | 140–2560 |
| 1 | 100 | 20.8 | 1.062 | 107 | 71–143 | 660 | 270–1090 |
| 5 | 100 | 22.5 | 1.059 | 101 | 67–135 | 690 | 290–1140 |
| 10 | 100 | 21.9 | 1.059 | 95 | 63–128 | 690 | 290–1140 |
| 15 | 100 | 22.0 | 1.061 | 78 | 43–114 | 4640 | 1640–7790 |
| 20 | 100 | 21.3 | 1.056 | 68 | 28–109 | 4800 | 1710–8060 |
| 25 | 100 | 21.5 | 1.057 | 63 | 17–109 | 180 | 70–310 |
| 30 | 100 | 21.5 | 1.052 | 93 | 43–143 | 170 | 70–290 |
| 35 | 100 | 21.4 | 1.053 | 92 | 56–128 | 3030 | 560–6180 |

Per. phase = Perovskite phase.
*A* = Crystallite size.
*c*/*a* = Tetragonality factor.
*D* = Average particle size.
*P* = Particle size distribution or range.

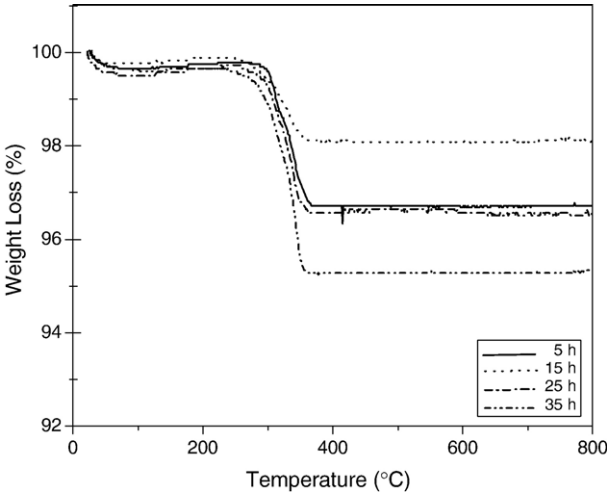


Fig. 2. TGA analysis of powder mixtures milled at different times.

The reactions of the uncalcined PT powders taking place during heat treatment were investigated by a combination of thermogravimetric and differential thermal analysis techniques (TG-DTA, Shimadzu) at a heating rate of 10 °C $min^{-1}$ in air from room temperature up to 1000 °C. All powders were subsequently examined at room temperature by X-ray diffraction (XRD; Siemens-D500 diffractometer) using Ni-filtered $CuK_\alpha$ radiation to identify the phases formed and optimum milling time for the production of $PbTiO_3$ powders having the smallest particle size. The relative amount of perovskite and secondary phases was determined from XRD patterns of the samples by measuring the major characteristic peak intensities

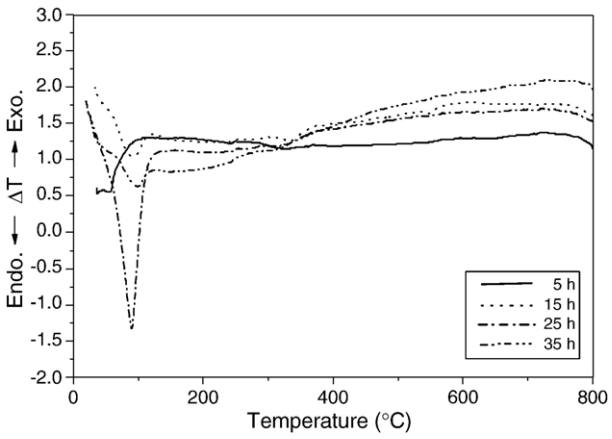


Fig. 3. DTA analysis of powder mixtures milled at different times.

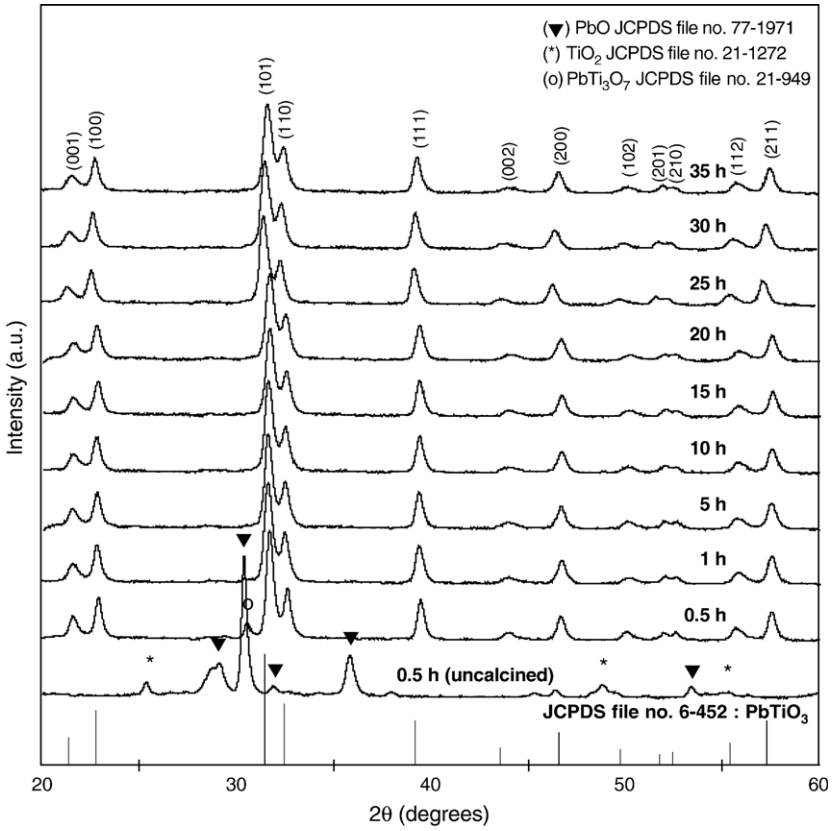


Fig. 4. XRD patterns of PT powders milled at different times (calcined at 600 °C for 1 h with heating/cooling rates of 20 °C $min^{-1}$).

for the perovskite (101) or $I_P$ and secondary (o) phases or $I_S$. The following qualitative equation was used [14].

$$\text{perovskite phase(wt\%)} = \frac{I_P}{I_P + I_S} \times 100 \quad (1)$$

The crystalline lattice constants, lattice strain and average particle size were also estimated from XRD patterns [15]. The particle size distributions of the powders were determined by laser diffraction technique (DIAS 1640 laser diffraction spectrometer) with the particle sizes and morphologies of the powders observed by scanning electron microscopy (JEOL JSM-840 A SEM). The particle sizes of PT powders milled at different times obtained from different measuring techniques are provided in Table 1.

## 3. Results and discussion

TGA and DTA results for the powders milled at different times are compared and shown in Figs. 2 and 3, respectively. In general, similar thermal characteristics are observed in all cases. As shown in Fig. 2, all

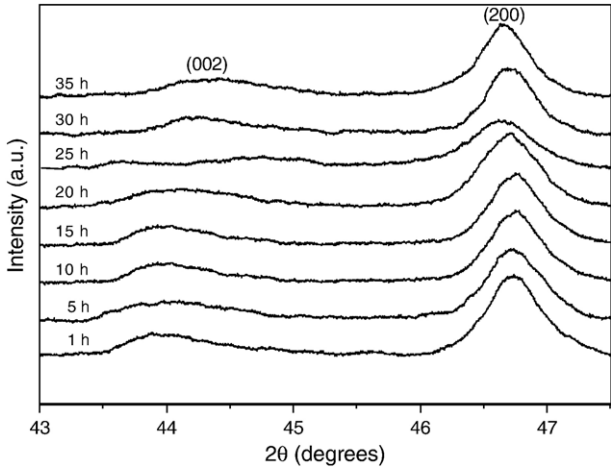


Fig. 5. Enlarged zone of XRD patterns showing (002) and (200) peaks broadening as a function of milling times.

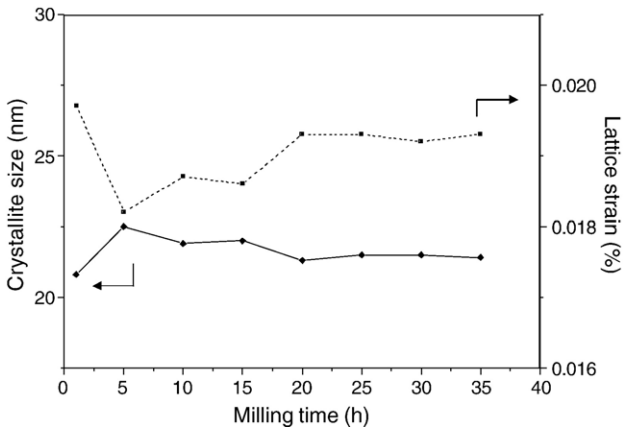


Fig. 6. Variation of crystalline size and lattice strain of PT powders as a function of milling times.

powders demonstrate two distinct weight losses below 400 °C. The first weight loss occurs below 100 °C and the second one above 200 °C. In the temperature range from room temperature to ~150 °C, all samples show exothermic peaks in the DTA curves at 120 °C (Fig. 3), which are related to the first weight loss. These DTA peaks can be attributed to the decomposition of the organic species originating from the milling process [11,16]. Corresponding to the second fall in specimen weight, by increasing the temperature up to ~800 °C, the solid-state reaction between lead oxide and titanium oxide occurs. The broad exothermic characteristic present in all the DTA curves represents that reaction, which has a maximum at ~600–750 °C. The slightly different temperature, intensities and shapes of the thermal peaks for the powders are probably related to the different sizes of the powders subjected to different milling times and, consequently, caused by the removal of organic species and rearrangement of differently bonded species in the network [16]. No further significant weight loss was observed for temperatures above 500 °C in the TGA curves, indicating that the minimum firing temperature to form PbO–$TiO_2$ compounds is in good agreement with XRD results (Fig. 4) and those of previous authors [17,18].

To further study the effect of milling time on phase formation, each of the powders milled for different times were calcined at 600 °C for 2 h in air, followed by phase analysis using XRD. For the purpose of estimating the concentrations of the phase present, Eq. (1) has been applied to the powder XRD patterns obtained, as given in Table 1. As shown in Fig. 4, for the uncalcined powder subjected to 0.5 h of vibro-

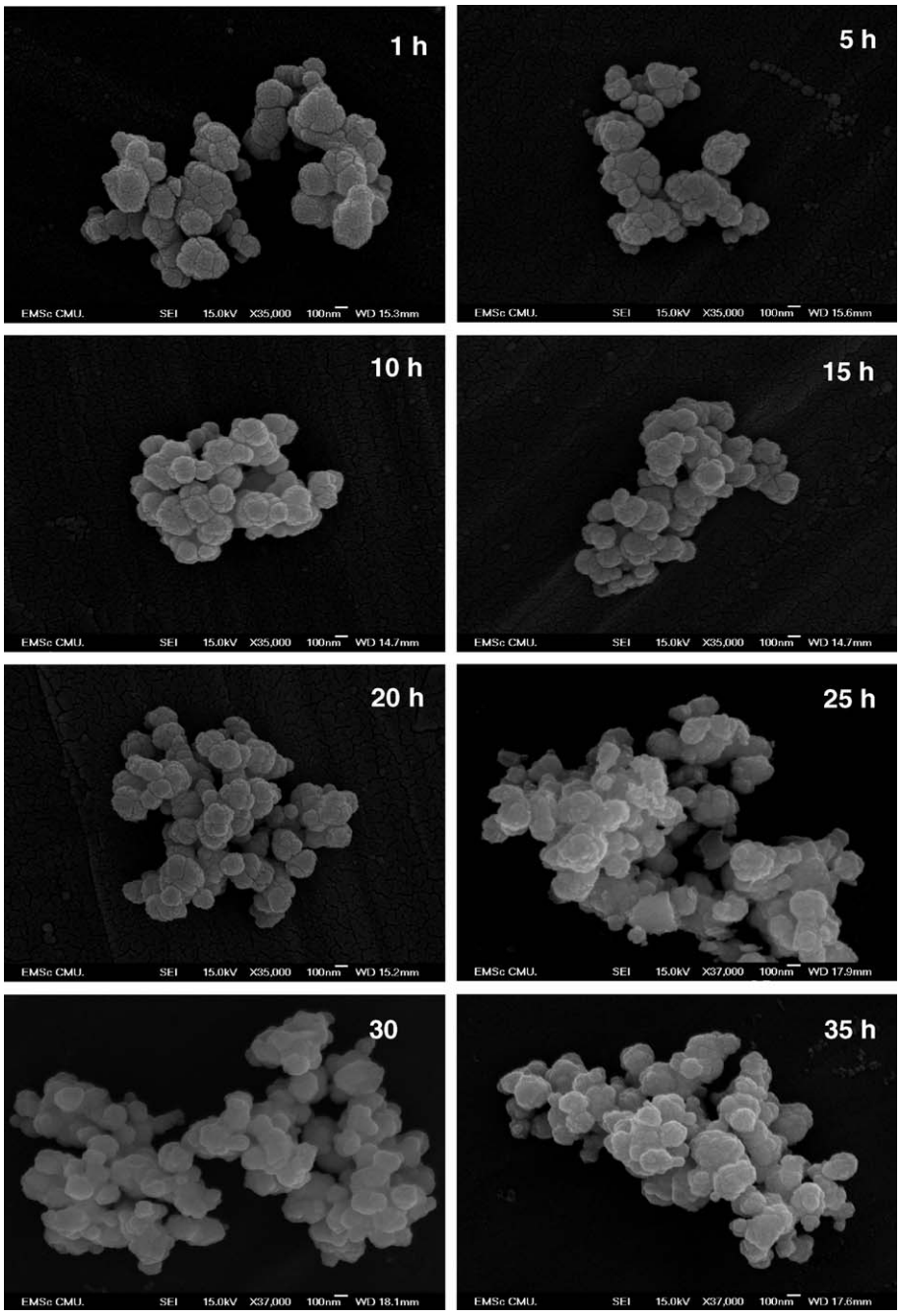


Fig. 7. SEM micrographs of PT powders milled at different times.

milling, only X-ray peaks of precursors PbO (▼) and $TiO_2$ (*) are present, indicating that no reaction had been initiated during the milling process. However, after calcinations at 600 °C, it is seen that the perovskite-type $PbTiO_3$ becomes the predominant phase in the powder milled for 0.5 h indicating that the reaction has occurred to a considerable extent. It is seen that ~11 wt.% of lead deficient phase, $PbTi_3O_7$ (o), reported by a number of workers [18,19] has been found only at a milling time of 0.5 h. This pyrochlore phase has a monoclinic structure with cell parameters $a$=107.32 pm, $b$=381.2 pm, c=657.8 pm and $\beta$=98.08° (JCPDS file number 21-949) [20]. This observation could be attributed mainly to the poor mixing capability under short milling time. With milling time of 1 h or more, it is apparent that a single phase perovskite PT (yield of 100% within the limitations of the XRD technique) was found to be possible after the same calcination process was applied.

In general, the strongest reflections found in the majority of these XRD patterns indicate the formation of the lead titanate, $PbTiO_3$. These can be matched with JCPDS file number 6-452 for the tetragonal phase, in space group $P4/mmm$ with cell parameters $a$=389.93 pm and $c$=415.32 pm [21], in consistent with other works [10,11]. It should be noted that no evidence for the introduction of impurity due to wear debris from the milling process was observed in any of the calcined powders (within the milling periods of 0.5–35 h), demonstrating the effectiveness of the vibro-milling technique for the production of high purity PT nanopowders.

Moreover, it has been observed that with increasing milling time, all diffraction lines broaden, e.g. (002) and (200) peaks, an indication of a continuous decrease in particle size and of the introduction of lattice strain, as shown in Fig. 5. These values indicate that the particle size affects the evolution of crystallinity of the phase formed by prolonged milling treatment (Fig. 6). For PT powders, the longer the milling time, the finer is the particle size, up to a certain level (Table 1). The results suggest that the steady state of the vibro-milling is attained at ~20 h of milling. Moreover, it is worthy to note that, in this condition, the mean crystalline size is close to ~21 nm. Also, the relative intensities of the Bragg peaks and the calculated tetragonality factor ($c/a$) for the powders tend to decrease with the increase of milling time. However, it is well documented that, as Scherer's analysis provides only a measurement of the extension of the coherently diffracting domains, the particle sizes estimated by this method can be significantly under

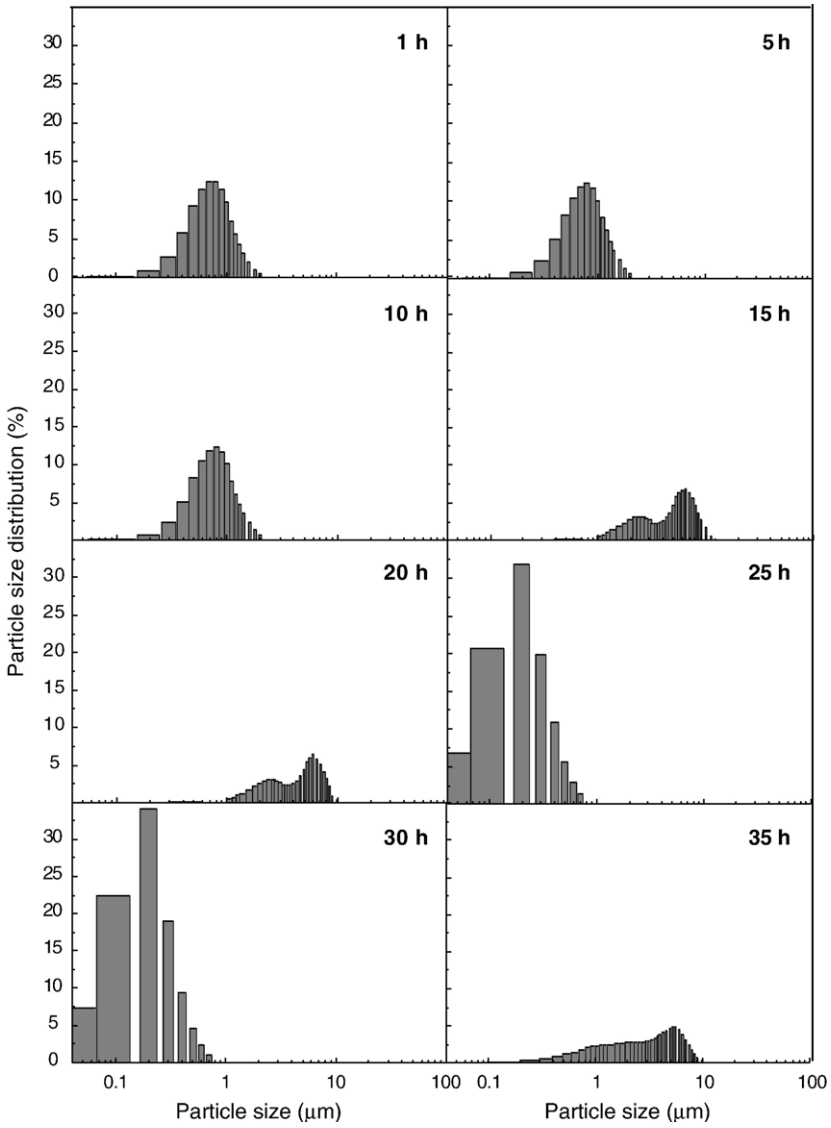


Fig. 8. Particle size distributions of PT powders milled at different times.

estimated [22]. In addition to strain, factors such as dislocations, stacking faults, heterogeneities in composition and instrumental broadening can contribute to peak broadening, making it almost impossible to extract a reliable particle size solely from XRD [15,23].

In this connection, scanning electron microcopy was also employed for particle size measurement (Table 1). The morphological evolution of the powders as a function of milling time was also revealed, as illustrated in the SEM micrographs (Fig. 7). At first sight, the morphological characteristic of PT powders with various milling times is similar for all cases. In general, the particles are agglomerated and basically irregular in shape, with a substantial variation in particle sizes. The powders consist of primary particles nanometers in size. Increasing the milling time over the range 0.5 to 35 h, the average size of the PT particle decreases significantly, until at 25 h, the smallest particle size (estimated from SEM micrographs to be ~17 nm) is obtained. However, it is also of interest to point out that a larger particle size was obtained for a milling time longer than 25 h. This may be attributed to the occurrence of hard agglomeration with strong inter-particle bonds within each aggregate resulting from dissipated heat energy of prolonged milling [24]. Fig. 7 also illustrates that vibro-milling has slightly changed the shape of the particles which become more equiaxed at long milling times. At the same time, the particle size is reduced. Fracture is considered to be the major mechanism at long milling times.

The effect of milling time on particle size distribution was found to be significant, as shown in Fig. 8. After milling times of 1, 5 and 10 h, the powders have a similar particle size distribution. They exhibit a single peak covering the size ranging from 0.2 to 1.1 μm. With increasing milling times to 15 and 20 h, the distribution curve of particle size separates into two groups. First is a monomodal distribution corresponding to the primary size of the $PbTiO_3$ particles. The second group (peak) is believed to arise mainly from particle agglomeration. By increasing the milling time to 25 and 30 h, a uniform particle size distribution with a much lower degree of particle agglomeration (<1 μm) is found. However, upon further increase of milling time up to 35 h, a bimodal distribution curve with peak broadening between 0.5 and 6.2 μm is observed again. Table 1 compares the results obtained for PT powders milled for different times via different techniques. Variations in these data may be attributed mainly to the formation of hard and large agglomerations found in the SEM results.

In this work, it is seen that the optimum milling time for the production of the smallest nanosized high purity PT powder was found to be at 25 h. The finding of this investigation indicates a strong relationship between the vibro-milling process and the yield of PT nanopowders. However, further investigation is required for the control and optimization of the PT formation. Studies on the effect of milling parameters and particle size distribution on phase formation kinetics would be useful for the particle size control. In case of the vibro-milling technique, other factors such as the milling speed, milling scale and type of milling media also need be taken into account.

## 4. Conclusion

The results infer that the milling time influences not only on the development of the solid-state reaction of lead titanate phase but also the particle size and morphology. The resulting PT powders have a range of particle size, depending on milling times. Production of a single-phase lead titanate nanopowder can be successfully achieved by employing a combination of 25 h milling time and calcination conditions of 600 °C for 2 h, with heating/cooling rates of 20 °C $min^{-1}$.

## Acknowledgement

This work was supported by the Thailand Research Fund (TRF) and the Faculty of Science, Chiang Mai University. One of the authors (R.W.) wishes to acknowledge Maejo University for financial support during her study and also the Graduate School of Chiang Mai University.

## References

[1] A.J. Moulson, J.M. Herbert, Electroceramics, 2nd ed.Wiley, Chichester, 2003.
[2] B. Jaffe, W.R. Cook, H. Jaffe, Piezoelectric Ceramics, Academic Press, New York, 1971.
[3] O. Bouquin, M. Lejeune, J.P. Boilot, J. Am. Ceram. Soc 74 (1991) 1152.
[4] T.R. Gururaja, A. Safari, A. Halliyal, Am. Ceram. Soc. Bull. 65 (1986) 1601.
[5] J.S. Wright, L.F. Francis, J. Mater. Res. 8 (1993) 1712.
[6] G.R. Fox, J.H. Adair, R.E. Newnham, J. Mater. Sci. 25 (1990) 3634.
[7] A. Rujiwatra, J. Jongphiphan, S. Ananta, Mater. Lett. 59 (2005) 1871.
[8] V.V. Dabhade, T.R. Rama Mohan, P. Ramakrishman, Appl. Surf. Sci. 182 (2001) 390.
[9] S. Ananta, Mater. Lett. 58 (2004) 2781.
[10] A. Udomporn, S. Ananta, Curr. Appl. Phys. 4 (2004) 186.
[11] A. Udomporn, S. Ananta, Mater. Lett. 58 (2003) 1154.
[12] S. Ananta, N.W. Thomas, J. Eur. Ceram. Soc. 19 (1999) 155.
[13] S. Ananta, R. Brydson, N.W. Thomas, J. Eur. Ceram. Soc. 20 (2000) 2315.
[14] S.L. Swartz, T.R. Shrout, Mater. Res. Bull. 17 (1982) 1245.
[15] H. Klug, L. Alexander, X-Ray Diffraction Procedures for Polycrystalline and Amorphous Materials, 2nd ed.Wiley, New York, 1974.
[16] S. Ananta, R. Tipakonitikul, T. Tunkasiri, Mater. Lett. 57 (2003) 2637.
[17] C.G. Pillai, P.V. Ravindran, Thermochim. Acta 66 (1996) 109.
[18] J. Tartaj, C. Moure, L. Lascano, P. Duran, Mater. Res. Bull. 36 (2001) 2301.
[19] M.L. Calzada, M. Alguero, L. Pardo, J. Sol–Gel Sci. Technol. 13 (1998) 837.
[20] Powder Diffraction File No. 21-949. International Centre for Diffraction Data, Newtown Square, PA, 2000.
[21] Powder Diffraction File No. 6-452. International Centre for Diffraction Data, Newtown Square, PA, 2000.
[22] C. Suryanarayana, Prog. Mater. Sci. 46 (2001) 1.
[23] A. Revesz, T. Ungar, A. Borbely, J. Lendvai, Nanostruct. Mater. 7 (1996) 779.
[24] P.C. Kang, Z.D. Yin, O. Celestine, Mater. Sci. Eng., A Struct. Mater.: Prop. Microstruct. Process. 395 (2005) 167.

Available online at www.sciencedirect.com
SCIENCE DIRECT
Current Applied Physics 6 (2006) 520–524
Current Applied Physics
An official journal of the KPS
www.elsevier.com/locate/cap
www.kps.or.kr

# Effects of uniaxial stress on dielectric properties of ferroelectric ceramics

Rattikorn Yimnirun *, Supattra Wongsaenmai, Athipong Ngamjarurojana, Supon Ananta

*Department of Physics, Faculty of Science, Chiang Mai University, Chiang Mai 50200, Thailand*

Available online 27 December 2005

**Abstract**

The effects of uniaxial stress on the dielectric properties of ceramics in PMN–PZT system are investigated. Ceramics with the formula $(x)Pb(Mg_{1/3}Nb_{2/3})O_3$–$(1-x)Pb(Zr_{0.52}Ti_{0.48})O_3$ when $x = 0.0$, 0.1, 0.3, 0.5, 0.7, 0.9 and 1.0 are prepared by a conventional mixed-oxides method. The sintered ceramics are perovskite materials with their physical properties proportionally depending on the PMN and PZT contents. The dielectric properties under the uniaxial stress of the unpoled and poled PMN–PZT ceramics are observed at stress levels up to 5 MPa. For the unpoled ceramics, the dielectric properties do not change significantly with the applied stress and the changes are independent of the ceramic compositions. For the poled ceramics, on the other hand, the dielectric constant of the PZT-rich compositions increases slightly, while that of the PMN-rich compositions decreases with increasing applied stress. In addition, changes in the dielectric loss tangent with stress are found to be composition independent. This study clearly shows the influences of the domain re-orientation, domain wall motion, degradation and depoling mechanisms on the variation of the dielectric properties of PMN–PZT ceramics under the uniaxial stress.


*PACS:* 77.22.Ch; 77.84.Dy

*Keywords:* Uniaxial stress; Dielectric properties; Ferroelectric; PMN–PZT

## 1. Introduction

Ferroelectric ceramics have been established as good candidates for actuator and transducer applications. Widely used materials include barium titanate ($BaTiO_3$ or BT) and lead-based materials such as lead magnesium niobate ($Pb(Mg_{1/3}Nb_{2/3})O_3$ or PMN) and lead zirconate titanate ($Pb(Zr_{1-x}Ti_x)O_3$ or PZT) [1]. In many of these applications, ceramics are normally used under conditions where stresses are applied [2,3]. Despite this fact, materials constants used in any design calculations are often obtained from a stress-free measuring condition, which in turn may lead to incorrect or inappropriate actuator and transducer designs. It is therefore important to determine the properties of these materials as a function of applied stress. Previous investigations on the stress-dependence dielectric and electrical properties of many ceramic systems, such as PZT and PMN-PT have clearly emphasized the importance of this matter [4,5].

As a prototypic relaxor ferroelectric, PMN exhibits a high dielectric constant and a broad range transition of dielectric constant with temperature as a function of frequency [6]. In addition, PMN ceramics exhibit low loss and non-hysteretic characteristics. These make PMN a good candidate for a large number of applications, such as multilayer capacitors, sensors and actuators. However, PMN ceramics have relatively low electromechanical coupling coefficients, as compared to PZT. On the contrary to PMN, PZT ceramics have found several actuator and transducer applications due to their high electromechanical coupling coefficients and higher temperature of operation [7]. However, PZT ceramics are fairly lossy as a result of their highly hysteretic behavior, which makes them unsuited for applications that require high delicacy and reliability. Furthermore, PZT ceramics normally have a very high Curie temperature ($T_C$) in the vicinity of

* Corresponding author. Fax: +66 53 357 512.
*E-mail address:* rattikornyimnirun@yahoo.com (R. Yimnirun).

1567-1739/$ - see front matter © 2005 Elsevier B.V. All rights reserved.
doi:10.1016/j.cap.2005.11.053

400 °C. Usually many applications require that $T_C$ is close to ambient temperature. Therefore, there is a general interest to reduce the $T_C$ of PZT ceramics to optimize their uses. Forming a solid-solution of PZT and relaxor ferroelectrics has been one of the techniques employed to improve the properties of ferroelectric ceramics. With the complementary features of PMN and PZT, the solid solutions between PMN and PZT are expected to synergetically combine the properties of both ceramics, which could exhibit more desirable piezoelectric and dielectric properties for several technologically demanding applications than single-phase PMN and PZT [8,9]. Our previous investigation has emphasized synthesis and dielectric properties of ceramics in PMN–PZT system [10]. Since there has been no report on the stress-dependent properties of this ceramic system, this study is undertaken to investigate the influence of uniaxial stress on the dielectric properties of ceramics in PMN–PZT system.

## 2. Experimental methods

The $Pb(Mg_{1/3}Nb_{2/3})O_3$–$Pb(Zr_{0.52}Ti_{0.48})O_3$ ceramic composites were prepared from PMN and PZT powders by a mixed-oxide method. Perovskite-phase PMN powders were obtained via a well-known columbite method [11]. PZT powders, on the other hand, were prepared by a more conventional mixed-oxide method. The $(x)Pb(Mg_{1/3}Nb_{2/3})O_3$–$(1-x)Pb(Zr_{0.52}Ti_{0.48})O_3$ (when $x = 0.0$, 0.1, 0.3, 0.5, 0.7, 0.9, and 1.0) ceramic composites were then prepared from the starting PMN and PZT powders by a mixed-oxide method at various processing conditions. Detailed procedures of each method are described in earlier publication [10]. Various characterization techniques were employed to determine the physical and chemical characteristics of the sintered PMN–PZT ceramics. The densities of the sintered ceramics were measured by Archimedes method. The phase formations of the sintered specimens were studied by X-ray diffraction, while microstructure analyses were undertaken using a scanning electron microscopy. Grain size was determined from SEM micrographs by a linear intercept method. Results of these characterizations are described in our previous report and some important data are listed in Table 1.

Table 1
Characteristics of PMN–PZT ceramics with optimized processing conditions

| Ceramic | Density ($g/cm^3$) | Grain size range (μm) | Average grain size (μm) |
|---|---|---|---|
| PZT | $7.59 \pm 0.11$ | 2–7 | 5.23 |
| 0.1PMN–0.9PZT | $6.09 \pm 0.11$ | 0.5–2 | 0.80 |
| 0.3PMN–0.7PZT | $7.45 \pm 0.10$ | 0.5–3 | 1.65 |
| 0.5PMN–0.5PZT | $7.86 \pm 0.05$ | 0.5–5 | 1.90 |
| 0.7PMN–0.3PZT | $7.87 \pm 0.07$ | 1–4 | 1.40 |
| 0.9PMN–0.1PZT | $7.90 \pm 0.09$ | 1–4 | 1.50 |
| PMN | $7.82 \pm 0.06$ | 2–4 | 3.25 |

For dielectric property characterizations, the sintered samples were lapped to obtain parallel faces, and the faces were then coated with silver paint as electrodes. The samples were heat-treated at 750 °C for 12 min to ensure the contact between the electrodes and the ceramic surfaces. The samples were subsequently poled in a silicone oil bath at a temperature of 120 °C by applying a dc field of 25 kV/cm for 30 min and field-cooled to room temperature. To study the effects of the uniaxial stress on the dielectric properties, a uniaxial compressometer was constructed. The details of the system are described elsewhere [12]. The dielectric properties were measured through spring-loaded pins connected to the LCZ-meter (Hewlett Packard, model 4276A). The capacitance and the dielectric loss tangent were determined at frequency of 1 kHz and room temperature (25 °C). The dielectric constant was then calculated from a parallel-plate capacitor equation, e.g. $\varepsilon_r = Cd/\varepsilon_0 A$, where $C$ is the capacitance of the sample, $d$ and $A$ are the thickness and the area of the electrode, respectively, and $\varepsilon_0$ is the dielectric permittivity of vacuum ($8.854 \times 10^{-12}$ F/m).

## 3. Results and discussion

### 3.1. Physical properties

The optimized density of sintered $x$PMN–$(14-x)$PZT ceramics is listed in Table 1. It is observed that the compositions with $x = 0.1$ and 0.3 show relatively lower density than other compositions. This suggests that the addition of a small amount of PMN to the PMN–PZT compositions results in a significant decrease in the density of the ceramics. However, further addition of PMN into the compositions increased the density again. A similar result was reported in previous investigation [13]. In addition, the grain size of the PMN–PZT ceramics, as determined from the SEM micrographs, varied considerably from <1 to 7 μm, as tabulated in Table 1. It is of interest to see that the average grain size of all the mixed compositions is much smaller than that of the pure PZT and PMN materials. The reason for the changes of the density and the smaller grain sizes in the mixed compositions is not clearly understood, but this may be a result of PMN's role as a grain-growth inhibitor in the PMN–PZT composites. Results from XRD studies indicate that PZT ceramic is identified as a single-phase material with a perovskite structure having tetragonal symmetry, while PMN ceramic is a perovskite material with a cubic symmetry [14]. All PMN–PZT ceramic composites exhibit pseudo-cubic crystal structure, as reported in previous investigations [8,13,14].

### 3.2. Uniaxial stress dependence of the dielectric propertie of the unpoled ceramics

The experimental results of the uniaxial stress-dependence of the dielectric properties of the unpoled PMN–PZT ceramics are shown in Figs. 1 and 2. There is a trivial

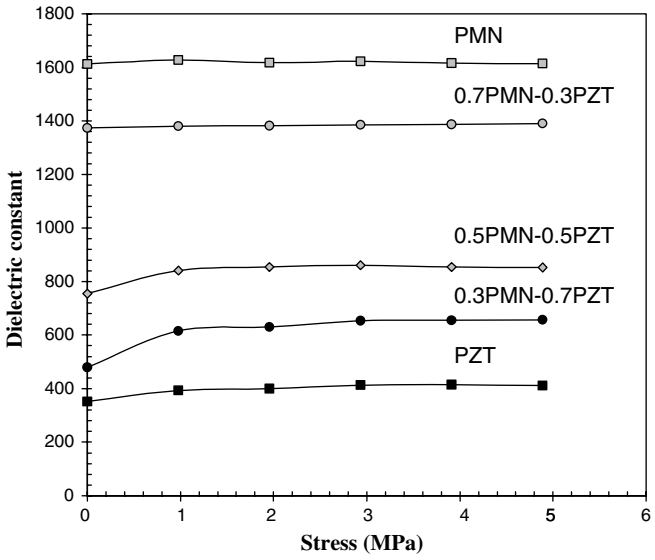


Fig. 1. Uniaxial stress dependence of dielectric constant of unpoled PMN–PZT ceramics.

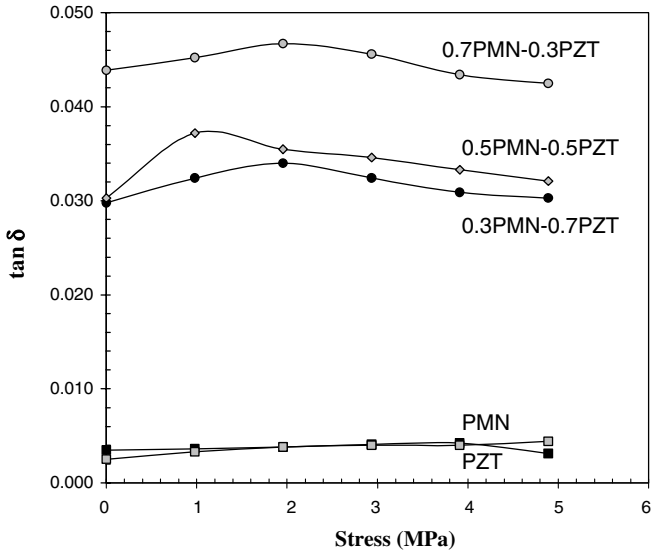


Fig. 2. Uniaxial stress dependence of dielectric loss tangent of unpoled PMN–PZT ceramics.

change of both the dielectric constant and the dielectric loss tangent of the ceramics when the applied stress increases from 0 to 1 MPa. However, these properties then become relatively constant when the applied stress increases further. This is a result of the randomness of the domain orientations in the unpoled ceramics. Since there is only a small portion of the domains that is aligned in the direction parallel or nearly parallel to the direction of the applied stress, the initial increase in the applied stress would then result in motion of these domains in favor of the applied stress, hence increasing dielectric constant and dielectric loss tangent. However, once all these domains are re-oriented, further increase in the applied stress would result in no change in the dielectric properties. The slight decrease in the dielectric loss tangent is probably an indication of the de-aging effect [15,16]. The non-180 °C domain re-orientations are the basic mechanism responsible for the changes in the dielectric properties with the applied stress. In addition, it was also found that the changes of the dielectric properties were composition independent.

### 3.3. Uniaxial stress dependence of the dielectric properties of the poled ceramics

The experimental results for the poled PMN–PZT ceramics are shown in Figs. 3 and 4. There is a significant change of both the dielectric constant and the dielectric loss tangent of the ceramics when the applied stress increases from 0 to 5 MPa. The changes of the dielectric constant with the applied stress can be divided into two different groups. For PMN-rich compositions (PMN, 0.9PMN–0.1PZT, and 0.7PMN–0.3PZT), the dielectric constant generally decreases with increasing applied stress. However, it should be noticed that only PMN and 0.9PMN–0.1PZT compositions show definite decreases in the dielectric constant, while the dielectric constant of the 0.7PMN–0.3PZT composition initially increases then decreases with very little difference in the dielectric constant between the 0 and 5 MPa. On the other hand, for PZT-rich compositions (PZT, 0.1PMN–0.9PZT, 0.3PMN–0.7PZT, and 0.5PMN–0.5PZT), the dielectric constant rises slightly when the applied stress increases from 0 to 1 MPa, and becomes relatively constant when the applied stress increases further. The dielectric loss tangent for most compositions, except for PMN and PZT, is found to first increase when the applied stress is raised from 0 to 1 MPa, and then decrease with further increasing stress. However, for PZT ceramic the dielectric loss tangent increases monotonously with the increasing stress, while PMN ceramic exhibits a slight

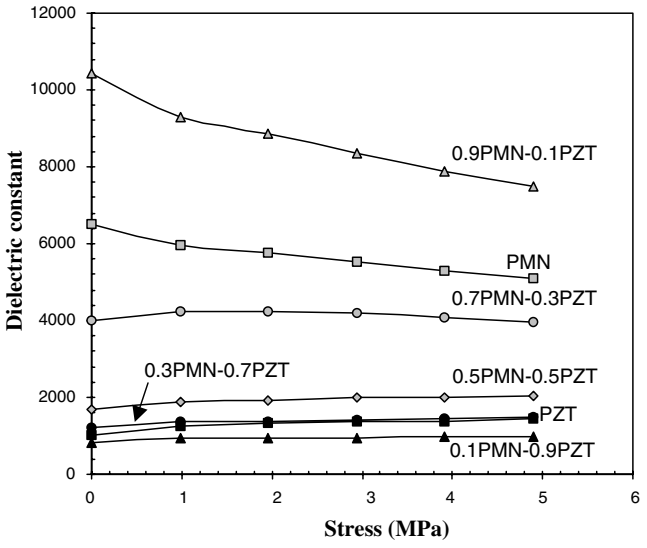


Fig. 3. Uniaxial stress dependence of dielectric constant of poled PMN–PZT ceramics.

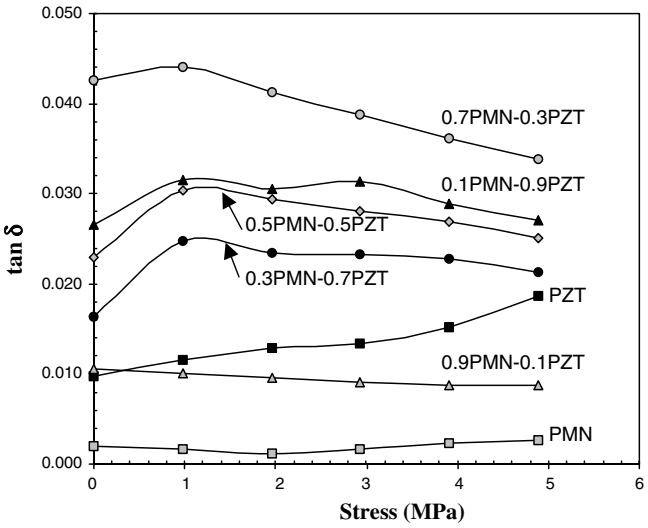


Fig. 4. Uniaxial stress dependence of dielectric loss tangent of poled PMN–PZT ceramics.

increase in the dielectric loss tangent followed by a drop, the turning point being around 2 MPa.

To understand these experimental results for the poled ceramics, various effects have to be considered. Normally, the properties of ferroelectric materials are derived from both the intrinsic contribution, which is the response from a single domain, and extrinsic contributions, which are from domain wall motions [15,16]. When a mechanical stress is applied to a ferroelectric material, the domain structure in the material will change to maintain the domain energy at a minimum; during this process some of the domains engulf other domains or change shape irreversibly. Under a uniaxial stress, the domain structure of ferroelectric ceramics may undergo domain switching, clamping of domain walls, de-aging, and de-poling [16].

In this study, the results for the case of PZT-rich compositions can easily be explained with the above statements. When the compressive uniaxial stress is applied in the direction parallel to the polar axis (poling) direction, the stress will move some of the polarization away from the poling direction resulting in a change in domain structures [15]. This change increases the non-180 °C domain wall density. Hence the increase of the dielectric constant is observed. The de-aging mechanism is also expected to play a role here. However, the stress clamping of domain walls and the de-poling mechanisms are not expected at this relative low stress level used in this study [15–17]. Therefore, a combination of the domain switching and the de-aging mechanisms is believed to be a reason for the slight increase of the dielectric constant with increasing applied stress in the PZT-rich compositions, as shown in Fig. 3. Since PMN is a relaxor ferroelectric material, the situation is very different for PMN-rich compositions. The stress dependence of the dielectric constant of the compositions is attributed to competing influences of the intrinsic contribution of non-polar matrix and the extrinsic contribution of re-polarization and growth of micro-polar regions [15,18]. Since the dielectric response of both contributions is affected by the applied stress in an opposite way, the behavior of the composites depends on the ratio between the micro-polar region and the non-polar matrix. Since the measurements are carried out at the room temperature, the micro-polar regions dominate the dielectric response of the composites [18]. Therefore, the dielectric constant of the PMN-rich compositions decreases with increasing applied stress, as seen in Fig. 3.

The cause of the stress dependence of the dielectric loss tangent is a little more straightforward than that of the dielectric constant. As depicted in Fig. 4, an increase in domain wall mobility clearly enhances the dielectric loss tangent in some compositions, while the de-aging in the materials normally causes the decrease of the dielectric loss tangent observed in some compositions [16,17]. More importantly, these results clearly demonstrate that the contribution of each mechanism to the dielectric responses of the PMN–PZT ceramic depends on the compositions and the stress level.

The results obtained for the poled ceramics are significantly different from those for the unpoled ones. In the poled ceramics, considerable changes of both the dielectric constant and dielectric loss tangent that depend upon the ceramic compositions are clearly observed. This distinct difference between the two ceramic groups can be intuitively attributed to the more active electrically re-oriented domains available in the poled ceramics. Clearly, these results demonstrate the contribution of the domain re-orientation procedure, e.g. poling, to the dielectric responses to external stresses in the PMN–PZT ceramics.

## 4. Conclusions

In this study, the $(x)Pb(Mg_{1/3}Nb_{2/3})O_3$–$(1-x)Pb(Zr_{0.52}Ti_{0.48})O_3$ (when $x = 0.0$, 0.1, 0.3, 0.5, 0.7, 0.9, and 1.0) ceramic composites were successfully prepared by a conventional mixed-oxide method at various processing conditions. The phase formation behavior, the microstructure features were studied using XRD and SEM techniques, respectively. The physical properties measurements revealed that the properties were relatively composition-dependent. The dielectric properties under the uniaxial stress of the unpoled and poled PMN–PZT ceramics were observed at stress levels up to 5 MPa using a calibrated uniaxial compressometer. For the unpoled PMN–PZT ceramics, the dielectric constant increased with increasing stress between 0 and 1 MPa and became relatively constant when the applied stress was further increased. On the other hand, the dielectric loss tangent first rises and then drops with increasing applied stress. Furthermore, the changes of the dielectric constant of these unpoled PMN–PZT ceramics are independent of the ceramic compositions. In the case of the poled ceramics, the results clearly show that the dielectric constant of the PMN-rich compositions decreases, while that of the PZT-rich compositions increases slightly, with increasing applied stress. However, the dielectric loss

tangent for most of the compositions first rises and then drops with increasing applied stress. It is very great interest to observe that the results for the unpoled PMN–PZT ceramics are significantly different from those for the poled PMN–PZT ceramics. This study shows that the applied stress has significant influences on the dielectric properties of the PMN–PZT ceramic composites.

## Acknowledgement

This work is supported by the Thailand Research Fund (TRF), Faculty of Science and Graduate School of Chiang Mai University.

## References

[1] L.E. Cross, Mater. Chem. Phys. 43 (1996) 108.
[2] K.V.R. Murty, S.N. Murty, K.C. Mouli, A. Bhanumathi, Proc. IEEE ISAF 1 (1992) 144.
[3] J.H. Yoo, H.S. Yoon, Y.H. Jeong, C.Y. Park, Proc. IEEE Ultra. Symp. 1 (1998) 981.
[4] D. Viehland, J. Powers, J. Appl. Phys. 89 (2001) 1820.
[5] J. Zhao, A.E. Glazounov, Q.M. Zhang, Appl. Phys. Lett. 74 (1999) 436.
[6] S.M. Gupta, A.R. Kulkarni, Mater. Chem. Phys. 39 (1994) 98.
[7] L.E. Cross, Ferroelectrics 76 (1987) 241.
[8] H. Ouchi, J. Am. Ceram. Soc. 51 (1968) 169.
[9] Y. Abe, Y. Yanagisawa, K. Kakagawa, Y. Sasaki, Solid State Commun. 113 (2000) 331.
[10] R. Yimnirun, S. Ananta, P. Laoratanakul, Mater. Sci. Eng. B 112 (2004) 79.
[11] S.L. Swartz, T.R. Shrout, Mater. Res. Bull. 17 (1982) 1245.
[12] R. Yimnirun, P.J. Moses, R.J. Meyer, R.E. Newnham, Rev. Sci. Instrum. 74 (2003) 3429.
[13] H. Ouchi, K. Nagano, S.J. Hayakawa, J. Am. Ceram. Soc. 48 (1965) 630.
[14] V. Koval, C. Alemany, J. Briancin, H. Brunckova, K. Saksl, J. Euro. Ceram. Soc. 23 (2003) 1157.
[15] Q.M. Zhang, J. Zhao, K. Uchino, J. Zheng, J. Mater. Res. 12 (1997) 226.
[16] G. Yang, S.F. Liu, W. Ren, B.K. Mukherjee, Proc. SPIE Symp. Smart Struct. Mater. 3992 (2000) 103.
[17] G. Yang, W. Ren, S.F. Liu, A.J. Masys, B.K. Mukherjee, Proc. IEEE Ultra. Symp. 1 (2000) 1005.
[18] J. Zhao, Q.M. Zhang, V. Mueller, Proc. IEEE ISAF 1 (1998) 361.

ELSEVIER

Materials Science and Engineering B 130 (2006) 246–253

MATERIALS SCIENCE & ENGINEERING B

www.elsevier.com/locate/mseb

# Effects of milling method and calcination condition on phase and morphology characteristics of $Mg_4Nb_2O_9$ powders

R. Wongmaneerung [a], T. Sarakonsri [b], R. Yimnirun [a], S. Ananta [a,*]

[a] *Department of Physics, Faculty of Science, Chiang Mai University, Chiang Mai, 50200, Thailand*
[b] *Department of Chemistry, Faculty of Science, Chiang Mai University, Chiang Mai, 50200, Thailand*

Received 9 November 2005; received in revised form 23 February 2006; accepted 19 March 2006

**Abstract**

Magnesium niobate, $Mg_4Nb_2O_9$, powders has been synthesized by a solid-state reaction. Both conventional ball- and rapid vibro-milling have been investigated as milling methods, with the formation of the $Mg_4Nb_2O_9$ phase investigated as a function of calcination conditions by DTA and XRD. The particle size distribution of the calcined powders was determined by laser diffraction technique, while morphology, crystal structure and phase composition were determined via a combination of SEM, TEM and EDX techniques. The type of milling method together with the designed calcination condition was found to show a considerable effect on the phase and morphology evolution of the calcined $Mg_4Nb_2O_9$ powders. It is seen that optimization of calcination conditions can lead to a single-phase $Mg_4Nb_2O_9$ in both milling methods. However, the formation temperature and dwell time for single-phase $Mg_4Nb_2O_9$ powders were lower with the rapid vibro-milling technique.


*Keywords:* Magnesium niobate; Milling; Calcination; Phase formation; X-ray diffraction

## 1. Introduction

To date, magnesium niobate, $Mg_4Nb_2O_9$, is one of the four possible magnesium–niobium oxides which have been recognized [1]. It has an ordered corundum-type hexagonal structure and has been investigated as a potential candidate for the synthesis of low loss microwave dielectric materials [2] and as buffer layer materials for manufacturing ferroelectric memory devices [3]. It is also an important material which shows self activated photoluminescence at room temperature [4]. You et al. [5] reported that cerium-doped $Mg_4Nb_2O_9$ exhibited improved luminescence properties. Recent work on the preparation of relaxor ferroelectric $Pb(Mg_{1/3}Nb_{2/3})O_3$ [6,7], has also shown that $Mg_4Nb_2O_9$ is a better precursor than the columbite $MgNb_2O_6$ [8,9] for the successful preparation of single-phase perovskite PMN which is becoming increasingly important for electroceramic components such as multilayer ceramic capacitors and electrostrictive actuators [10–12].

The evolution of a method to produce particular powders of precise stoichiometry and desired properties is complex, depending on a number of variables such as raw materials, their purities, processing history, temperature, time, etc. For example, the synthesis of stoichiometric lead magnesium niobate (PMN) using $Mg_4Nb_2O_9$ as a key precursor by a conventional solid-state reaction [7] requires an additional amount of PbO to convert the pyrochlore phase to PMN. However, the effect of excess PbO on PMN preparation is still a matter of debate, and appears to depend critically on the amount of PbO added [13–15]. Determination of the appropriate excess of PbO is currently a matter of trial and error. Furthermore, it has been reported that residual MgO present in the sample after the reaction has to be removed by treating with dilute nitric acid. Interestingly, a two-stage mixed oxide route has also been employed with minor modifications in the synthesis of $Mg_4Nb_2O_9$ itself [16,17]. In general, production of single-phase $Mg_4Nb_2O_9$ is not straightforward, as minor concentrations of the $MgNb_2O_6$ phases and/or MgO inclusion are sometimes formed alongside the major phase of $Mg_4Nb_2O_9$ [15,17,18].

The development of $Mg_4Nb_2O_9$ powders, to date, has not been as extensive as that of $MgNb_2O_6$. Much of the work concerning the compound $Mg_4Nb_2O_9$ has been directed towards determining luminescent [4,5] or microwave dielectric [2] properties, and fabrication of $Mg_4Nb_2O_9$ single crystal [19] or PMN powders [6,7]. Only limited attempts have been made to improve

* Corresponding author. Tel.: +66 53 943367; fax: +66 53 943445.
*E-mail address:* suponananta@yahoo.com (S. Ananta).

0921-5107/$ – see front matter © 2006 Elsevier B.V. All rights reserved.
doi:10.1016/j.mseb.2006.03.027

the yield of $Mg_4Nb_2O_9$ powders derived from the solid-state reaction by optimizing milling method or calcination condition [13,20,21]. Moreover, the optimization of a combination between the milling method and the calcination condition in the mixed oxide process has not been studied. The purpose of this work was to explore a simple mixed oxide synthetic route for the production of $Mg_4Nb_2O_9$ powders and compare the characteristics of the resulting powders. Two milling techniques were employed as the mixing method. A conventional ball milling was compared against a rapid vibro-milling in terms of their phase formation, particle size, morphology and microchemical compositions of the powders calcined at various conditions.

## 2. Experimental procedure

The starting materials used in the present study were commercially available magnesium oxide, MgO and niobium oxide, $Nb_2O_5$ (Fluka, 98% purity). These two oxide powders exhibited an average particle size in the range of 5.0–10.0 μm. $Mg_4Nb_2O_9$ powders were synthesized by the solid-state reaction of appropriate amounts of MgO and $Nb_2O_5$ powders that were mixed using two wet-milling methods (Fig. 1). The ball-milling operation was carried out for 48 h [7,13,20,22] with zirconia balls [22] in isopropanal. For comparison, a McCrone vibro-milling technique [9] was carried out on another set of powders with corundum cylindrical media in isopropanal for 1 h [21]. After drying at 120 °C for 2 h, various calcination conditions, i.e. temperatures ranging from 550 to 1100 °C and dwell times ranging from 2 to 5 h with heating/cooling rates ranging from 10 to 30 °C/min. [22] were applied in order to investigate the formation of $Mg_4Nb_2O_9$ phase in powders from both milling methods. The reactions of the uncalcined powders taking place during heat treatment were investigated by thermal gravimetric and differential thermal analysis (TG-DTA, Shimadzu) using a heating rate of 10 °C/min. in air from room temperature up to 1100 °C. Calcined powders were subsequently examined by room temperature X-ray diffraction (XRD; Philips PW 1729 diffractometer) using Ni filtered Cu Kα radiation, to identify the phases formed and optimum calcination conditions for the manufacture of $Mg_4Nb_2O_9$ powder. The mean crystallite size was determined using the diffraction peak (1 0 4) of the corundum pattern by using Scherrer equation [23]. Particle size distributions of the powders were determined by laser diffraction technique (DIAS 1640 laser diffraction spectrometer), with the grain size and morphologies of the powders observed by scanning electron microscopy (SEM; JEOL JSM-840A). The chemical composition and structure of the phases formed were elucidated by transmission electron microscopy (CM 20 TEM/STEM) operated at 200 keV and fitted with an energy-dispersive X-ray (EDX) analyzer with an ultra-thin window. EDX spectra were quantified with the virtual standard peaks supplied with the Oxford Instruments eXL software. Powder samples were dispersed in solvent and deposited by pipette on to 3 mm holey copper grids for TEM observation. In addition, attempt was made to evaluate the crystal structures of the observed compositions/phases by correcting the XRD and TEM diffraction data.

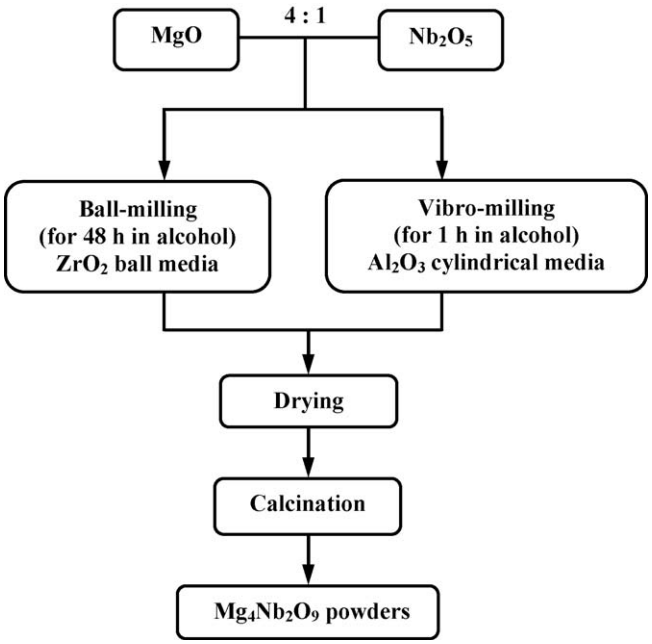


Fig. 1. Flow chart for preparing $Mg_4Nb_2O_9$ powders by ball- and vibro-milling methods.

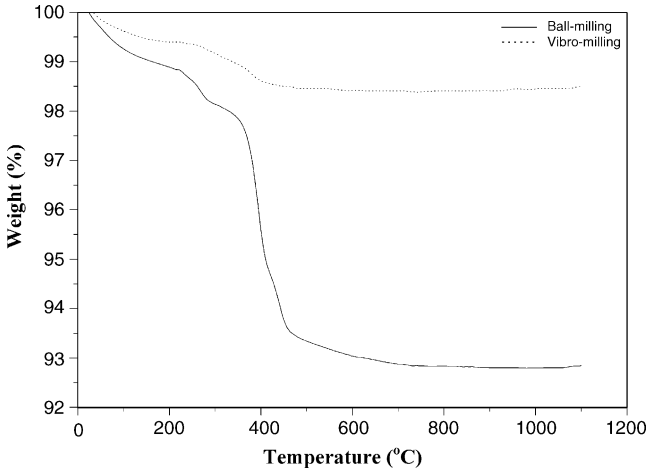


Fig. 2. TGA curves of the two MgO–$Nb_2O_5$ mixtures derived from (a) ball-milling and (b) vibro-milling methods.

## 3. Results and discussion

TGA and DTA results for the mixture of MgO and $Nb_2O_5$ milled by both methods are shown in Figs. 2 and 3, respectively. In general, similar trend of thermal characteristics is observed in both precursors. As shown in Fig. 2, the precursors prepared with both milling methods exhibit two distinct weight losses below 600 °C. The first weight loss occurs below 200 °C and the second one above 250 °C. In the temperature range from room temperature to ∼150 °C, both samples show small exothermic peaks in the DTA curves at ∼120 °C (Fig. 3), which are related to the first weight loss. These DTA peaks can be attributed to the decomposition of the organic species such as rubber lining from the milling process similar to those reported earlier [20]. In comparison between the two milling methods,

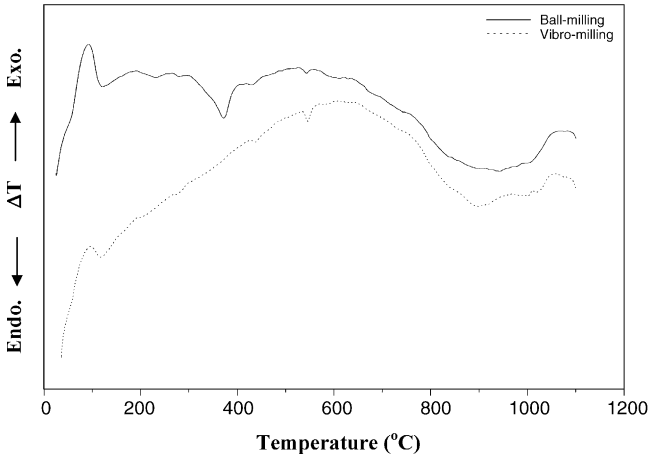


Fig. 3. DTA curves of the two MgO–$Nb_2O_5$ mixtures derived from (a) ball-milling and (b) vibro-milling methods.

after the first weight loss, the ball-milling precursor (solid line) shows a slightly less weight loss over the temperature range of ~150–250 °C, followed by a much more sharp fall in specimen weight with increasing temperature from ~250–500 °C. This precursor also exhibits a significantly larger overall weight loss (~7.25%) than that of the vibro milling (~1.50%). This may be accounted for by the fact that the vibro-milling method provides faster size reduction rate and is able to enhance mixing capability with lower contamination possibility due to shorter milling time applied as suggested by several authors [9,24,25].

Corresponding to the second fall in specimen weight, by increasing the temperature up to ~700 °C, the solid-state reaction occurs between magnesium oxide and niobium oxide. The broad exothermic characteristic in both DTA curves represents that reaction, which has a maximum at ~550 and 620 °C for ball- and vibro-milling precursors, respectively. No significant weight loss was observed for the temperatures above 800 °C in the TG curves (Fig. 2), indicating that the minimum firing temperature to obtain MgO–$Nb_2O_5$ compounds is in good agreement with XRD results (Figs. 4 and 5) and other workers [6,9,16]. However, the DTA curves show that there are other small peaks with maximum at ~1080 °C (for ball-milling) and 1050 °C (for vibro-milling). It is to be noted that there is no obvious interpretation of these peaks, although it is likely to correspond to a phase transition reported by a number of workers [14,17,22]. The different temperature, intensities, and shapes of the thermal peaks for the two precursors are probably related to the different milling conditions between the two methods, and consequently caused by the removal of organic species (such as rubber lining) and reactivity of species differently milled (difference in size and size distribution) and mixed in the powders. These data were used to define the range of temperatures for XRD investigation to between 550 and 1100 °C.

To further study the phase development with increasing calcination temperature in each of the two precursors, they were calcined for 2 h in air with a constant heating/cooling rates of 10 °C/min at various temperatures, up to 1100 °C, followed by phase analysis using XRD. As shown in Figs. 4 and 5, for the powders calcined at 550 °C, only X-ray peaks of MgO and

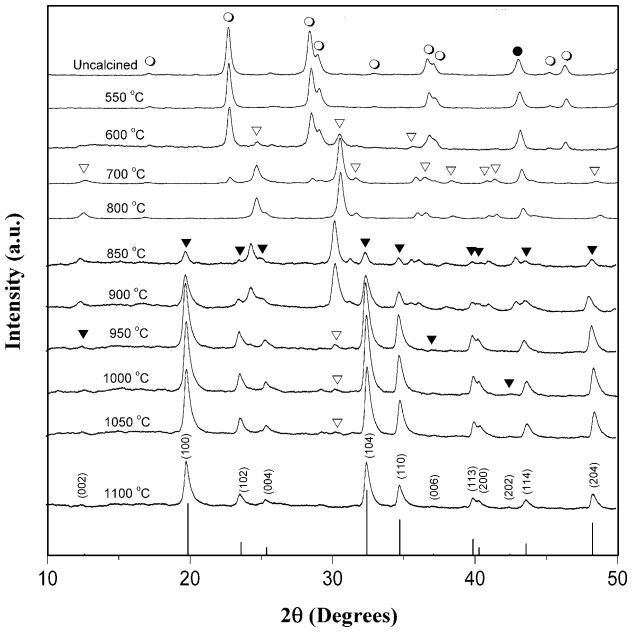


Fig. 4. Powder XRD patterns of the ball-milling powders calcined at various conditions for 2 h with constant heating/cooling rates of 10 °C/min (●, MgO; ◯, $Nb_2O_5$; ▽, $MgNb_2O_6$; ▼, $Mg_4Nb_2O_9$; ICDD file No. 38–1459: $Mg_4Nb_2O_9$).

$Nb_2O_5$ are present, indicating that the elimination of organic species occurs below 500 °C, which agrees with the TG-DTA results determined previously. The strongest reflections of the mixed phases of MgO (●) and $Nb_2O_5$ (◯) can be correlated with ICDD file Nos. 71–1176 [26] and 28–317 [27], respectively.

From Figs. 4 and 5, it is seen that little crystalline phase of $MgNb_2O_6$ (▽), earlier reported by many researchers [6,17,28] was found at 600 °C as separated phases in both calcined powders. This $MgNb_2O_6$ phase (ICDD file No. 33–0875 [29])

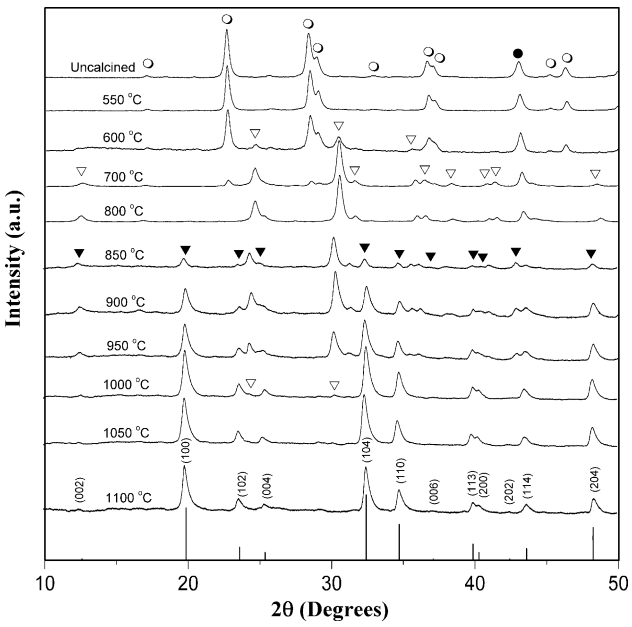


Fig. 5. Powder XRD patterns of the vibro-milling powders calcined at various conditions for 2 h with constant heating/cooling rates of 10 °C/min (●, MgO; ◯, $Nb_2O_5$; ▽, $MgNb_2O_6$; ▼, $Mg_4Nb_2O_9$; ICDD file No. 38–1459: $Mg_4Nb_2O_9$).

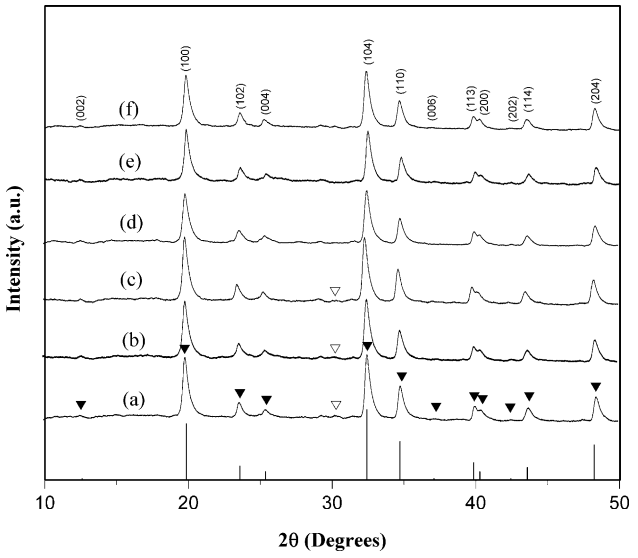


Fig. 6. Powder XRD patterns of the ball-milling powders calcined at 1050 °C with heating/cooling rates of 10 °C/min. for (a) 2 h, (b) 3 h, (c) 4 h and (d) 5 h, and at 1050 °C for 5 h with heating/cooling rates of (e) 20 °C/min and (f) 30 °C/min (▽, $MgNb_2O_6$; ▼, $Mg_4Nb_2O_9$; ICDD file No. 38–1459: $Mg_4Nb_2O_9$).

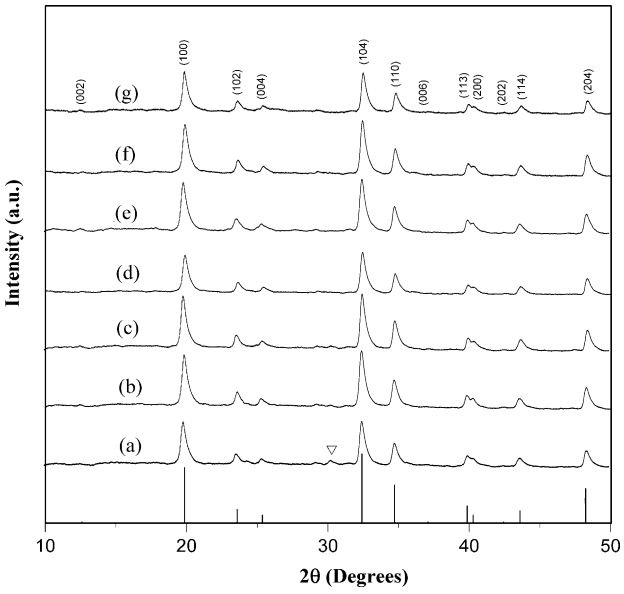


Fig. 7. Powder XRD patterns of the vibro-milling powders calcined at 1050 °C with heating/cooling rates of 10 °C/min. for (a) 1 h, (b) 2 h, (c) 3 h, (d) 4 h and (e) 5 h, and at 1050 °C for 5 h with heating/cooling rates of (f) 20 °C/min and (g) 30 °C/min (▽, $MgNb_2O_6$; ICDD file No. 38–1459: $Mg_4Nb_2O_9$).

has a columbite-type structure with an orthorhombic unit cell ($a = 5.70$ Å, $b = 14.19$ Å and $c = 5.032$ Å) with space group $I4_1/amd$ (No. 141), in agreement with literature [14,17,28]. As the temperature increased to 700 °C, the intensity of the $MgNb_2O_6$ peaks in both calcined powders was further enhanced and became the predominant phase, in consistent with the TG-DTA results. From Figs. 4 and 5, it is seen that the peaks corresponding to MgO and $Nb_2O_5$ phases were completely eliminated after calcination at 800 °C in both powders. These observations are associated to the DTA peaks found at the same temperature range within the broad exothermic effects (Fig. 3). After calcination at 850 °C, some new peaks (▼) of the desired $Mg_4Nb_2O_9$ started to appear, mixing with $MgNb_2O_6$ and MgO phases in both powders, in consistent with Ananta [20]. To a first approximation, this $Mg_4Nb_2O_9$ phase (ICDD file No. 38–1459 [30]) has a corundum-type structure with a hexagonal unit cell ($a = 5.162$ Å and $c = 14.024$ Å) with space group (no. 165), in consistent with other researchers [5,19,20].

Upon calcination at 1100 °C, the major phase of $Mg_4Nb_2O_9$ has been clearly identified in the ball-milling powders and most of second phases were eliminated. In particular, the peaks corresponding to $MgNb_2O_6$ disappeared. However, in comparison, a single phase of $Mg_4Nb_2O_9$ is already formed when the vibro-milling precursor was calcined at 1050 °C. Apart from calcination temperature, the effect of dwell time was also found to be significant (Figs. 6 and 7). It is seen that an essentially monophasic $Mg_4Nb_2O_9$ of corundum structure is obtainable in the ball-milling powders when the dwell time was extended to 5 h at 1050 °C (Fig. 6), which is 3 h longer than that of the vibro-milling precursor (Fig. 7). In this work, an attempt was also made to calcine these powders under various heating/cooling rates (Figs. 6(d–f) and 7(e–g)). In this connection, it is shown that the yield of $Mg_4Nb_2O_9$ phase did not vary significantly with different heating/cooling rates ranging from 10 to 30 °C/min, in good agreement with earlier results reported by Ananta et al. [20,31] for the mixture of the two kinds of refractory oxides.

The amount of corundum phase present in each of the powders was estimated using the following equation:

$$\text{corundum phase (wt.\%)} = \left[\frac{I_{\text{Cor}}}{(I_{\text{Cor}} + I_{\text{Col}})}\right] \times 100 \quad (1)$$

This equation is analogous to well-known equation [6,8] widely employed in connection with the fabrication of complex perovskite materials. It should be seen as a first approximation since its applicability requires comparable maximum intensities of the peaks of corundum and columbite phases. Here $I_{\text{Cor}}$ refers to the intensity of the corundum (1 0 4) peak and $I_{\text{Col}}$ the intensity of the columbite (1 3 1) peak [32]. For the purpose of estimating the concentration of the phase present, Eq. (1) has been applied to the powder XRD patterns obtained as given in Table 1.

It is well established that the columbite-type $MgNb_2O_6$ tends to form together with the corundum-type $Mg_4Nb_2O_9$, depending on calcination conditions [18,20,32]. In the work reported here, evidence for the formation of $MgNb_2O_6$ phase, which coexists with the $Mg_4Nb_2O_9$ phase, is found after calcination at temperature ~850–950 °C, similar to those reported by Ananta [20] and Yu et al. [22]. The formation temperature and dwell times for high purity $Mg_4Nb_2O_9$ observed in the powders derived from a combination of a mixed oxide synthetic route and a careful calcination condition (especially with a rapid vibro-milling technique) are slightly lower than those reported for the powders prepared via many other conventional mixed oxide methods [3–5,13].

Based on the DTA and XRD data, it may be concluded that, over a wide range of calcination conditions, single-phase $Mg_4Nb_2O_9$ cannot be straightforwardly formed via a solid-state mixed oxide synthetic route, as verified by a number of

Table 1
Calculated amount of $Mg_4Nb_2O_9$ phase as a function of calcination conditions and milling methods

| Calcination conditions | | Qualitative concentrations of phases[a] | | | |
|---|---|---|---|---|---|
| Temperature (°C) | Dwell time (h) | Ball-milling | | Ball-milling | |
| | | $Mg_4Nb_2O_9$ (wt.%) | $MgNb_2O_6$ (wt.%) | $Mg_4Nb_2O_9$ (wt.%) | $MgNb_2O_6$ (wt.%) |
| 850 | 2 | 20.88 | 79.12 | 5.00 | 95.00 |
| 900 | 2 | 42.44 | 57.56 | 21.33 | 78.67 |
| 950 | 2 | 91.22 | 8.78 | 58.81 | 41.19 |
| 1000 | 2 | 93.69 | 6.31 | 93.44 | 6.56 |
| 1050 | 1 | – | – | 98.29 | 1.71 |
| 1050 | 2 | 93.96 | 6.04 | 100.00 | 0.00 |
| 1050 | 3 | 99.02 | 0.98 | 100.00 | 0.00 |
| 1050 | 4 | 99.13 | 0.87 | 100.00 | 0.00 |
| 1050 | 5 | 100.00 | 0.00 | 100.00 | 0.00 |
| 1100 | 2 | 100.00 | 0.00 | 100.00 | 0.00 |

[a] The estimated precision of the concentrations for the two phases is ±1%.

researchers [16,17,20]. The experimental work carried out here suggests that the optimal calcination conditions for single-phase $Mg_4Nb_2O_9$ are 1050 °C for 5 h or 1100 °C for 2 h (ball-milling) and 1050 °C for 2 h (vibro-milling), with heating/cooling rates as fast as 30 °C/min. The optimized formation temperature of single-phase $Mg_4Nb_2O_9$ was lower for the vibro-milling method probably due to the higher degree of mixing with more effective size reduction. Therefore, in general, the methodology presented in this work provides a simple method for preparing corundum $Mg_4Nb_2O_9$ powders via a solid-state mixed oxide synthetic route. It is interesting to note that, by using either ball-milling or vibro-milling methods with its respective optimized calcination condition, the reproducible, lower cost and flexible process involving simple synthetic route can produce high purity corundum $Mg_4Nb_2O_9$ (with impurities undetected by XRD technique) from relatively impure and inexpensive commercially available raw materials.

SEM micrographs of the calcined $Mg_4Nb_2O_9$ powders derived from ball- and vibro-milling methods are shown in Fig. 8(a) and (b), respectively. In general, the particles are agglomerated and basically irregular in shape, with a substantial variation in particle size. Observed diameters range from 0.5 to 1.6 and 0.1 to 1.8 μm for ball- and vibro-milling methods, respectively (Table 2). However, it is seen that higher degree of agglomeration with more rounded particle morphology is observed in the powders produced by vibro-milling. The strong inter-particle bond within each aggregate is evidenced by the formation of a well-established necking between neighbouring particles. This observation could be attributed to the mechanism of surface energy reduction of the ultrafine powders, i.e. the smaller the powder the higher the specific surface area [24,25]. In general, it is seen that higher and longer heat treatment of ball-milling powders leads to larger particle sizes with hard agglomeration. The averaged particle size of vibro-milling $Mg_4Nb_2O_9$ powders with finer particle size is regarded as

Table 2
Particle size range of $Mg_4Nb_2O_9$ particles measured by different techniques

| Measurement techniques | Particle size range | |
|---|---|---|
| | Ball-milling | Vibro-milling |
| XRD (nm, ±2.0) | 23.9 | 23.4 |
| Laser diffraction (μm, ±0.2) | 2.0–5.0 | 0.3–6.5 |
| SEM (μm, ±0.1) | 0.5–1.6 | 0.1–1.8 |
| TEM (μm, ±0.01) | 0.01–1.0 | 0.01–0.03 |

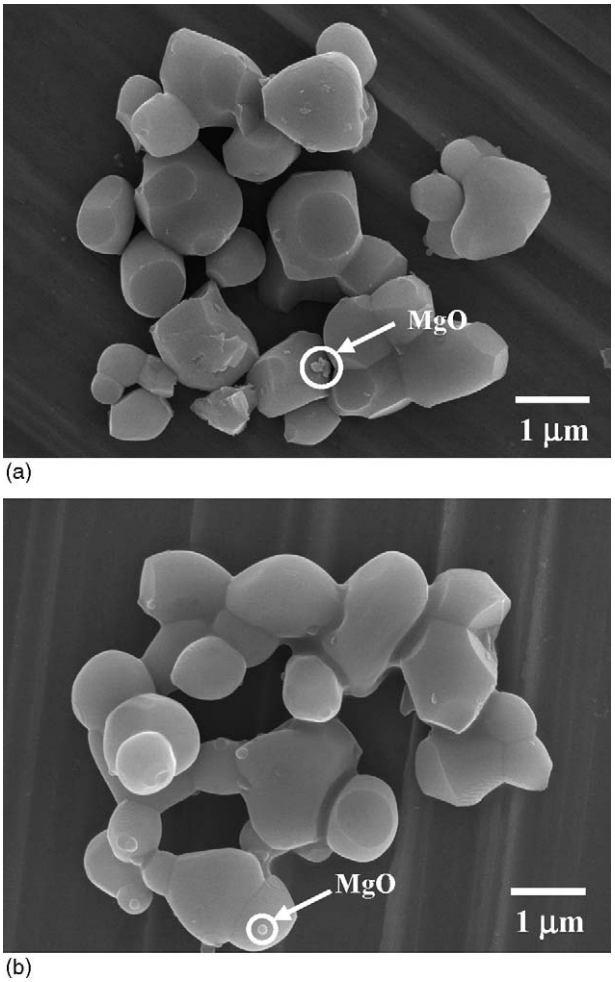


Fig. 8. SEM micrographs of the (a) ball-milling and (b) vibro-milling $Mg_4Nb_2O_9$ powders after calcined at their optimal conditions.

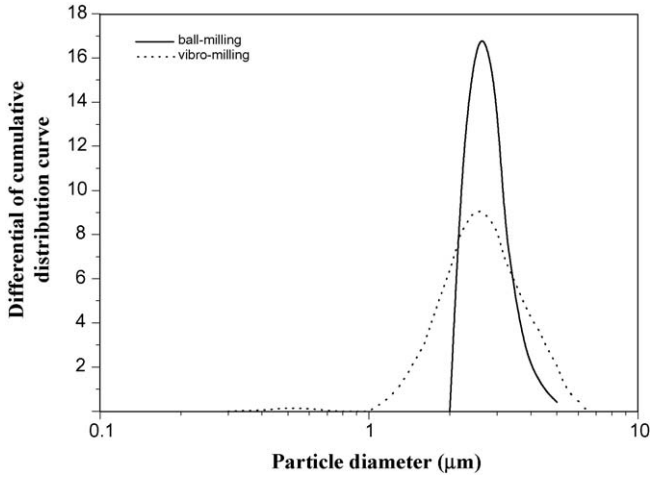


Fig. 9. The particle size curves of the ball- and vibro-milling $Mg_4Nb_2O_9$ powders after calcined at their optimal conditions.

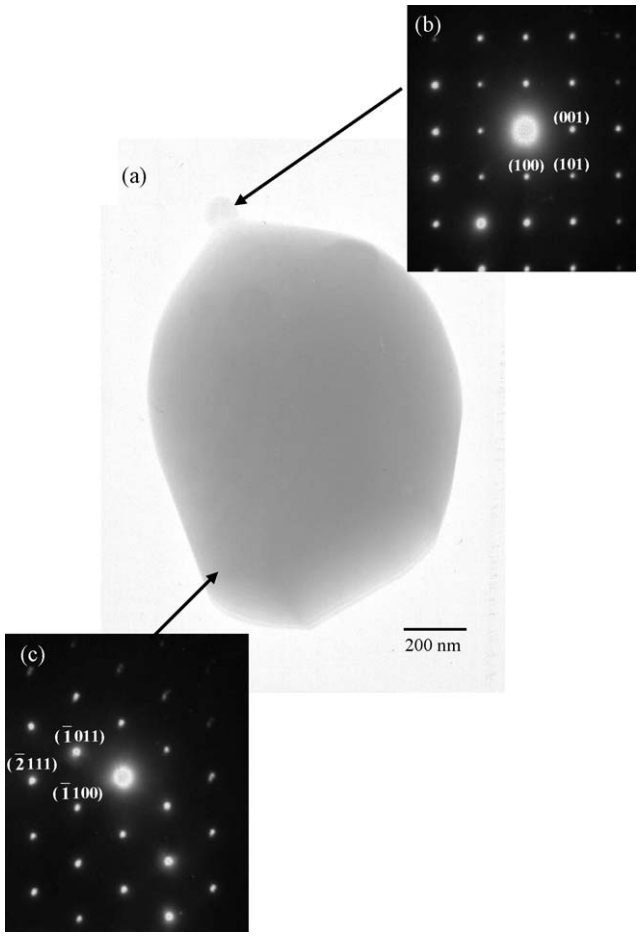


Fig. 10. (a) TEM micrograph of ball-milling $Mg_4Nb_2O_9$ particles and SAED patterns of (b) the major phase of hexagonal $Mg_4Nb_2O_9$ (zone axes [1 1 1]) and (c) the minor phase of orthorhombic $MgNb_2O_6$ (zone axes [0 1 0]).

advantage for better reactivity. A combination of SEM and EDX techniques has demonstrated that an MgO-rich phase (spherical particle with diameter of ~50–100 nm) exists neighbouring the $Mg_4Nb_2O_9$ parent phase, as circled in Figs. 8(a) and 9b). The existence of discrete nano-sized MgO phase points to the poor reactivity of MgO, although the concentration is too low for detection by XRD in consistent with earlier work by Ananta [20]. Fig. 9 shows the particle size distribution curves of calcined $Mg_4Nb_2O_9$ powders derived from both milling methods. As listed in Table 2, the particle size falls within the range of 2.0–5.0 and 0.3–6.5 μm for powders from ball- and vibro-milling methods, respectively. Even taking into account that the analysis does not reveal the real dimension of single particles (due to agglomeration effects as expected from the SEM results in Fig. 8), a uniform frequency distribution curve was observed for the ball-milling powders whilst broad distribution curve with tiny tail at front covering the range of 0.3–0.8 μm in sizes was found for the vibro-milling powders (dashed line), reflecting more of the size of agglomerates than the real size of particles, in good agreement with the SEM results previously determined.

Bright field TEM images of discrete particles of the calcined $Mg_4Nb_2O_9$ powders are shown in Fig. (ball-milling) and Fig. 11 (vibro-milling), indicating the particle sizes and shapes at higher magnifications. The observed morphology reveals the considerable difference in both size and shapes between the two particles. Primary particle in vibro-milling powders is clearly smaller in size than the ball-milling powders. As seen in Fig. 10(a), the ball-milling powders consist mainly of irregular round shape primary particles with a diameter of ~1 μm or less. In addition to the primary particles, the powders have another kind of very fine particle (brighter area)

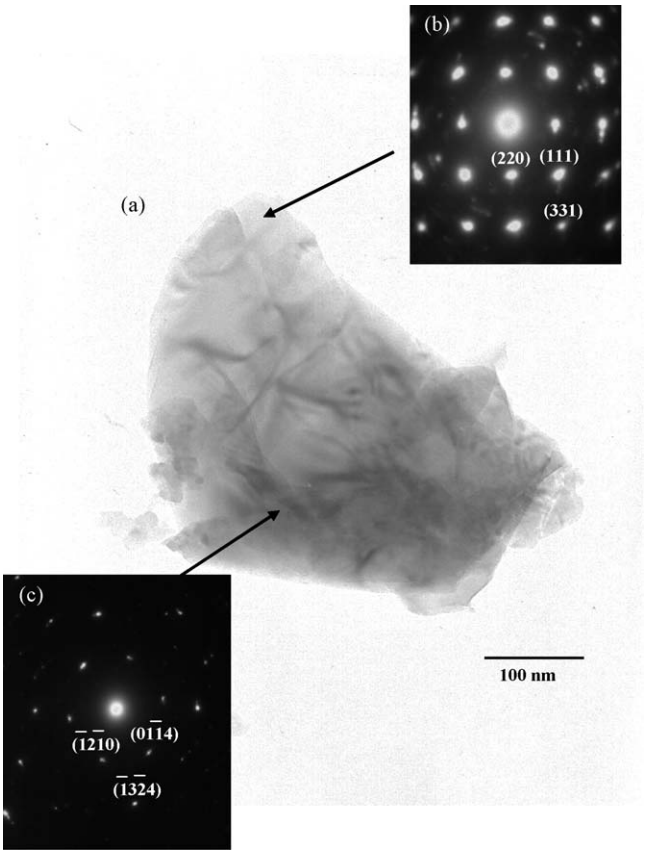


Fig. 11. (a) TEM micrograph of vibro-milling $Mg_4Nb_2O_9$ particles and SAED patterns of (b) the major phase of hexagonal $Mg_4Nb_2O_9$ (zone axes [$\bar{8}\,\bar{4}$ 1]) and (c) the minor phase of orthorhombic $MgNb_2O_6$ (zone axes [0 0 1]).

with diameter of about 93 nm (it is referred to as nanoparticle). Only single nanoparticle can be observed in this TEM micrograph. In contrast, the vibro-milling powders consist mainly of submicrometer-sized primary particles accompanying with several dark and bright areas (Fig. 11(a)). The particle diameters in these TEM micrographs are also given in Table 2. It is possible to observe in Table 2 that the particle sizes determined by XRD technique have almost the same value in nanometer range for different milling methods. It should be noted that the calculated values from the XRD technique were determined from the XRD peak-broadening and actually present the crystallite sizes [33], whereas the values from other methods as listed in Table 2 represent the particle sizes, which include polycrystalline, agglomerates, defects, etc. [23,33]. In addition, these other methods also provide information on particle morphology and powder quality, which is not available from the XRD technique alone. Thus the combination of the data listed in Table 2 provides better assessment of the powders produced from different milling techniques.

By employing a combination of both selected area electron diffraction (SAED) and crystallographic analysis, the major phase of hexagonal $Mg_4Nb_2O_9$ (Figs. 10(b) and 11(b)) and minor phase of $MgNb_2O_6$ nanoparticles in orthorhombic form were identified (Figs. 10(c) and 11(c)), in good agreement with the XRD results. In general, EDX analysis using a 20 nm probe from a large number of particles of the two calcined powders

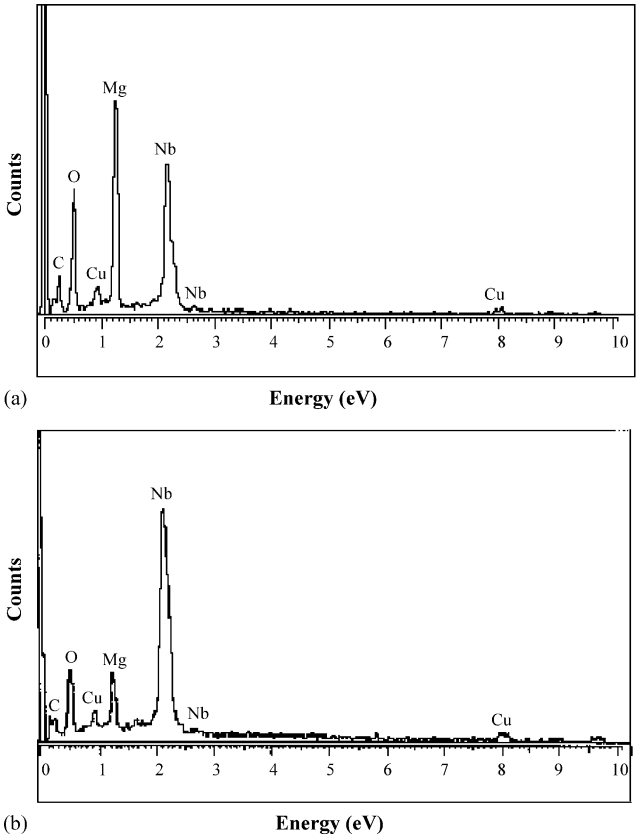


Fig. 12. EDX analysis of (a) the major phase $Mg_4Nb_2O_9$ and (b) the minor phase $MgNb_2O_6$ (some signals of C and Cu come from coated electrodes and sample stubs, respectively).

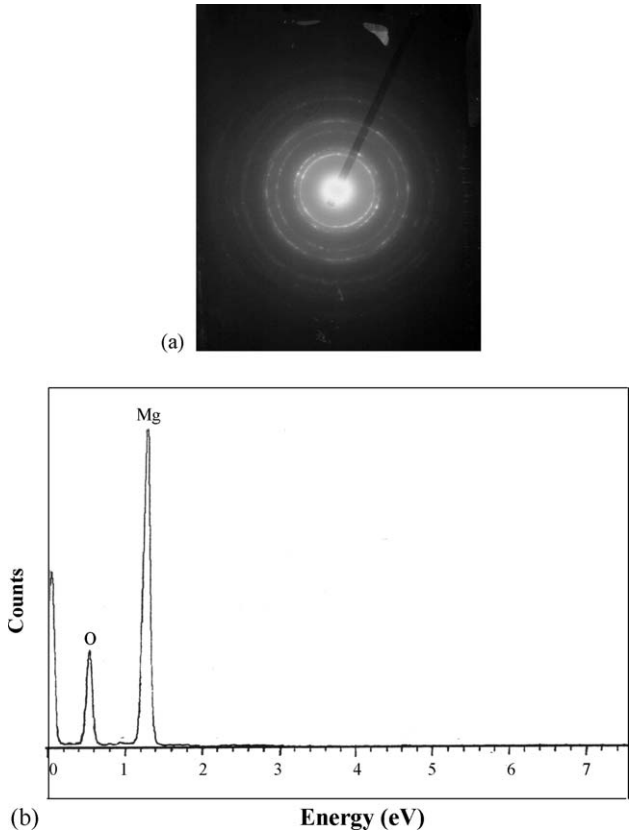


Fig. 13. (a) SAED pattern of the unreacted MgO phase and (b) EDX analysis of the MgO-rich phase.

confirmed the parent composition to be $Mg_4Nb_2O_9$ (Fig. 12(a)). Minor phase of $MgNb_2O_6$ was also confirmed by this technique, as illustrated in Fig. 12(b). It is interesting to noted that limited evidence for the presence of the unreacted starting precursor MgO (Fig. 13(a) the ring patterns indicating the polycrystalline nature and hence fine scale of this phase Fig. 13(b)) in good agreement with the SEM results, and nano-scale particle of $MgNb_2O_6$ was also found in the TEM–EDX investigation, even though this could not be detected by XRD. It is, therefore, intriguing to note the advantage of a combination between TEM and EDX techniques, which lies in its ability to reveal microstructural features often missed by the XRD diffraction method which requires at least 5 wt.% of the component [23].

## 4. Conclusions

It has been shown that pure corundum $Mg_4Nb_2O_9$ powders can be formed by the reaction of niobium oxide with magnesium oxide via either ball-milling or vibro-milling methods at about 1050–1100 °C. Evidence for the formation of a columbite $MgNb_2O_6$ minor phase, which coexists with the corundum $Mg_4Nb_2O_9$ parent phase, is found at calcination temperatures ranging from 800 to 1050 °C. Between the two methods, it is seen that lower optimized calcination temperature and dwell time for the production of pure $Mg_4Nb_2O_9$ powders can be obtained by using vibro-milling method. This technique was superior to ball-milling as measured by the required minimum firing temperature

and dwell time for the yield of single-phase $Mg_4Nb_2O_9$ in the powders together with the smallest particle size achieved.

## Acknowledgments

The authors gratefully acknowledge the Thailand Research Fund (TRF), the Department of Physics, the Faculty of Science and the Graduate School, Chiang Mai University for all supports.

## References

[1] S. Pagola, R.E. Carbonio, J.A. Alonso, M.T. Fernández-Díaz, J. Solid State Chem. 134 (1997) 76.
[2] A. Yokoi, H. Ogawa, A. Kan, H. Ohsato, Y. Higashida, J. Eur. Ceram. Soc. 25 (2005) 2871.
[3] C.W. Hwang, S.K. Lee, Japanese Patent No. JP97-293619 (1998).
[4] A. Wachtel, J. Electrochem. Soc. 111 (1964) 534.
[5] Y.C. You, N. Park, K.H. Jung, H.L. Park, K.C. Kim, S.I. Mho, T.W. Kim, J. Mater. Sci. Lett. 13 (1994) 1682.
[6] P.A. Joy, K. Sreedhar, J. Am. Ceram. Soc. 80 (1997) 770.
[7] C.H. Lu, H.S. Yang, Mater. Sci. Eng. B 84 (2001) 159.
[8] S.L. Swartz, T.R. Shrout, Mater. Res. Bull. 17 (1982) 1245.
[9] S. Ananta, N.W. Thomas, J. Eur. Ceram. Soc. 19 (1999) 155.
[10] G. Haertling, J. Am. Ceram. Soc. 82 (1999) 797.
[11] A.J. Moulson, J.M. Herbert, Electroceramics, 2nd ed., Wiley, Chichester, 2003.
[12] K. Uchino, Piezoelectrics and Ultrasonic Applications, Kluwer, 1998.
[13] E. Goo, T. Yamamoto, K. Okazaki, J. Am. Ceram. Soc. 69 (1986) C-188.
[14] D.H. Kang, K.H. Yoon, Ferroelectrics 87 (1988) 255.
[15] P.A. Joy, Mater. Lett. 32 (1997) 347.
[16] Y.C. You, H.L. Park, Y.G. Song, H.S. Moon, G.C. Kim, J. Mater. Sci. Lett. 13 (1994) 1487.
[17] K. Sreedhar, N.R. Pavaskar, Mater. Lett. 53 (2002) 452.
[18] N.K. Kim, Mater. Lett. 32 (1997) 127.
[19] N. Kumada, K. Taki, N. Kinomura, Mater. Res. Bull. 35 (2000) 1017.
[20] S. Ananta, Mater. Lett. 58 (2004) 2530.
[21] S. Ananta, Mater. Lett. 58 (2004) 2834.
[22] Y.H. Yu, C.D. Feng, W.L. Yao, Y. Yang, C.E. Li, H.X. Yan, J. Mater. Sci. Lett. 20 (2001) 2189.
[23] H.P. Klug, L.E. Alexander, X-ray Diffraction Procedures, 2nd ed., Wiley, New York, 1974.
[24] J.S. Reeds, Principles of Ceramics Processing, 2nd ed., Wiley, New York, 1995.
[25] D. Richerson, Modern Ceramic Engineering, 3rd ed., CRC Press, New York, 2005.
[26] Powder Diffraction File No. 71–1176, International Centre for Diffraction Data, Newton Square, PA, 2000.
[27] Powder Diffraction File No. 28–317, International Centre for Diffraction Data, Newton Square, PA, 2000.
[28] S. Ananta, Mater. Lett. 58 (2004) 2781.
[29] Powder Diffraction File No. 33–875, International Centre for Diffraction Data, Newton Square, PA, 2000.
[30] Powder Diffraction File No. 38–1459, International Centre for Diffraction Data, Newton Square, PA, 2000.
[31] S. Ananta, R. Tipakontitikul, T. Tunkasiri, Mater. Lett. 57 (2003) 2637.
[32] S. Ananta, R. Brydson, N.W. Thomas, J. Eur. Ceram. Soc. 19 (1999) 355.
[33] B.D. Cullity, Elements of X-Ray Diffraction, 2nd ed., Addison-Wesley Publishing Company Inc., Reading, 1978.

INSTITUTE OF PHYSICS PUBLISHING JOURNAL OF PHYSICS D: APPLIED PHYSICS
J. Phys. D: Appl. Phys. **39** (2006) 3097–3102 doi:10.1088/0022-3727/39/14/032

# Change of dielectric properties of ceramics in lead magnesium niobate-lead titanate system with compressive stress

**Rattikorn Yimnirun, Muangjai Unruan, Yongyut Laosiritaworn and Supon Ananta**

Department of Physics, Faculty of Science, Chiang Mai University, Chiang Mai 50200, Thailand

Received 27 February 2006, in final form 12 June 2006
Published 30 June 2006
Online at stacks.iop.org/JPhysD/39/3097

**Abstract**
Effects of compressive stress on the dielectric properties of PMN–PT ceramics were investigated. The ceramics with the formula $(1-x)Pb(Mg_{1/3}Nb_{2/3})O_3$-$(x)PbTiO_3$ or $(1-x)$PMN–$(x)$PT ($x = 0.1$–$0.5$) were prepared by a conventional mixed-oxide method and then characterized with x-ray diffraction (XRD) and scanning electron microscopy. Dense perovskite-phase PMN–PT ceramics with uniform microstructure were successfully obtained. The dielectric properties under compressive stress were observed at stress up to 230 MPa using a home-built compressometer. The experimental results revealed that the superimposed compression stress significantly reduced both the dielectric constant and the dielectric loss tangent of 0.9PMN–0.1PT ceramic, while the changes were not as significant in the other PMN–PT ceramic compositions. In addition, the dielectric properties were considerably lowered after a stress cycle. Since change in the dielectric properties with applied stress was attributed to the competing influences of the intrinsic and the extrinsic contributions, the observations were mainly interpreted in terms of domain switching through non-180° domain walls, de-ageing, clamping of domain walls and the stress induced decrease in the switchable part of spontaneous polarization.

(Some figures in this article are in colour only in the electronic version)

## 1. Introduction

A family of materials which are of great interest due to their high polarizabilities is the lead-based relaxor ferroelectrics, particularly lead magnesium niobate, $Pb(Mg_{1/3}Nb_{2/3})O_3$ (PMN) and its solid solution with lead titanate, $PbTiO_3$ (PT), the so-called PMN–PT. These compounds have dielectric constants in excess of 20 000, making them potential candidates for capacitive applications. In addition, they also exhibit electrostrictive behaviour at temperatures above their phase transition temperatures. This behaviour extends their use to transducer and actuator applications [1–5]. $(1-x)Pb(Mg_{1/3}Nb_{2/3})O_3$-$(x)PbTiO_3$ or $(1-x)$PMN–$(x)$PT ceramic compositions with $x < 0.2$ have been studied for electrostrictive applications [4–7], while those with $x > 0.2$ can be utilized as piezoelectric materials [4, 6, 8, 9]. The differences between the electrostrictive and piezoelectric compositions of PMN–PT are due to differences in the degree of long-range polar order [4, 7, 10]. In the compositions with lower PT content, relaxor ferrfoelectric characteristics with polar clusters or nanodomains are observed [4, 11, 12]. On the other hand, long-range polar order with normal micrometre-sized ferroelectric domains exists in the compositions with higher PT content [4, 9, 10].

Practically, when used in specific applications PMN–PT ceramics are often subjected to mechanical loading, either deliberately in the design of the device itself or because the device is used to change shapes as in many smart structure applications or the device is used under environmental stresses [8, 13–17]. A prior knowledge of how the material properties change under different load conditions is crucial for the proper design of a device and for suitable selection of

  

materials for a specific application. Despite this fact, material constants used in any design calculations are often obtained from a stress-free measuring condition, which in turn may lead to incorrect or inappropriate actuator and transducer designs. It is therefore important to determine the properties of these materials as a function of applied stress. Previous investigations on the stress-dependence electrical properties of many ceramic systems have clearly emphasized the importance of this matter [7, 15, 18–23]. Recently, the uniaxial stress dependence of dielectric properties has been investigated in materials such as BT, PZT, PMN and PMN–PZT [19–22]. The results clearly showed that the effects of stress on the dielectric properties depended significantly on ceramic compositions and stress levels. Since PMN–PT ceramics are practically very important, there have been previous reports on the electromechanical properties of electrostrictive 0.9PMN–0.1PT and piezoelectric 0.7PMN–0.3PT ceramics under various mechanical and electrical loading conditions [7,15,23,24]. However, there has been no systematic study on the influence of an applied stress on the dielectric properties of ceramics in the PMN–PT system. Therefore, it is the aim of this study to determine the dielectric properties of the $(1-x)$PMN–$(x)$PT ceramics as a function of compressive stress.

## 2. Experimental method

PMN–PT ceramics were prepared from starting PMN and PT powders by a conventional mixed-oxide method. Perovskite-phase PMN powders were obtained from the columbite method, while PT powders were prepared by a simple mixed-oxide method [25]. To obtain the perovskite-phase PMN, the magnesium niobate powders were first prepared by mixing MgO (99.0%) and $Nb_2O_5$ (99.9%) powders and then calcining the mixed powders at 1100 °C for 3 h, to yield so called columbite powders ($MgNb_2O_6$). After that, the columbite powders were mixed with PbO (99.9%) by the ball-milling method and calcined at 800 °C for 1 h to form the perovskite-phase PMN powders. With a simple mixed-oxide route, PT powders were prepared from PbO (99.9%) and $TiO_2$ (99.9%) starting powders. These powders were ball-milled and calcined at 600 °C for 1 h.

The $(1-x)Pb(Mg_{1/3}Nb_{2/3})O_3$–$(x)PbTiO_3$ ceramics were then prepared from starting PMN and PT powders by the mixed-oxide method. After mixing the powders by the ball-milling method and drying process, the mixed powders were pressed hydraulically to form disc-shaped pellets 10 mm in diameter and 2 mm thick, with 3 wt% polyvinyl alcohol as a binder. The pellets were placed on the alumina powder-bed inside alumina crucible and surrounded with atmosphere powders of the same composition. Finally, for optimization purposes the pellets were sintered at temperatures between 1220 and 1240 °C for 2 h. Optimum sintering conditions for all ceramics were established by identifying the conditions for maximizing both the bulk density and the yield of perovskite. However since the PMN–PT compositions having high PT content in the range $0.6 \leqslant x \leqslant 0.9$ could not be fabricated in a bulk form of high density, these compositions could not be characterized any further for the rest of the study. Their comparatively large $c/a$ values, which give rise to serious internal stress, are responsible for the frequent crack

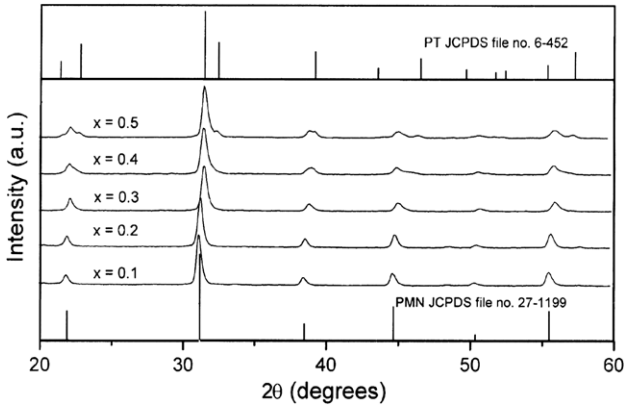


**Figure 1.** XRD diffraction patterns of the sintered $(1-x)$PMN–$(x)$PT ceramics.

developments around the phase transition temperature during the cooling of these sintered samples. In the present study, only compositions in the pseudo-binary system $(1-x)$PMN–$x$PT ($0.1 \leqslant x \leqslant 0.5$) have been successfully fabricated from the calcined $(1-x)$PMN–$x$PT powders, employing a normal sintering method, i.e. the pressureless sintering technique. Similar optimum sintering conditions of 1240 °C for 2 h with 15 °C $min^{-1}$ were observed in samples at compositions of $x$ between 0.1 to 0.3 while for compositions with PT content of $x = 0.4$ and 0.5 the optimum condition was found at 1220 °C for 2 h with 15 °C $min^{-1}$ [25]. The phase-formation of the sintered ceramics was studied by the x-ray diffraction (XRD) technique. The densities of sintered specimens were measured by Archimedes method. The microstructure analyses were undertaken by scanning electron microscopy (SEM: JEOL Model JSM 840A). The grain size was determined from SEM micrographs by a linear intercept method.

Before studying the dielectric properties, the specimens were lapped to obtain parallel faces. After coating with silver paint as electrode at the faces, the specimens were heated at 750 °C for 12 min to ensure contact between the electrode and the surface of the ceramic. All the ceramics were then poled to a full remanent state prior to testing. A compressometer was constructed [19, 26, 27] to study the effects of the compressive stress on the dielectric properties of the ceramics. The dielectric properties were measured by LCR-meter (Instrek LCR-821). The room temperature (25 °C) capacitance and the dielectric loss tangent were obtained at a frequency of 1 kHz under compressive stress up to 230 MPa. The dielectric constant was then calculated from a parallel-plate capacitor equation, e.g. $\varepsilon_r = Cd/\varepsilon_0 A$, where $C$ is the capacitance of the specimens, $d$ and $A$ are, respectively, the thickness and the area of the electrode and $\varepsilon_0$ is the dielectric permittivity of vacuum ($8.854 \times 10^{-12}$ F $m^{-1}$).

## 3. Results and discussion

The XRD patterns of sintered ceramics with maximum perovskite phase and bulk density are presented in figure 1, where complete crystalline solutions of perovskite structure are formed throughout the composition range between $x = 0.1$ and 0.5. In general, only a (pseudo) cubic symmetry is observed at low values of PT concentration, in good

**Table 1.** Characteristics of PMN–PT ceramics with optimized processing conditions.

| Ceramic | Density[a] ($g\,cm^{-3}$) | Grain size range ($\mu$m) | Average grain size[b] ($\mu$m) | $T_C$ (1 kHz) (°C) | Stress-free dielectric properties[c] $\varepsilon_r$ | tan $\delta$ |
|---|---|---|---|---|---|---|
| 0.9PMN–0.1PT | 7.98 | 0.42–3.66 | 2.07 | 45 | 10 713 | 0.083 |
| 0.8PMN–0.2PT | 7.94 | 0.44–3.02 | 2.02 | 100 | 2 883 | 0.079 |
| 0.7PMN–0.3PT | 7.86 | 0.41–2.80 | 1.72 | 150 | 1 976 | 0.045 |
| 0.6PMN–0.4PT | 7.83 | 0.41–3.45 | 1.93 | 210 | 1 909 | 0.031 |
| 0.5PMN–0.5PT | 7.78 | 0.48–3.72 | 2.11 | 260 | 1 375 | 0.022 |

[a] The estimated precision of the density is ±1%.
[b] The estimated precision of the average grain size is ±1%.
[c] Measured at 1 V $mm^{-1}$ (25 °C and 1 kHz).

agreement with other workers [28, 29]. By the influence of PT, however, several peaks split for $x \geqslant 0.4$, indicating the development of tetragonal symmetry, consistent with earlier work on PMN–PT ceramics [9, 30]. As listed in table 1, density values are found to decrease slightly with $x$ (in units of grams per centimetre cube the value decreases gradually from 7.98 in 0.9PMN–0.1PT to 7.78 in 0.5PMN–0.5PT). SEM-micrographs of fractured surfaces of all compositions are shown in figure 2. In general, similar microstructure characteristics are observed in these samples, i.e. uniformly sized grains with a high degree of grain close-packing. Almost no abnormal grain growth is observed. All ceramic compositions display very similar grain size range between 0.4 and 3.7 $\mu$m. By applying the linear intercept method to SEM micrographs of polished and thermally etched specimens, mean grain sizes of about 1.72–2.11 $\mu$m are estimated for these samples as given in table 1. These characteristics indicate that dense perovskite-phase PMN–PT ceramics with uniform microstructure have been obtained. Since the physical and microstructure features of all ceramic compositions are not significantly different, these parameters should not play an important role in the composition-dependent dielectric properties under the compressive stress discussed in the following paragraphs.

The room temperature dielectric properties measured under stress-free condition are listed in table 1. It is clearly seen that the dielectric constant ($\varepsilon_r$) of $(1-x)$PMN–$(x)$PT ceramics decreases with increasing PT content. The dielectric constant decreases from 10713 in 0.9PMN–0.1PT to 1375 in 0.5PMN–0.5PT. In addition, a decreasing trend has been observed for the stress-free dielectric loss tangent (tan $\delta$), which shows a decrease in value from 0.083 in 0.9PMN–0.1PT to 0.022 in 0.5PMN–0.5PT. This observation could be attributed to a high dielectric constant of PMN and a closer to ambient temperature $T_C$ for PMN–PT compositions with higher PMN content [1, 4, 5]. Comparable stress-free dielectric properties have also been reported in earlier publications [2, 5, 29, 30].

The experimental results of the compressive stress dependence of the dielectric properties during loading and unloading for the ceramics in the PMN–PT system are displayed in figures 3 and 4. For better comparison, the dielectric properties of each composition under stress are normalized to the stress-free values. Clearly, there is a considerable change in both the dielectric constant and the dielectric loss tangent when the compressive stress increases from 0 to 230 MPa and returning to stress-free condition. As

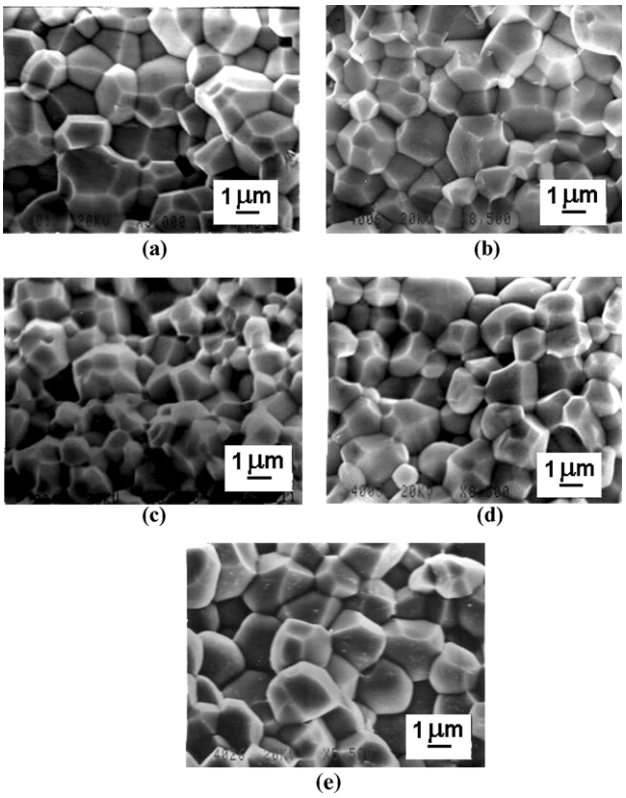


**Figure 2.** SEM micrographs of fracture surfaces of $(1-x)$PMN–$(x)$PT ceramics (*a*) 0.9PMN–0.1PT; (*b*) 0.8PMN–0.2PT; (*c*) 0.7PMN–0.3PT; (*d*) 0.6PMN–0.4PT and (*e*) 0.5PMN–0.5PT.

depicted in figure 3, the changes of the dielectric constant with the stress can be divided into two groups. For 0.9PMN–0.1PT ceramic, the dielectric constant decreases drastically with the stress. The dielectric constant decreases more than 70% when the stress reaches 230 MPa and only returns to slightly less than 50% of its original value when the stress is removed. The changing of the dielectric constant with increasing and decreasing stress does not follow the same path. On the other hand, for other PMN–PT ceramics, i.e. with $x$ values of 0.2–0.5, the change is minimal. The dielectric constant is actually rather stable within this range of the stress. The dielectric constant of these compositions initially increases then decreases with very little difference in the dielectric constant between stress-free and maximum stress

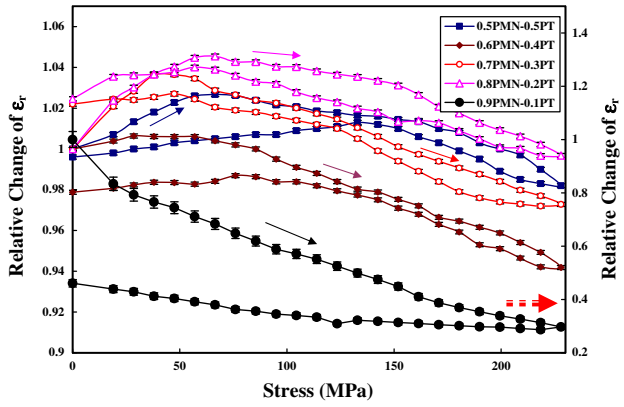


**Figure 3.** Relative changes of the dielectric constant ($\varepsilon_r$) with compressive stress for $(1-x)$PMN–$(x)$PT ceramics (measured at 25 °C and 1 kHz; secondary $Y$-axis is only for 0.9PMN–0.1PT and solid arrows indicate loading direction).

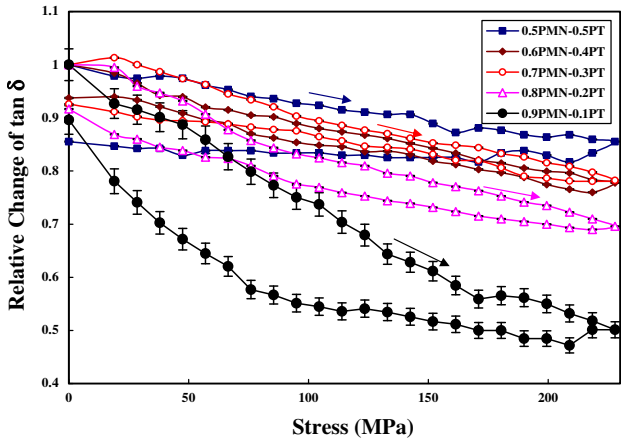


**Figure 4.** Relative changes of dielectric loss tangent (tan $\delta$) with compressive stress for $(1-x)$PMN–$(x)$PT ceramics (measured at 25 °C and 1 kHz; solid arrows indicate loading direction).

conditions. In addition, the dielectric constants during loading and unloading are not significantly different.

Since the dielectric constant of the sample was measured through the capacitance, there is a change in sample capacitance due to the geometrical deformation under stress. The variation of the sample dielectric constant ($\Delta\varepsilon_r$) can be expressed as $\varepsilon_r^* X^*((1+2\upsilon)/E)$, where $X$ is the applied stress, $\upsilon$ is the Poisson's ratio and $E$ is the Young's modulus [26, 31]. By applying the estimated values of $\upsilon \sim 0.3$ and $E \sim 100$ GPa for PMN–PT ceramics [7, 23, 24, 32] and $\varepsilon_r$ given in table 1, it can be estimated that at the maximum stress of 230 MPa, the variation in the sample dielectric constant due to the geometrical deformation is <0.5%. Therefore, this variation should not be an important factor in the variation of the dielectric constant under stress seen in figure 3.

Figure 4 shows the results of the compressive stress dependence of the dielectric loss tangent. The dielectric loss tangent decreases monotonously with increasing the stress and then increases slightly when stress is removed. The dielectric loss tangent is also found to decrease considerably after a stress cycle. This is clearly seen in 0.9PMN–0.1PT ceramics, where the change in the dielectric loss tangent value is very significant, as it decreases about 50% at the maximum stress and almost returns to its original value after a stress cycle. The changes in the other compositions are less significant with increasing PT content.

It is also noticed that the changes in the dielectric properties with the compressive stress obtained in this study are in parts similar to those for the $(1-x)$PMN–$(x)$PZT system in the earlier investigation [19]. By comparison, the 0.9PMN–0.1PT behaves more like PMN-rich compositions in that study, while the other PMN–PT compositions act more like the PZT-rich compositions. It should also be noted that the $T_C$ range of 16–160 °C for the $(1-x)$PMN–$(x)$PZT system with $x = 0.1$–$0.7$ [33, 34] is nearly similar to that of the PMN–PT ceramics used in this study, as listed in table 1. More importantly, it is interesting to observe that a mixture of different normal and relaxor ferroelectrics responds to the applied stress in a similar manner.

To understand these experimental results, at least qualitatively, various effects have to be considered. Normally, the properties of ferroelectric materials are derived from both the intrinsic contribution of domains and extrinsic contributions of re-polarization and growth of micro-polar regions [19–23]. When a compressive stress is applied to the ferroelectric materials, the domain structure in the materials will change to maintain the domain energy at a minimum; during this process some of the domains engulf other domains or change shape irreversibly. Under the applied stress, the domain structure of ferroelectric ceramics may undergo domain switching through non-180° domain walls, de-ageing, clamping of domain walls and stress induced decrease in the switchable part of spontaneous polarization [21, 23, 35].

The situation for the PMN–PT system is quite complex because this system is a mixing between the relaxor ferroelectric PMN and the normal ferroelectric PT. Therefore, there is a competing mechanism between the two types of materials, depending upon temperature and composition. Since 0.9PMN–0.1PT is a relaxor ferroelectric with $T_C \sim 45$ °C and the experiment was carried out at room temperature (~25 °C) which is slightly below $T_C$, the experimental observations, which show decreases in both dielectric constant and dielectric loss tangent with increasing stress, can be attributed to competing influences of the intrinsic contribution of the non-polar matrix and the extrinsic contribution of re-polarization and growth of micro-polar regions. Since the dielectric response of both contributions is affected by the applied stress in an opposite way, the behaviour of 0.9PMN–0.1PT depends on the ratio between the micro-polar region and the non-polar matrix, in this case the non-polar matrix still dominates [21, 22]. Hence, the dielectric responses of the 0.9PMN–0.1PT ceramic are observed to decrease significantly with increasing compressive stress, as seen in figures 3 and 4. Earlier works on PMN and 0.9PMN–0.1PT ceramics also reported a similar observation [22, 23]. However, under stress as high as 230 MPa microcracks may develop, particularly in 0.9PMN–0.1PT, which in turn could lead to a significant change in the dielectric properties. Therefore, an additional experiment was carried out to investigate the existence of the microcracks. The stressed specimens were annealed at 300 °C for 3 h [36], then poled at the same condition used earlier. The dielectric properties were re-measured under a stress-free condition. The results showed a full recovery of the dielectric

properties, within experimental errors. This indicated that there were no microcracks in the stressed specimens.

For the other PMN–PT compositions with higher $T_C$, the extrinsic contribution of re-polarization and growth of micro-polar regions becomes dominant. When the compressive stress is applied in the direction parallel to the poling direction, the stress will move some of the polarization away from the poling direction resulting in a change in domain structures [20]. This change increases the non-180° domain wall density. Hence increase in the dielectric constant is observed. The de-ageing mechanism, which also increases the dielectric constant, is also expected to play a role here. After poling, ceramics undergo an ageing process during which some of the domain walls become pinned by impurities and structural imperfections. When a large enough stress is applied to the aged samples, it causes structural changes and redistribution of impurities [21]. As a result, the domain walls that were pinned during ageing can become active again. This de-ageing can increase dielectric responses [20, 23]. Therefore, a combination of the domain switching and the de-ageing mechanisms is believed to be a reason for the slight increase in the dielectric constant during low-stress application. With further increase in the stress, the stress clamping of domain walls, which results in a decrease of domain wall mobility, and the stress induced decrease in the switchable part of spontaneous polarization are expected to play a role in the decrease in the dielectric constant [21,23,35]. Therefore, the dielectric constant of these compositions is seen to be rather stable with the applied stress, as seen in figure 3. Similar observation has also been reported in soft PZT [20,23].

The cause of the stress dependence of the dielectric loss tangent is a little more straightforward than that of the dielectric constant. As depicted in figure 4, the clamping of the domain walls under the compressive stress results in a decrease of domain wall mobility and reduces the dielectric loss tangent [21]. This is a reversible effect with the domain wall mobility returning to near original values when the applied stress is removed, as seen in figure 4 that dielectric loss tangents return to near original values after a stress cycle. In addition, a significant decrease in the dielectric constant after a full cycle of stress application has been observed, particularly in 0.9PMN–0.1PT, and attributed to the stress induced decrease in the switchable part of the spontaneous polarization at high stress [23, 35].

## 4. Conclusions

In this study, the dielectric properties of $(1-x)\mathrm{Pb}(\mathrm{Mg}_{1/3}\mathrm{Nb}_{2/3})\mathrm{O}_3$–$(x)\mathrm{PbTiO}_3$ or $(1-x)$PMN–$(x)$PT ($x = 0.1$–$0.5$) ceramics prepared by a conventional mixed-oxide method are measured under compressive stress from 0 to 230 MPa. Phase formation behaviour and microstructure features of these ceramics are studied by an XRD and SEM methods, respectively. Perovskite-phase PMN–PT ceramics with homogeneous microstructure are obtained. The dielectric properties of 0.9PMN–0.1PT ceramic are found to decrease significantly with compressive stress, while the changes are not as significant in the other PMN–PT ceramic compositions. In addition, the dielectric properties are considerably lowered after a stress cycle. The change in dielectric properties with the applied stress is attributed to competing influences of intrinsic and extrinsic contributions. The observations are then mainly interpreted in terms of domain switching through non-180° domain walls, de-ageing, clamping of domain walls and the stress induced decrease in the switchable part of spontaneous polarization.

## Acknowledgments

This work is supported by the Thailand Research Fund (TRF). Additional support from the Faculty of Science and Graduate School of Chiang Mai University are gratefully acknowledged. The authors would also like to express their gratitude to Aurawan Udomporn for help in sample preparation and characterization.

## References

[1] Xu Y H 1991 *Ferroelectric Materials and Their Applications* (Amsterdam: North Holland)
[2] Moulson A J and Herbert J M 2003 *Electroceramics: Materials, Properties, Applications* (Chichester: Wiley)
[3] Haertling G H 1999 *J. Am. Ceram. Soc.* **82** 797
[4] Cross L E 1987 *Ferroelectrics* **76** 241
[5] Jang S 1979 *PhD Thesis* Pennsylvania State University
[6] Uchino K 1997 *Piezoelectric Actuators and Ultrasonic Motors* (Boston, MA: Kluwer)
[7] Viehland D, Li J, McLaughlin E, Powers J, Janus R and Robinson H 2004 *J. Appl. Phys.* **95** 1969
[8] Shrout T R, Chang Z, Kim N and Markgraf S 1990 *Ferroelectr. Lett. Sect.* **12** 63
[9] Viehland D, Kim M, Xu Z and Li J 1995 *Appl. Phys. Lett.* **67** 2471
[10] Smolenskii G and Agranovskaya A 1960 *Sov. Phys. Solid State* **1** 1429
[11] Randall C, Barber D and Whatmore R 1987 *J. Microsc.* **45** 275
[12] Dai X, Xu Z and Viehland D 1994 *Phil. Mag.* B **70** 33
[13] Kuwata J, Uchino K and Nomura S 1982 *Japan. J. Appl. Phys.* **21** 1298
[14] Park S and Shrout T R 1997 *J. Appl. Phys.* **82** 1804
[15] Viehland D and Powers J 2001 *Appl. Phys. Lett.* **78** 3112
[16] Stansfield D 1991 *Underwater Electroacoustic Transducers* (Bath, UK: Bath University Press)
[17] Mitrovic M, Carmen G P and Straub F K 2001 *Int. J. Solids Struct.* **38** 4357
[18] Zhou D, Kamlah M and Munz D 2005 *J. Euro. Ceram. Soc.* **25** 425
[19] Yimnirun R, Ananta S, Meechoowas E and Wongsaenmai S 2003 *J. Phys. D: Appl. Phys*. **36** 1615
[20] Zhang Q M, Zhao J, Uchino K and Zheng J 1997 *J. Mater. Res.* **12** 226
[21] Yang G, Liu S F, Ren W and Mukherjee B K 2000 *Proc. SPIE Symp. on Smart Struct. Mater.* **3992** 103
[22] Steiner O, Tagantsev A K, Colla E L and Setter N 1999 *J. Euro. Ceram. Soc.* **19** 1243
[23] Zhao J and Zhang Q M 1996 *Proc. IEEE Int. Symp. Appl. Ferroelectr.* **2** 971
[24] Zhao J, Glazounov A E and Zhang Q M 1999 *Appl. Phys. Lett.* **74** 436
[25] Udomporn A 2004 *PhD Thesis* Chiang Mai University
[26] Yimnirun R, Moses P J, Meyer R J and Newnham R E 2003 *Rev. Sci. Instrum.* **74** 3429
[27] Yimnirun R, Ananta S, Ngamjarurojana A and Wongsaenmai S 2005 *Appl. Phys.* A **81** 1227
[28] Kong L B, Ma J, Zhu W and Tan O K 2002 *Mater. Res. Bull.* **37** 23
[29] Liou Y C 2003 *Mater. Sci. Eng*. B **103** 281
[30] Brown L F, Carlson R L, Sempsrott J M, Standford G T and Fitzgerald J J 1997 *Proc. IEEE Ultrason. Symp.* **1** 561

[31] Preu P and Haussuhl S 1983 *Solid State Commun.* **45** 619
[32] Viehland D and Powers J 2001 *J. Appl. Phys.* **89** 1820
[33] Yimnirun R, Ananta S and Loaratanakul P 2004 *Mater. Sci. Eng.* B **112** 79
[34] Yimnirun R, Ananta S and Loaratanakul P 2005 *J. Euro. Ceram. Soc.* **25** 3225
[35] Yimnirun R, Loasiritaworn Y and Wongsaenmai S 2006 *J. Phys. D: Appl. Phys*. **39** 759
[36] Liao J, Jiang X P, Xu G S, Luo H S and Yin Q R 2000 *Mater. Charact.* **44** 453

*Ferroelectrics*, 331:9–18, 2006

ISSN: 0015-0193 print / 1563-5112 online
DOI: 10.1080/00150190600732850

Taylor & Francis
Taylor & Francis Group

# Change in the Dielectric Properties of Normal and Relaxor Ferroelectric Ceramic Composites in BT-PZT and PMN-PZT Systems by an Uniaxial Compressive Stress

RATTIKORN YIMNIRUN*

Department of Physics, Faculty of Science, Chiang Mai University, Chiang Mai 50200, Thailand

*Effects of an uniaxial compressive pre-stress on the dielectric properties of normal and relaxor ferroelectric ceramic composites in BT-PZT and PMN-PZT systems are investigated. The dielectric properties are observed under the compressive pre-stress levels up to 15 and 5 MPa for BT-PZT and PMN-PZT, respectively, using a uniaxial compressometer. Both the dielectric constant and the dielectric loss tangent of the BT-PZT ceramics increase significantly with increasing applied stress. Larger changes in the dielectric properties with the applied stress are observed in the PZT-rich compositions. For PMN-PZT ceramics, the dielectric constant of the PZT-rich compositions increases slightly, while that of the PMN-rich compositions decreases with increasing applied stress. On the other hand, changes in the dielectric loss tangent with stress are found to be compositional independent. The experimental results are explained with the domain wall motion and de-aging mechanisms from the application of the compressive pre-stress. More importantly, this study undoubtedly shows that the applied stress significantly influences the dielectric properties of both ceramic composite systems.*

**Keywords** Dielectric properties; ferroelectrics; BT-PZT; PMN-PZT; uniaxial stress

## Introduction

Among many smart systems, ceramic actuators and transducers are finding an increasingly wide range of applications. Ferroelectric ceramics have been established as good candidates for these applications. In many of these applications, ferroelectric ceramics are often subjected to mechanical loading, either deliberately in the design of the device itself or because the device is used to change shapes as in many smart structure applications or the device is used under environmental stresses [1–3]. Despite the fact, materials constants used in any design calculations are often obtained from a stress-free measuring condition, which in turn may lead to incorrect or inappropriate actuator and transducer designs. It is therefore important to determine the properties of these materials as a function of applied stress. Previous investigations on the stress-dependence dielectric and electrical properties of many ceramic systems, such as PZT and PMN-PT have clearly emphasized the importance of this matter [4, 5].

Received July 15, 2005; accepted October 31, 2005.
*Corresponding author. E-mail: rattikornyimnirun@yahoo.com

Among perovskite ferroelectric materials, barium titanate ($BaTiO_3$ or BT), lead zirconate titanate ($Pb(Zr_{1-x}Ti_x)O_3$ or PZT) and lead magnesium niobate ($Pb(Mg_{1/3}Nb_{2/3})O_3$ or PMN) ceramics have been investigated extensively and continuously since the late 1940s [6–9]. BT, PMN, and PZT are representative perovskite normal ferroelectric, relaxor ferroelectric, and piezoelectric prototypes, respectively, because of their excellent electrical properties. These three types of ceramics possess distinct characteristics that make each ceramic suitable for different applications. Forming a composite of these ferroelectrics has been one of the techniques employed to improve the properties of ferroelectric ceramics for specific requirements for each application.

One of the most studied piezoelectric compounds, $Pb(Zr_{0.52}Ti_{0.48})O_3$, a morphotropic phase boundary (MPB) compound of PZT, has great piezoelectric properties with a high Curie temperature ($T_C$) of $\sim$390°C. BT exhibits high dielectric constant and superior electrostrictive responses with a lower $T_C$ ($\sim$120°C) [6–9]. In addition, BT is mechanically superior to PZT [10], whereas PZT ceramics can be easily sintered at temperature much lower than BT ceramics, which usually require high sintering temperatures even as high as 1400°C [10]. With their complementary features, the composites between PZT and BT are expected to exhibit better properties than those of the single-phase PZT and BT [6–9]. Furthermore, the properties can also be tailored over a wider range, by changing the compositions, to meet the strict requirements for specific applications [1, 6–9].

PMN exhibits a high dielectric constant and a broad range transition of dielectric constant, with temperature as a function of frequency [6]. In addition, PMN ceramics exhibit low loss and non-hysteretic characteristics. These make PMN a good candidate for a large number of applications, such as multilayer capacitors, sensors and actuators. However, PMN ceramics have relatively low electromechanical coupling coefficients, as compared to PZT. In contrast to PMN, PZT ceramics have found several actuator and transducer applications due to their high electromechanical coupling coefficients and higher temperature of operation [8, 9]. However, PZT ceramics also possess highly hysteretic behavior, which makes them unsuited for applications that require high delicacy and reliability. Furthermore, PZT ceramics normally have very high Curie temperature ($T_C$) in the vicinity of 400°C. Usually many applications require that $T_C$ is close to ambient temperature. Therefore, there is a general interest to reduce the $T_C$ of PZT ceramics to optimize their uses. With the complementary features of PMN and PZT, the composites between PMN and PZT are expected to synergetically combine the properties of both ceramics, which could exhibit more desirable piezoelectric and dielectric properties for several technologically demanding applications than single-phase PMN and PZT [11, 12].

Prior investigations have already revealed interesting results on the structure, and the dielectric and ferroelectric properties of the BT-PZT and PMN-PZT ceramics [10, 13–15]. However, there has been no report on the influences of the applied stress on the dielectric properties of ceramics in the BT-PZT and PMN-PZT systems. Therefore, this study is undertaken to investigate the influences of the uniaxial compressive pre-stress on the dielectric properties of ceramics in $x$BT-(1-$x$)PZT and $x$PMN-(1-$x$)PZT systems.

## Experimental Procedure

The $BaTiO_3$–$Pb(Zr_{0.52}Ti_{0.48})O_3$ and $Pb(Mg_{1/3}Nb_{2/3})O_3$–$Pb(Zr_{0.52}Ti_{0.48})O_3$ ceramic composites are prepared from starting BT, PZT, and PMN powders by a mixed-oxide method. BT and PZT powders are first prepared by a conventional mixed-oxide method. On the other hand, perovskite-phase PMN powders are obtained via a well-known columbite

method [16]. Subsequently, the $(x)BaTiO_3$–$(1\text{-}x)Pb(Zr_{0.52}Ti_{0.48})O_3$ (when x = 0.0, 0.05, 0.15, 0.25, 0.35, 0.45, 0.55, 0.65, 0.75, 0.85, 0.95, and 1.0) and the $(x)Pb(Mg_{1/3}Nb_{2/3})O_3$–$(1\text{-}x)Pb(Zr_{0.52}Ti_{0.48})O_3$ (when x = 0.0, 0.1, 0.3, 0.5, 0.7, 0.9, and 1.0) ceramic composites are then prepared from the starting BT, PZT and PMN powders by the similar mixed-oxide method described above at various processing conditions. The detailed descriptions of powders and ceramics processing and characterizations are presented thoroughly in earlier publications [10, 14, 15].

For dielectric property characterizations, the sintered samples are lapped to obtain parallel faces, and the faces are then coated with silver paint as electrodes. The samples are heat-treated at 750°C for 12 min to ensure the contact between the electrodes and the ceramic surfaces. The samples are subsequently poled in a silicone oil bath at a temperature of 120°C by applying a dc field of 20 kV/cm for 30 min for BT-PZT ceramics, while for PMN-PZT ceramics the poling condition is 25 kV/cm for 30 min and field-cooled to room temperature. To study the effects of the uniaxial stress on the dielectric properties, the uniaxial compressometer is constructed. The uniaxial compressive stress applied parallel to the electric field direction is supplied by the servohydraulic load frame and the applied stress level is monitored with the pressure gage of the load frame. The details of the system are described elsewhere [17, 18]. The dielectric properties are measured through spring-loaded pins connected to the LCZ-meter (Hewlett Packard, model 4276A). The capacitance and the dielectric loss tangent are determined at a frequency of 1 kHz and room temperature (25°C). The dielectric constant is then calculated from a parallel-plate capacitor equation, e.g. $\varepsilon_r = Cd/\varepsilon_0 A$, where C is the capacitance of the sample, d and A are the thickness and the area of the electrode, respectively, and $\varepsilon_0$ is the dielectric permittivity of vacuum ($8.854 \times 10^{-12}$ F/m).

## Experimental Results

The room temperature dielectric properties measured are under stress-free condition and are listed in Table 1. It is clearly seen that dielectric constant ($\varepsilon_r$) of xBT-(1-x)PZT ceramics increases with increasing BT content. The dielectric constant increases from 813 in PZT to 1429 in BT. For the PMN-PZT system, except for PZT, the dielectric constant increases steadily with increasing PMN content ($\varepsilon_r$ increases from ~700 in 0.1PMN-0.9PZT to ~10300 in 0.9PMN-0.1PZT). The PMN is expected to show a larger value of the dielectric constant, but the lower value is attributed to the detrimental effect of the secondary pyrochlore phase. In addition, the stress-free dielectric loss tangent (tan $\delta$) for BT-PZT system does not change significantly with compositions. Even though the dielectric loss tangent of PMN is very small, larger values of the dielectric loss tangent in PMN-PZT compositions is due mainly to lossy behavior of PZT. More details on the stress-free dielectric properties are available in other publications [14, 15].

The experimental results of the uniaxial compressive pre-stress dependence of the dielectric properties of the ceramics in BT-PZT system are shown in Figs. 1 and 2. There is a significant change of both the dielectric constant and the dielectric loss tangent of the ceramics when the applied stress increases from 0 to 15 MPa. The changes of the dielectric constant with the applied stress can be divided into three different groups. For PZT ceramic, the dielectric constant increases exponentially with applied stress. It can be seen that the dielectric constant is enhanced by approximately 8% at 15 MPa applied stress. For PZT-rich compositions (0.05BT-0.95PZT, 0.15BT-0.85PZT, 0.25BT-0.75PZT, 0.35BT-0.65PZT and 0.45BT-0.55PZT), the dielectric constant increases rather linearly with increasing applied

**Table 1**
Dielectric properties of $x$BT-(1-$x$)PZT and $x$PMN-(1-$x$)PZT ceramics measured at room temperature (25°C and 1 kHz) under stress-free condition

| | $x$BT-(1-$x$)PZT | | | | | | | | | | | $x$PMN-(1-$x$)PZT | | | | | | | |
|---|---|---|---|---|---|---|---|---|---|---|---|---|---|---|---|---|---|---|---|
| x value | 1 | 0.95 | 0.85 | 0.75 | 0.65 | 0.55 | 0.45 | 0.35 | 0.25 | 0.15 | 0.05 | 0 | 0 | 0.1 | 0.3 | 0.5 | 0.7 | 0.9 | 1 |
| $\varepsilon_r$ | 1429 | 1288 | 1223 | 1077 | 1060 | 952 | 890 | 875 | 857 | 839 | 809 | 813 | 813 | 700 | 1400 | 2200 | 5600 | 10300 | 6000 |
| tan $\delta$ | 0.004 | 0.005 | 0.004 | 0.005 | 0.007 | 0.005 | 0.006 | 0.005 | 0.004 | 0.006 | 0.007 | 0.011 | 0.011 | 0.02 | 0.03 | 0.04 | 0.06 | 0.001 | 0.001 |

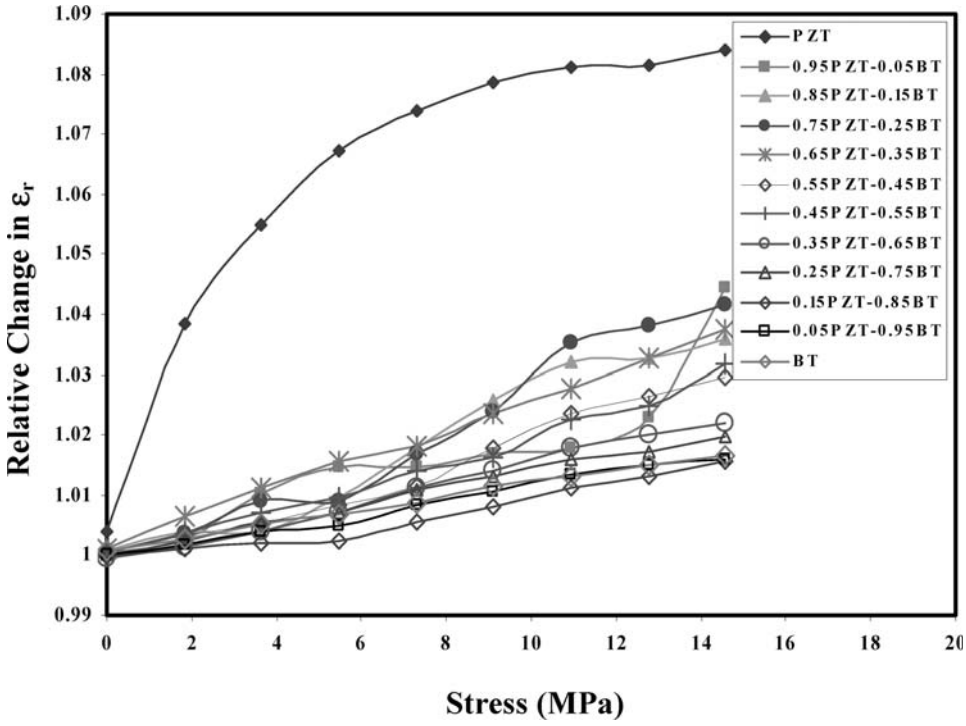


**Figure 1.** Relative changes of the dielectric constant ($\varepsilon_r$) as a function of compressive pre-stress for ($x$)BT-(1-$x$)PZT ceramics.

stress. The changes in the dielectric constant between 2 to 4% at 15 MPa applied stress are obviously smaller than that observed in PZT. For BT-rich compositions (BT, 0.95BT-0.05PZT, 0.85BT-0.15PZT, 0.75BT-0.25PZT and 0.65BT-0.35PZT), the dielectric constant only rises slightly (<2%) and in a linear manner when the applied stress increases to the maximum amplitude. The dielectric loss tangent for all compositions is found to increase significantly and non-linearly when the applied stress is raised from 0 to 15 MPa. The largest changes occur in PZT and 0.25BT-0.75PZT with the dielectric loss tangent enhancement of nearly 80% and 50%, respectively. For the other compositions, the increase in the dielectric loss tangent varies between 10 and 40% at 15 MPa applied stress. Again the changes of the dielectric loss tangent of BT-rich compositions are comparatively smaller than those of PZT-rich compositions, similar to what have been observed in the case of the dielectric constant. Similar experimental results have been reported previously for soft PZT [19, 20], un-doped PZT with various Zr/Ti ratio [21], and Ca-doped BT [22], in which the dielectric properties are found to increase with increasing magnitude of the compressive pre-stress.

The experimental results for the PMN-PZT ceramics are shown in Figs. 3 and 4. To prevent mechanical failures usually occurring in PMN-PZT, the experiments are carried out at the compressive pre-stress levels up to 5 MPa. However, there is a significant change of both the dielectric constant and the dielectric loss tangent of the ceramics even if the maximum applied stress is only 5 MPa. The changes of the dielectric constant

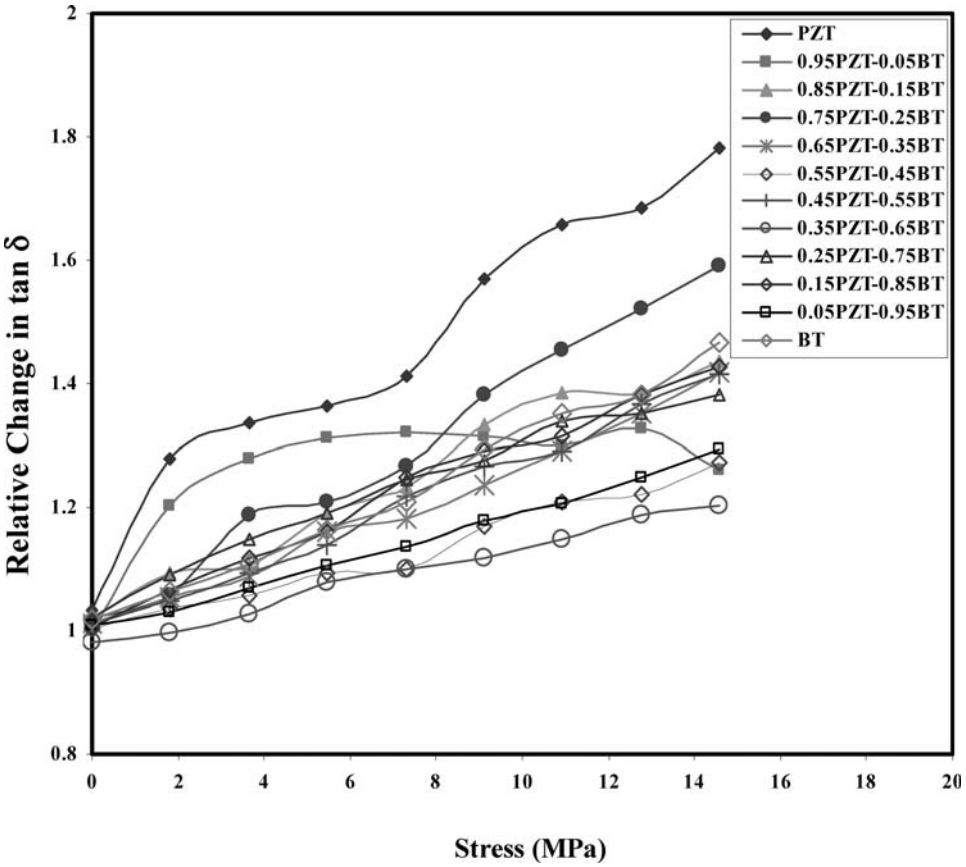


**Figure 2.** Relative changes of the dielectric loss tangent (tan $\delta$) as a function of compressive pre-stress for ($x$)BT-(1-$x$)PZT ceramics.

with the compressive pre-stress can be divided into two different groups. For PMN-rich compositions (PMN, 0.9PMN-0.1PZT, and 0.7PMN-0.3PZT), the dielectric constant generally decreases with increasing applied stress. However, it should be noticed that only PMN and 0.9PMN-0.1PZT compositions show definite decreases in the dielectric constant, while the dielectric constant of the 0.7PMN-0.3PZT composition initially increases then decreases with very little difference in the dielectric constant between the 0 and 5 MPa. On the other hand, for PZT-rich compositions (PZT, 0.1PMN-0.9PZT, 0.3PMN-0.7PZT, and 0.5PMN-0.5PZT), the dielectric constant rises slightly when the compressive pre-stress increases from 0 to 1 MPa, and becomes relatively constant when the pre-stress level increases further. The dielectric loss tangent for most compositions, except for PMN and PZT, is found to first increase when the pre-stress is raised from 0 to 1 MPa, and then decrease with further increasing stress. However, for PZT ceramic the dielectric loss tangent increases monotonously with the increasing stress, while PMN ceramic exhibits a slight increase in the dielectric loss tangent followed by a drop, the turning point being around 2 MPa.

To understand these experimental results, various effects have to be considered. Normally, the properties of ferroelectric materials are derived from both the intrinsic

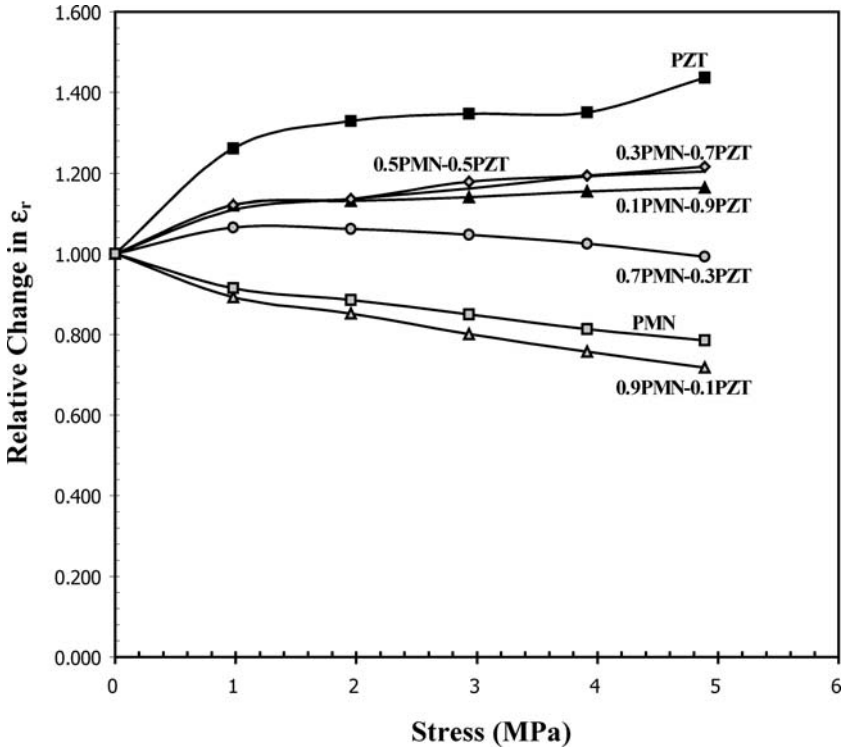


**Figure 3.** Relative changes of the dielectric constant ($\varepsilon_r$) as a function of compressive pre-stress for ($x$)PMN-(1-$x$)PZT ceramics.

contribution, which is the response from a single domain, and extrinsic contributions, which are from domain wall motions [5, 23, 24]. When a mechanical stress is applied to a ferroelectric material, the domain structure in the material will change to maintain the domain energy at a minimum; during this process some of the domains engulf other domains or change shape irreversibly. Under a uniaxial stress, the domain structure of ferroelectric ceramics may undergo domain switching, clamping of domain walls, de-aging, and de-poling [24].

For the case of BT-PZT system, the results on the uniaxial compressive pre-stress dependence of the dielectric properties can easily be explained with the above statements. When the uniaxial compressive pre-stress is applied in the direction parallel to the polar axis (poling) direction, the stress will move some of the polarization away from the poling direction resulting in a change in domain structures [4, 23, 24]. This change increases the non-180° domain wall density. Hence the increase of the dielectric constant with the applied stress is observed. The de-aging mechanism is also expected to play a role here. However, the stress clamping of domain walls and the de-poling mechanisms are not expected at this relatively low stress level used in this study [25]. Therefore, a combination of the domain switching and the de-aging mechanisms is believed to be a reason for the increase of the dielectric constant with increasing applied stress in the BT-PZT system, as shown in Fig. 1.

For the PMN-PZT system, the results for the case of PZT-rich compositions can easily be explained in the same way as in the BT-PZT system. Since PMN is a relaxor ferroelectric

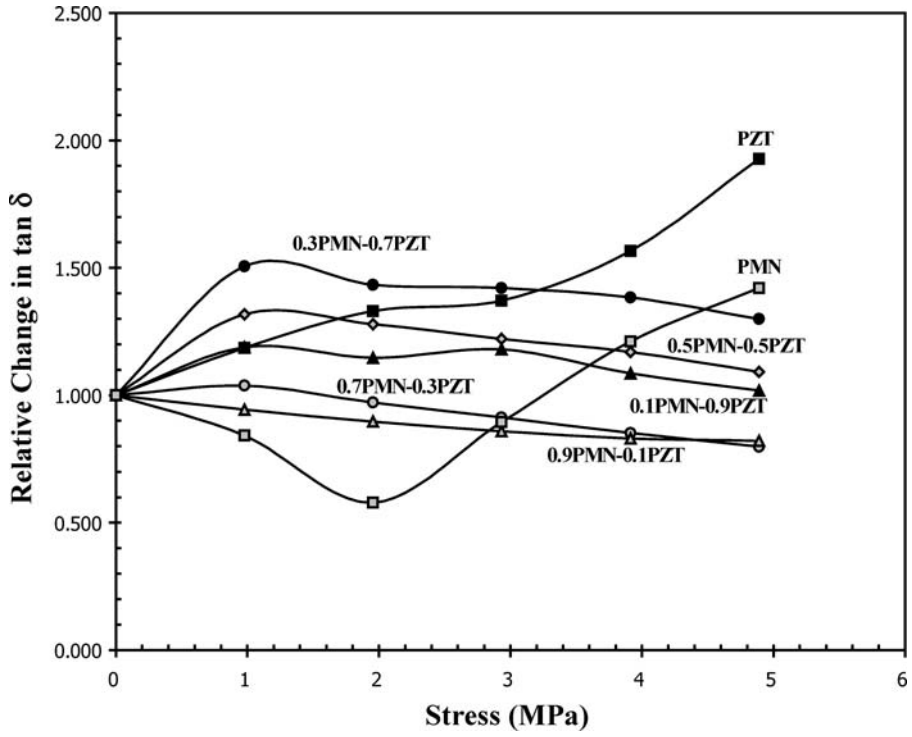


**Figure 4.** Relative changes of the dielectric loss tangent (tan $\delta$) as a function of compressive pre-stress for ($x$)PMN-(1-$x$)PZT ceramics.

material, the situation is very different for PMN-rich compositions. The stress dependence of the dielectric constant of the compositions is attributed to competing influences of the intrinsic contribution of non-polar matrix and the extrinsic contribution of re-polarization and growth of micro-polar regions [4, 25]. Since the dielectric response of both contributions is affected by the applied stress in an opposite way, the behavior of the composites depends on the ratio between the micro-polar region and the non-polar matrix. Since the measurements are carried out at the room temperature, the micro-polar regions dominate the dielectric response of the composites [25]. Therefore, the dielectric constant of the PMN-rich compositions decreases with increasing applied stress, as seen in Figure 3.

The cause of the stress dependence of the dielectric loss tangent for both systems is a little more straightforward than that of the dielectric constant. Stress-induced depinning of the domain walls is expected to occur under the applied compressive pre-stress. As depicted in Figures 2 and 4, an increase in domain wall mobility clearly enhances the dielectric loss tangent in some compositions, while the de-aging in the materials normally causes the decrease of the dielectric loss tangent observed in some compositions [23, 24].

These results clearly demonstrate that the contribution of each mechanism to the dielectric responses of the BT-PZT and PMN-PZT ceramic composites depends on the compositions and the stress level. Finally, it should be noted here that the dielectric behaviors under the applied stress for BT-PZT system, which is a mixture of normal ferroelectrics, are significantly different from those observed in a mixture between normal and relaxor ferroelectrics, i.e. PMN-PZT system, in which the dielectric responses to the applied stress

depend more on the compositions and the stress level, and the dielectric properties of some compositions decrease with increasing applied stress.

## Conclusions

In this study, the $(x)BaTiO_3–(1-x)Pb(Zr_{0.52}Ti_{0.48})O_3$ (when $x = 0.0$, 0.05, 0.15, 0.25, 0.35, 0.45, 0.55, 0.65, 0.75, 0.85, 0.95, and 1.0) and $(x)Pb(Mg_{1/3}Nb_{2/3})O_3–(1-x)Pb(Zr_{0.52}Ti_{0.48})O_3$ (when $x = 0.0$, 0.1, 0.3, 0.5, 0.7, 0.9, and 1.0) ceramic composites are successfully prepared by a conventional mixed-oxide method at various processing conditions. The dielectric properties under the uniaxial compressive pre-stress of the BT-PZT and PMN-PZT ceramics are observed at stress levels up to 15 and 5 MPa, respectively, using a uniaxial compressometer. The dielectric constant and the dielectric loss tangent of the BT-PZT ceramics increase significantly with increasing applied stress. Larger changes in the dielectric properties with the applied stress are observed in the PZT-rich compositions. For PMN-PZT system, the dielectric constant of the PMN-rich compositions decreases, while that of the PZT-rich compositions increases slightly, with increasing applied stress. On the other hand, the dielectric loss tangent for most of the compositions first rises and then drops with increasing applied stress. The experimental results are explained in terms of domain wall and de-aging mechanisms. More importantly, it is of interest to find that the results for the mixture normal ferroelectrics such as BT-PZT ceramics are significantly different from those for the mixture of normal and relaxor ferroelectrics such as PMN-PZT ceramics. Finally, this study undoubtedly shows that the applied stress has significant influence on the dielectric properties of both BT-PZT and PMN-PZT ceramic composites.

## Acknowledgment

The author would like to express his sincerest and deepest gratitude for guidance and teaching by Prof. Robert E. Newnham throughout his career. Contributions from colleagues, S. Wongsaenmai, S. Chamunglap, and S. Ananta, are gratefully acknowledged. This work is supported by the Thailand Research Fund (TRF).

## References

1. L. E. Cross, Relaxor ferroelectrics. *Ferroelectrics* **76**, 241–267 (1987).
2. Y. H. Xu, Ferroelectric Materials and Their Applications. Los Angeles: North Holland; (1991).
3. D. Viehland and J. Powers, Effects of uniaxial stress on the electromechanical properties of $0.7Pb(Mg_{1/3}Nb_{2/3})O_3$-$0.3PbTiO_3$ crystals and ceramics. *J. Appl. Phys*. **89**(3), 1820–1825 (2001).
4. J. Zhao and Q. M. Zhang, Effect of mechanical stress on the electromechanical performance of PZT and PMN-PT ceramics. *Proceedings of the IEEE International Symposium on Applications of Ferroelectrics* **2**, 971–974 (1996).
5. J. Zhao, A. E. Glazounov, and Q. M. Zhang, Change in electromechanical properties of 0.9PMN-0.1PZT relaxor ferroelectrics induced by uniaxial compressive stress directed perpendicular to the electric field. *Appl. Phys. Lett*. **74**, 436–438 (1999).
6. G. H. Haertling, Ferroelectric ceramics: history and technology. *J. Am. Ceram. Soc*. **82**(4), 797–818 (1999).
7. L. E. Cross, Review: ferroelectric materials for electromechanical transducer applications. *Mater. Chem. Phys*. **43**, 108–115 (1996).
8. A. J. Moulson and J. M. Herbert, Electroceramics: Materials, Properties, Applications, 2nd Ed., John Wiley & Sons Ltd (2003).

9. B. Jaffe and W. R. Cook, Piezoelectric Ceramics, R.A.N. Publishers (1971).
10. W. Chaisan, S. Ananta, and T. Tunkasiri, Synthesis of barium titanate-lead-zirconate titanate solid solutions by a modified mixed-oxide synthetic route. *Cur. Appl. Phys*. **4**, 182–185 (2004).
11. J. H. Yoo, H. S. Yoon, Y. H. Jeong, and C. Y. Park, Piezoelectric characteristics of PMN-PZT ceramics for piezoelectric transformer. *Proceedings of the IEEE Ultrasonic Symposium*. 981–984 (1998).
12. A. V. Shilnikov, A. V. Sopit, A. I. Burkhanov, and A. G. Luchaninov, The dielectric response of electrostrictive (1-x)PMN-xPZT ceramics. *J. Euro. Ceram. Soc*. **19**, 1295–1297 (1999).
13. B. K. Gan, J. M. Xue, D. M. Wan, and J. Wang, Lead zirconate titanate-barium titanate by mechanical activation of mixed oxides. *Appl. Phys. A*. **69**, 433–436 (1999).
14. R. Yimnirun, S. Ananta, and P. Laoratanakul, Effects of PMN-mixed-oxide modification on dielectric properties of PZT ceramics. *Mater. Sci. Eng. B*. **112**, 79–86 (2004).
15. R. Yimnirun, S. Ananta, and P. Laoratanakul, Dielectric and ferroelectric properties of PMN-PZT ceramics prepared by mixed-oxide method. *J. Euro. Ceram. Soc*. (2005) (in press).
16. S. L. Swartz and T. R. Shrout, Fabrication of perovskite lead magnesium niobate. *Mater. Res. Bull*. **17**, 1245–1250 (1982).
17. R. Yimnirun, P. Moses, R. J. Meyer, and R. E. Newnham, Dynamic compressometer for converse electrostriction measurements. *Rev. Sci. Instrum*. **74**, 3429–3432 (2003).
18. R. Yimnirun, S. Ananta, E. Meechoowas, and S. Wongsaenmai, Effects of uniaxial stress on dielectric properties of lead magnesium niobate-lead zirconate titanate ceramics. *J. Phys. D: Appl. Phys*. **36**, 1615–1619 (2003).
19. D. Zhou, M. Kamlah, and D. Munz, Effects of uniaxial prestress on the ferroelectric hysteretic response of soft PZT. *J. Euro. Ceram. Soc*. **25**, 425–432 (2005).
20. J. M. Calderon-Moreno, Stress induced domain switching of PZT in compression tests. *Mater. Sci. Eng. A*. **315**, 227–230 (2004).
21. D. Audigier, C. l. Richard, C. l. Descamps, M. Troccaz, and L. Eyraud, PZT uniaxial stress dependence: experimental results. *Ferroelectrics* **154**, 219–224 (1994).
22. I. J. Fritz, Ultrasonic, dilatometric, and dielectric study of uniaxial stress effects in a barium-calcium titanate ceramic. *J. Appl. Phys*. **49**, 788–794 (1978).
23. G. Yang, W. Ren, S. F. Liu, A. J. Masys, and B. K. Mukherjee, Effects of uniaxial stress and DC bias field on the piezoelectric, dielectric, and elastic properties of piezoelectric ceramics. *Proceedings of the IEEE Ultrasonic Symposium* 1005–1008 (2000).
24. G. Yang, S. F. Liu, E. Ren, and B. K. Mukherjee, Uniaxial stress dependence of the piezoelectric properties of lead zirconate titanate ceramics. *Proceedings of SPIE Symposium on Smart Structures and Materials* **3992**, 103–113 (2000).
25. Q. M. Zhang, J. Zhao, K. Uchino, and J. Zheng, Change of the weak-field properties of $Pb(ZrTi)O_3$ piezoceramics with compressive uniaxial stresses and its links to the effect of dopants on the stability of the polarizations in the materials. *J. Mater. Res*. **12**(1), 226–234 (1997).

Available online at www.sciencedirect.com
SCIENCE DIRECT®
Materials Letters 60 (2006) 2666–2671
materials letters
www.elsevier.com/locate/matlet

# Effects of milling time and calcination condition on phase formation and particle size of lead titanate nanopowders prepared by vibro-milling

R. Wongmaneerung, R. Yimnirun, S. Ananta *

*Department of Physics, Faculty of Science, Chiang Mai University, Chiang Mai 50200, Thailand*

Received 10 August 2005; accepted 22 January 2006
Available online 13 February 2006

**Abstract**

Effect of calcination conditions on phase formation and particle size of lead titanate ($PbTiO_3$) powders synthesized by a solid-state reaction with different vibro-milling times was investigated. Powder samples were characterized using XRD, SEM, TEM and EDX techniques. A combination of the milling time and calcination conditions was found to have a pronounced effect on the phase formation and particle size of the calcined $PbTiO_3$ powders. The calcination temperature for the formation of single-phase perovskite lead titanate was lower when longer milling times were applied. More importantly, by employing an appropriate choice of the milling time and calcination conditions, perovskite lead titanate ($PbTiO_3$) nanopowders have been successfully prepared with a simple solid-state reaction method.


*Keywords:* Lead titanate; Perovskite; Nanopowders; Calcination; Phase formation

## 1. Introduction

Lead titanate, $PbTiO_3$ (PT), is one of the perovskite-type ferroelectric materials having unique properties such as high transition temperature (~490 °C), excellent pyroelectric coefficient and large spontaneous polarization [1,2]. These characteristics make it an interesting candidate for many applications e.g. ultrasonic transducers, microactuators and multilayer capacitors [3,4]. To fabricate them, a fine powder of perovskite phase with the minimized degree of particle agglomeration is needed as starting material in order to achieve a dense and uniform microstructure at the sintering temperature [5,6].

Recently, the studies of nanoparticles are also a very attractive field. The evolution of a method to produce nanopowders of precise stoichiometry and desired properties is complex, depending on a number of variables such as starting materials, processing history, temperature, etc. The advantage of using a solid-state reaction method via mechanical milling for preparation of nanosized powders lies in its ability to produce mass quantities of powder in the solid state using simple equipment and low cost starting precursors [7,8]. Although some research has been done in the preparation of PT powders via a vibro-milling technique [9,10], to our knowledge a detailed study considering the role of both milling times and firing conditions on the preparation of PT nanopowders has not been reported. Thus, in the present study, the primary attention was aimed towards the production of stoichiometric $PbTiO_3$ nanopowders by a mixed oxide method. The powder characteristics of the vibro-milling derived $PbTiO_3$ have also been thoroughly investigated.

## 2. Experimental procedure

The raw materials used were commercially available lead oxide, PbO and titanium oxide, $TiO_2$ (Fluka, >99% purity). The two oxide powders exhibited an average particle size in the range of 3.0 to 5.0 μm. $PbTiO_3$ powder was synthesized by the solid-state reaction of these raw materials. A McCrone Micronizing Mill was employed for preparing the stoichiometric $PbTiO_3$ powders as described in a previous work [11]. In order to improve the reactivity of the constituents, the milling process was carried out for various milling times ranging from 20 to 30 h (instead of 30 min [10]) with corundum media in

* Corresponding author. Tel.: +66 53 943367; fax: +66 53 357512.
*E-mail address:* supon@chiangmai.ac.th (S. Ananta).

0167-577X/$ - see front matter © 2006 Elsevier B.V. All rights reserved.
doi:10.1016/j.matlet.2006.01.062

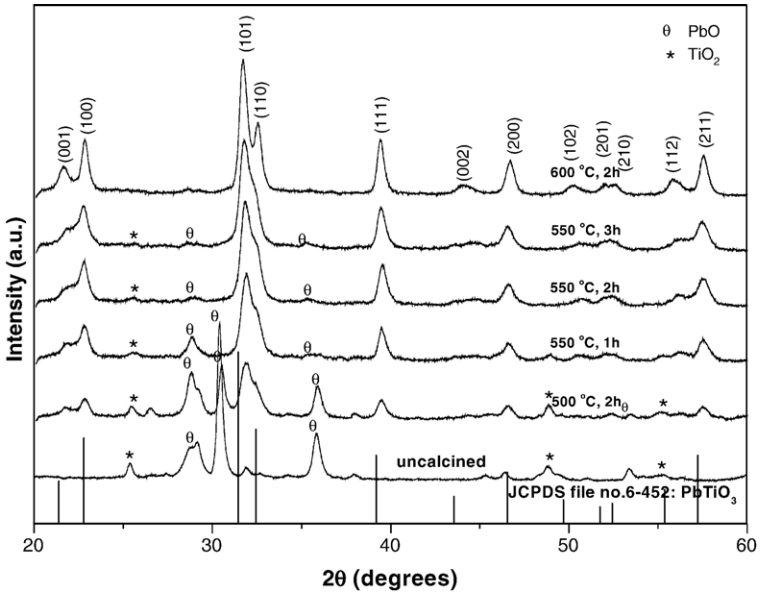


Fig. 1. XRD patterns of PT powders milled for 20 h and calcined at various conditions.

isopropyl alcohol (IPA). After drying at 120 °C for 2 h, various calcination conditions, i.e. temperature ranging from 500 to 600 °C, dwell times ranging from 1 to 4 h and heating/cooling rates ranging from 5 to 20 °C.min$^{-1}$, were applied (the powders were calcined inside a closed alumina crucible) in order to investigate the formation of $PbTiO_3$.

All powders were examined by room temperature X-ray diffraction (XRD; Siemens-D500 diffractometer) using Ni-filtered $CuK_\alpha$ radiation, to identify the phases formed, optimum milling time and firing conditions for the production of single-phase $PbTiO_3$ powders. The crystalline lattice constants, tetragonality factor ($c/a$), mean lattice strain and average particle size were also estimated from XRD patterns [12]. The particle size distributions of the powders were determined by laser diffraction technique (DIAS 1640 laser diffraction spectrometer) with the particle sizes and morphologies of the powders observed by scanning electron microscopy (JEOL JSM-840A SEM). The structures and chemical compositions of the phases formed were elucidated by transmission electron microscopy (CM 20 TEM/STEM operated at 200 keV) and an energy-dispersive X-ray (EDX) analyzer with an ultra-thin window.

## 3. Results and discussion

Powder XRD patterns of the calcined powders after different milling times are given in Figs. 1–3, with the corresponding JCPDS patterns. As shown in Fig. 1, for the uncalcined powder subjected to 20

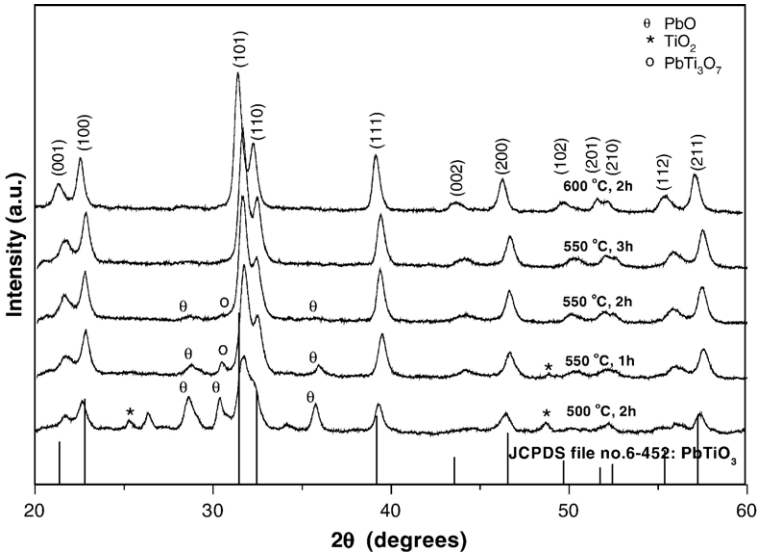


Fig. 2. XRD patterns of PT powders milled for 25h and calcined at various conditions.

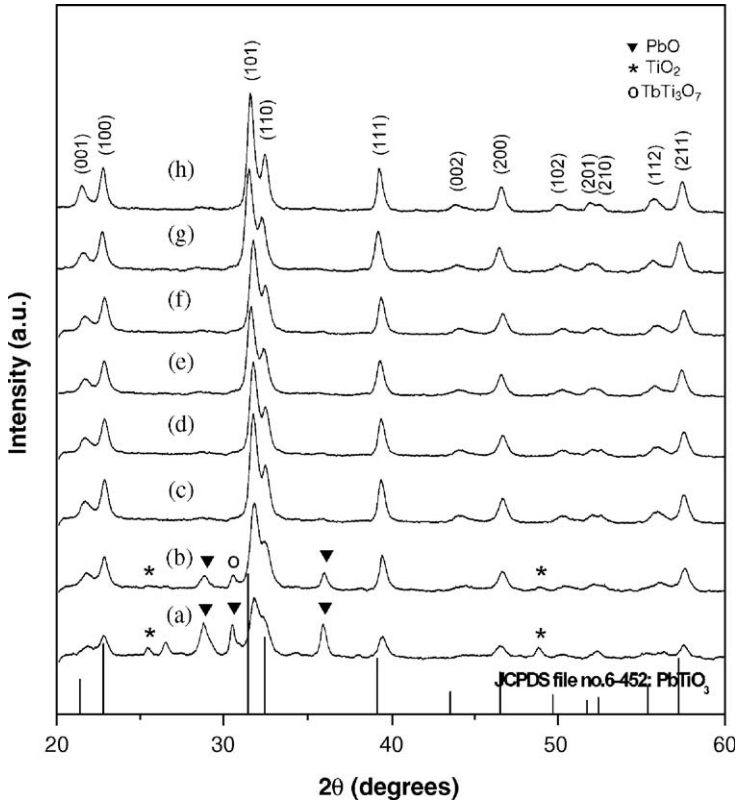


Fig. 3. XRD patterns of PT powders milled for 30 h and calcined at (a) 500 °C for 2 h, (b) 550 °C for 1 h, (c) 550 °C for 2 h, (d) 550 °C for 3 h, (e) 600 °C for 2 h, with heating/cooling rates of 5 °C/min and 550 °C for 3 h with heating/cooling rates of (f) 10 °C/min, (g) 20 °C/min and (h) 30 °C/min.

h of vibro-milling, only X-ray peaks of precursors PbO (▼) and $TiO_2$ (∗) are present, indicating that no reaction was yet triggered during the vibro-milling process. However, after calcination at 500 and 550 °C, it is seen that the perovskite-type $PbTiO_3$ becomes the predominant phase indicating that the reaction has occurred to a considerable extent. Further calcination at 550 °C with dwell time of 1 h or more does not result in a very much increase in the amount of $PbTiO_3$ whereas the traces of unreacted PbO and $TiO_2$ could not be completely eliminated. This could be attributed to the poor reactivity of lead and titanium species [9,10]. However, it should be noted that after calcination at 600 °C for 2 h, the single phase of perovskite PT (yield of 100% within the limitations of the XRD technique) was obtained.

In general, the strongest reflections apparent in the majority of these XRD patterns indicate the formation of $PbTiO_3$. These can be matched with JCPDS file number 6–452 for the tetragonal phase, in space group *P*4/*mmm* with cell parameters $a=389.93$ pm and $c=415.32$ pm [13], consistent with other works [9,10]. For 20 h of milling, the optimum calcination temperature for the formation of a high purity $PbTiO_3$ phase was found to be about 600 °C.

To further study the phase development with increasing milling times, an attempt was also made to calcine mixed powders milled at 25 h and 30 h under various conditions as shown in Figs. 2 and 3, respectively. In this connection, it is seen that by varying the calcination temperature, the minimum firing temperature for the single phase formation of each milling batch is gradually decreased with increasing milling time (Figs. 1–3). The main reason for this behavior is that a complete solid-state reaction probably takes place more easily when the particle size is milled down to accelerate an atomic diffusion mechanism resulting in the suitable level of homogeneous mixing. It is therefore believed that the solid-state reaction to form perovskite PT phase occurs at lower temperatures with decreasing the particle size of the oxide powders.

However, there is evidence that, even for a wide range of calcination conditions, single-phase $PbTiO_3$ cannot be produced easily, in agreement with literature [10,14]. A noticeable difference is noted when employing the milling time longer than 20 h (Figs. 2 and 3), since they lead to a considerable formation of lead deficient phase, $PbTi_3O_7$ (o), earlier reported by a number of workers [15,16]. This pyrochlore phase has a monoclinic structure with cell parameters $a=107.32$ pm, $b=381.2$ pm, $c=657.8$ pm and $\beta=98.08°$ (JCPDS file number 21–949) [17]. This observation could be attributed mainly to the poor reactivity of lead and titanium species [9,10] and also the limited mixing capability of the mechanical method [18].

From Figs. 2 and 3, it is clear that the intensity of the perovskite peaks was further enhanced when the dwell times of the calcinations process were extended up to 3 h at the expenses of PbO, $TiO_2$ and $PbTi_3O_7$ phases. An essentially monophasic $PbTiO_3$ of perovskite structure was obtained at 550 °C when the calcination time was increased to 3 h and 2 h for the milling time of 25 h and 30 h, respectively, as shown in Figs. 2 and 3(c). This was apparently a consequence of the enhancement in crystallinity of the perovskite phase with increasing degree of mixing and dwell time, in good agreement with other works [18,19].

In the present study, an attempt was also made to calcine the powders with 30 h of milling times under various heating/cooling rates (Fig. 3). In this connection, it is shown that the yield of $PbTiO_3$ phase did not vary significantly with different heating/cooling rates ranging from 5 to 30 °C $min^{-1}$, in good agreement with the early observation for the $PbTiO_3$ powders subjected to 0.5 h of vibro-milling times [10]. It should be noted that no evidence of the introduction of impurity due